RESEARCH ON THE DEVELOPMENT OF ELECTRICAL EVALUATION METHOD FOR STATIC AND DYNAMIC PROPERTIES OF MAGNETIC VORTEX SYSTEMS IN PATTERNED FERROMAGNETIC DOTS

崔, 暁敏

https://doi.org/10.15017/1544002

出版情報：九州大学, 2015, 博士（工学）, 課程博士
バージョン：
権利関係：全文ファイル公表済

RESEARCH ON THE DEVELOPMENT OF ELECTRICAL EVALUATION METHOD FOR STATIC AND DYNAMIC PROPERTIES OF MAGNETIC VORTEX SYSTEMS IN PATTERNED FERROMAGNETIC DOTS

By
Xiaomin Cui

SUBMITTED IN PARTIAL FULFILLMENT OF THE
REQUIREMENTS FOR THE DEGREE OF
DOCTOR OF PHILOSOPHY
AT
KYUSHU UNIVERSITY
FUKUOKA, JAPAN
AUGUST 1, 2015

KYUSHU UNIVERSITY
GRADUATE SCHOOL OF INFORMATION SCIENCE AND ELECTRICAL ENGINEERING

The undersigned hereby certify that they have read and recommend to the Faculty of Graduate Studies for acceptance a thesis entitled "**Research on the development of electrical evaluation method for static and dynamic properties of magnetic vortex systems in patterned ferromagnetic dots**" by **Xiaomin Cui** in partial fulfillment of the requirements for the degree of **Doctor of Philosophy**.

Dated: August 1, 2015

Examing Committee:

Prof. Tanemasa Asano, Supervisor

Prof. Takashi Kimura

Prof. Kimihide Matsuyama

Prof. Hiromi Yuasa

KYUSHU UNIVERSITY

Date: **August 1, 2015**

Author: **Xiaomin Cui**

Title: **Research on the development of electrical evaluation method for static and dynamic properties of magnetic vortex systems in patterned ferromagnetic dots**

Department: **Graduate School of Information Science and Electrical Engineering**

Degree: **Ph.D.** Convocation: Year:

Signature of Author

To My Husband and Family

Table of Contents

List of Figures

Abstract

Magnetic domain structure forms the patterned structures with increasing magneto-static energy reflected by the geometrical shape while ferromagnet is miniaturized to micron or sub-micron size. Among them, the stabilized unique curling spin configuration in circular or regular polygon ferromagnetic dot is known as magnetic vortex. Magnetic vortex represents unique spin arrangement with robust stability and its characteristics make the cornerstone of a series of promising spin-based electronics including magnetoelectric random access memory, microwave assisted filters, vortex based oscillators or even medical use such as bio-functionalized microdiscs. Magnetic vortex includes two degrees of freedom chirality (rotation direction of the magnetic moment) and polarity (the magnetization direction of the vortex core). However, the identification of chirality requires certain special equipment such as magnetic force microscope or soft x-ray microscope, attributing to the high spatial symmetry of the spin arrangement. In this thesis, relatively simple evaluation methods for magnetic vortex properties in ferromagnetic dots have been developed. The results are summarized as below.

First, the measurement of anisotropic magneto-resistance in a single micron sized ferromagnetic dot offers the information of vortex nucleation position by introducing the asymmetrically configured electrodes. The inhomogeneous current distribution created by the large difference of the electrical resistivity between the ferromagnetic disk and nonmagnetic electrodes enables the detection of different AMR curves, leading to the characterization of vortex chirality. The vortex chirality is also confirmed in the AMR device to depend on the magnitude of the maximum magnetic field. Second, a sensitive detection method with separately prepared injection and detection circuits is developed for investigating the vortex core dynamics while the core is excited by an amplitude-modulated alternating magnetic field.

By taking advantage of the two-fold symmetrical resistance distribution in a ferromagnetic disk, the detectable 2nd harmonic voltage is achieved at remanent state corresponding to the vortex core excitation by a microwave magnetic field. Moreover, the nonlinear behavior of resonant frequency as a function of the microwave power suggests a deviation from the ideal situation, which may attribute to the higher order contribution of the magnetostatic potential under high amplitude.

Furthermore, the magnetic structure in isosceles triangular dot has been examined using magnetic force microscope and two magnetic vortices has been created by an initialized external field with specific direction. The resonant dynamical properties of the triangle with two vortices have been probed. Those results have revealed the effective control of magnetic vortices numbers in the isosceles triangle, and demonstrated large splitting between the two resonant peaks, which has been reproduced by the micromagnetic simulation.

Finally, the dynamic response of chained square type ferromagnetic dots has also been studied by applying an external field with different directions. The experimental results demonstrate field dependence of resonant frequency of vortex core showing unique directional dependence on external field. A significant modulation on resonant frequency has also been achieved when external field is perpendicular with the strip line.

The developed detection techniques of vortex core dynamics and demonstrated experimental results provide valuable means for exploring intrinsic property of vortex, enrich understanding towards vortex static and dynamic properties, and eventually pave the way for the development of magnetic vortex based memories, reconfigurable logic or microwave assisted filters.

Acknowledgements

In full gratitude I would like to acknowledge the following individuals who have encouraged, inspired, supported, assisted and sacrificed themselves to help my pursuit of doctoral degree during the whole process of my doctoral course period. The valuable experience would be cherished forever because of those wonderful people around me.

First of all, I would like to address my sincere gratitude to al the members in the defense committee, Prof. Tanemasa Asano, Prof. Kimihide Matsuyama, Prof. Hiromi Yuasa and Prof. Takashi Kimura for all their contributions, valuable suggestions and comments. Particularly, I express my special appreciate and thanks to my supervisor Prof. Takashi Kimura. I have been amazingly fortunate to have a supervisor who is not only a enthusiastic and energetic researcher, but also a patient advisor for guiding me to this fascinating research field of magnetic science. I appreciate all his contributions of time, interesting ideas, and funding to make my PhD experience and stimulating. I thank him for providing friendly research environment and advanced scientific equipment for experimental research so that I could fabricate the micron or nano-sized devices. I still remember that he taught me patiently how to use electron beam lithography. I also thank him for allowing me to take part in both the domestic and international conferences so that I could not only learn about the frontiers of this research field but also give poster or oral presentations as a good practice. He also invites many excellent researchers to give us lectures or presentations for enriching our knowledge magnificently. In addition, I really appreciate his long discussions, carefully reading, insightful comments and constructive criticisms during my preparation of manuscripts which helped me focus and understand my work better. Most importantly, I am grateful to him for holding me to a high research standard and I want to become a good researcher as good as him.

I am very grateful for my previous assistant professor Satoshi Yakata for teaching me how to do the microwave assisted electrical measurement and how to adjust the equipment to obtain a better signal. I am also thankful to him for not only introducing the fundamental knowledge about magnetic vortex dynamics but also offering amazing suggestions and fruitful discussions. What's more, he taught me to use Igor for processing data. I

got used to my job fast under his continuous guidance and encouragement. In addition, I would like to thank our assistant professors Kohei Ohnishi and Kazumasa Yamada for their continuous support both on the experimental research and daily life for creating a qualify work environment for me.

I also want to mention that specially gratitude is addressed to assistant professor Terumitsu Tanaka from Matsuyama labratory who is a expert for performing the micromagnetic simulation research for the magnetostatic and dynamic properties for the Isosceles triangular device. His simulation result is a great contribution to my thesis. I am very grateful for his valuable suggestions and fruitful discussions.

I am very grateful for our excellent technician Atsushi Kenjo who helps to improve and maintain all the equipment in the clean-room and the measurement stage for my measurement setup. He also helps me to enhance my Japanese on professional and physics level in the daily life. He is an energetic old man who would always encourage me to become a nice person no matter how old I am. He is also interested into all kinds of new electronic products and I learn a lot about the frontier electronic products.

I would also like to thank our wonderful and warm-hearted secretary Mika Ishima who is always sweet and friendly woman who gave me a lot help during the preparation of the paperwork. Additionally, she always bring us delicious sweets and presents. Thanks to her, I get to know many traditional stuff in Japanese culture. She absolutely made my life easier and more enjoyable in Japan.

I am also grateful for my current and former colleagues Makoto Hidegara, Kohei Kiseki, Congpu Mu and Qisen Dang for their good and pleasant cooperation in micromagnetic simulation using OOMMF, sample fabrication process, magnetic dynamic measurement and numerous discussions. I also thank Tatsuya Nomura, Kazuto Yamanoi, Yu Takaira, Masatoshi Kawakita, Yuma Ono and all the other members for creating a warm environment, teaching and helping me in the Japanese learning and my life in Japan.

Besides, I would like to thank Miyao Sensee, Sadoh Sensee for allowing me staying in their office for several months during the year 2014. I had a good time when I was there. I also want to thank the kindness and good care from Yamamoto San, who is the assistant in Sadoh laboratory.

I also want to express my special gratitude to my supervisor Prof. Guotian Ye during Master course for his continuous encouragement on English learning and his guidance for starting out in a scientific research.

Particularly, none of this work would have been possible without the love, patience and understanding of my parents, my younger sister and brother during all these years. I would like to express my heart-felt gratitude to my husband Shaojie. He has always been there to support and encourage me to overcome the difficulties in my research and life. I am also

very thankful for his generous help, valuable suggestion, comments even grammar check for my thesis preparation throughout this endeavor.

Finally, I would like to acknowledge that China Scholarship Council for their the financial support of my living expense in Japan. I really appreciate the precious change they provided so that I could receive the good education and research for my PhD study. What's more, it enriches my vision to see the world and specifically to the frontier research of spintronics.

Fukuoka, Japan Xiaomin Cui
July, 1, 2015

Chapter 1

Introduction

1.1 Motivation

Magnetic domains stand for the elementary objects which establishes the relationship among fundamental physical behaviors, macroscopic properties and the future applications of ferromagnetic materials.[1, 2] As a magnetic domain structure with relatively lowest energy at remanence, magnetic vortex forms as a curling spin configuration with a out-of-plane vortex core which could be used as a cell for a number of emerging spintronic applications such as the high density memory devices, and vortex based spin oscillators and other medical use like biofunctionalized microdiscs.[3–7] The existence of vortex structure in ferromagnetic dots has been experimentally confirmed by conducting the sensitive magneto-optical measurement and magnetic force microscopy imaging.[3, 8] In addition, magnetic vortex exhibits abundant fundamental dynamic behaviors during the low frequency precession mode[9–13]. The appropriate characterization method (especially electrical measurement technique) may deep the understanding towards the basic vortex core motion of magnetic nanostructures, provide valuable information for independent manipulation for vortex chirality or polarity, and pave the way for the application of magnetic vortex structure. On the basis of some regulations of present electrical detection methods, development of more flexible, quantitative but simple evaluation technique and exploit of novel dynamic properties of magnetic

vortex become indispensable.

1.2 Outline of the chapters

This dissertation mainly concentrates on experimentally study of the magnetostatic and dynamic properties of the magnetic vortex stabilized in micron or submicron-sized ferromagnetic dots during the past three years.

The background and motivation of this research are introduced in chapter 1. In chapter 2, the theoretical background related to the understanding of magnetic vortices and the measurement techniques are summarized. In chapter 3, the fabrication process of the ferromagnetic devices and the measurement system for evaluating magnetostatic and dynamic properties are provided. The experimental results from chapter 4 to chapter 6 are for the ferromagnetic circular disks. In chapter 4, the measurement of anisotropic magnetoresistance for detecting the vortex nucleation position in a single micron ferromagnetic disk is demonstrated by the asymmetrically configured electrode, which extensively offers the information of the chirality of the magnetic vortex. Chapter 5 is devoted to a sensitive method for electrically detecting the resonant oscillation of the magnetic vortex induced by the amplitude-modulated ac magnetic field in the chained ferromagnetic disks with separately prepared injection and detection circuits. In chapter 6, a sensitive and reliable method for characterizing the vortex core dynamics at the remanent state is developed by monitoring the detectable 2nd harmonic voltage excited by the microwave magnetic field due to a two-fold symmetric resistance distribution as a function of the vortex core in the ferromagnetic disk. Finally, in chapter 7, the studies on magnetostatic and dynamic properties have been extended to the isosceles triangle and square shaped ferromagnetic dots. In the first section, the numbers and the chirality in the isosceles triangle have been successfully manipulated by applying an initialized external field and the domain structure with single vortex and two vortices has been confirmed by employing the magnetic force

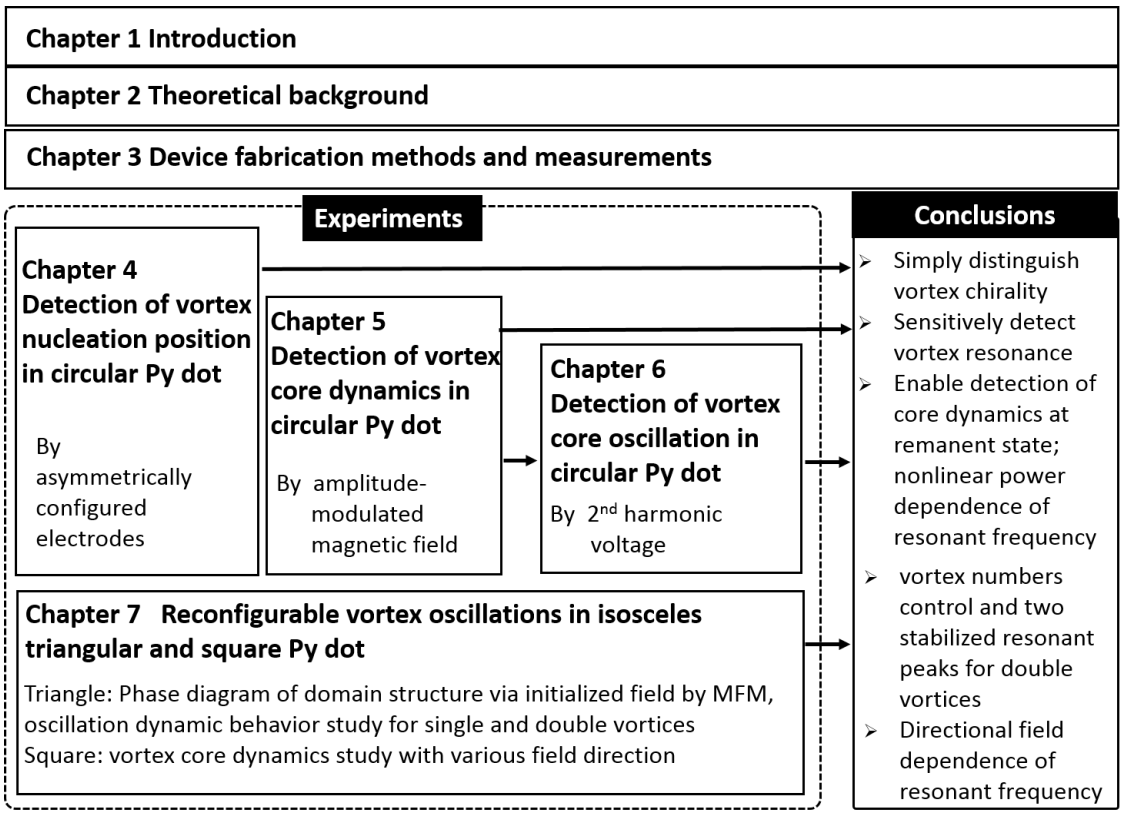

Figure 1.1: The flow chart of the chapters.

microscope, respectively. Besides, the resonant dynamic properties of the stabilized double vortices in the isosceles triangle have been studied by the transmission impedance technique. The two resonant frequency peaks suggest the existence of high resonant frequency mode and low resonant frequency mode as a function of the field possibly because of the strong magnetic coupling. In addition, the experimental results are reproduced by performing the micromagnetic simulations. In the other section, a large variation of the resonant frequency as a function of the field is indicated in the square chained dots which probably due to the large change of the defined potential attributing to the displacement of vortex core under external field. Finally, the dissertation closes with a conclusion in chapter 8.

The flow chart for the chapters is shown in the figure 1.1.

Chapter 2

Theoretical background

Magnetism in nanoscale or sub-micron scale has attracted a wealth of interest not only for providing fascinating fundamental physics but also for their promising potential in technological applications. In this chapter, we reviewed the theoretical background required for understanding the experimental research in the following chapters.

2.1 Ferromagnetic material

2.1.1 Ferromagnetism

Ferromagnetism describes the material that could exhibit spontaneous magnetization with parallel alignment of spins in the absence of an external magnetic field. As we know, in addition to the negative electronic charge, the electron also has an intrinsic spin angular momentum which is separate from the angular momentum resulting from its orbital motion. This angular momentum is called spin. Electrons with spin possesses a magnetic dipole moment and it can be either spin up or spin down as shown in Fig.2.1 (a). According to Pauli exclusion principle, two identical electrons can not occupy the same quantum state simultaneously. Therefore, when two electrons are residing in the same orbital, the spins of electrons have to be antiparallel to satisfy the above rule. In ordinary materials, the magnetic dipole moments of each atom produce opposite magnetic field which would cancel each other because each dipole points in a random direction. But the magnetization

in ferromagnetic materials spontaneously aligns ordering arising from the spin magnetic moment in conjunction with the orbital angular momentum of the electron about its nucleus. However, the ferromagnet would lose their alignment when the temperature reaches a critical temperature. That critical temperature is called Curie temperature because the disorder coming from thermal becomes dominant comparing with the energy-lowering due to the magnetic ordering.

Transition metals Iron, Cobalt, Nickel,and their alloys are most common ferromagnetic materials. Among those materials, permalloy (shorted as Py) is one of widely used soft ferromagnetic alloys with the composition of 80% Ni and 20% Fe. In this thesis, Py is employed for the study of static and dynamical properties of magnetic vortices. For Py ($Ni_{80}Fe_{20}$), the 3d shell of electrons is partially filled which would create a substantial magnetic moment. The interaction of the magnetic moment between neighbored 3d subshell electrons produces the energy band. However, there is energy shift between the bands of the spin up and spin down configurations due to the exchange interaction. Figure 2.1 (b) shows the schematic image of the density of electronic states at 3d shell in a ferromagentic materials.

2.1.2 Energy component

The magnetization configuration in a ferromagnetic dot shows a tight correlation with the energy distribution in the ferromagnetic system. The energy relationships in a ferromagneticstructure would be discussed as follows. The total energy is mainly determined by the competition of exchange energy (E_{ex}), demagnetization energy (E_{de}), Zeeman energy (E_{z}), anisotropy energy (E_{ani}).[14–17] Correspondingly, the total energy in a ferromagnetic system could be expressed as

$$E_{\mathrm{tot}} = E_{\mathrm{ex}} + E_{\mathrm{de}} + E_{\mathrm{z}} + E_{\mathrm{ani}} \tag{2.1.1}$$

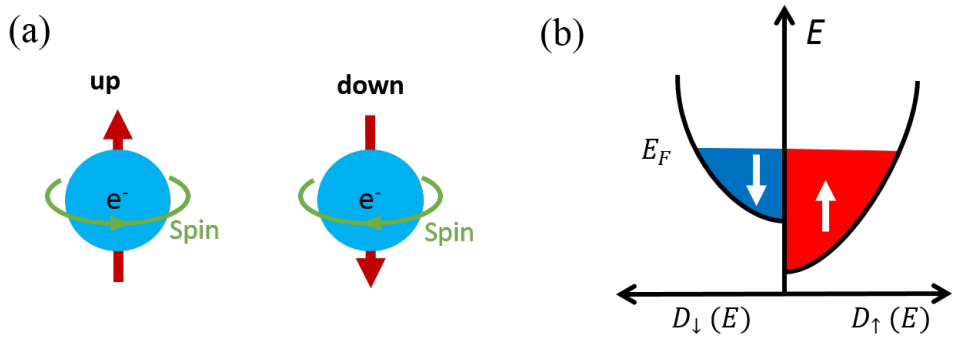

Figure 2.1: (a) Configurations of the electron with up spin or down spin angular momentum, respectively; (b) A schematic representation of the density of electronic states for the 3d shell in a ferromagnetic material where the filled electron states below the Fermi level E_F are marked as red and blue colors; E is the electron energy; $D_\uparrow$(E) and $D_\downarrow$(E) are the density of states for spin up (majority states) and spin down (minority states), respectively.

Exchange energy

The exchange interaction (exchange energy) is a quantum mechanical effect between identical particles, which arises from the wave function of the indistinguishable particles being subject to exchange symmetry, that is, either remaining unchanged (symmetric) or changing its sign (asymmetric) when two particles are exchanged.[18, 19] The exchange interaction keeps the spins being alignment randomly under the influence of certain thermal fluctuations. In the micromagnetic regime, the exchange force per volume could be expressed

$$E_{\text{ex}} = \int A(\nabla \mathbf{m})^2 dV = -\int \frac{\mu_0 M_s}{2} \mathbf{m} \cdot \mathbf{H}_{\text{ex}} dV \tag{2.1.2}$$

Where A, μ_0 and $\mathbf{H}_{\text{ex}}$ are the exchange stiffness constant, permeability of the vacuum and the effective exchange field, respectively. However, Stoner and Slater developed a theory where they consider the exchange energy as an internal field.[20, 21] The exchange energy changes while the orientation of the elementary magnets changes.

Demagnetization energy

The magnetization inside a magnet can generate a magnetic field due to the interaction of the magnetization, which is the demagnetizing field (H). The demagnetizing field behaves with the purpose of decreasing the total magnetic moment in a ferromagnet.[22, 23] Moreover, the shape anisotropic effect in the ferromagnet is attributed to the demagnetization field. The demagnetization energy depends on the integral of volume of the magnet, as shown following,

$$E_{\mathrm{de}} = -\int \frac{\mu_0 M_s}{2} \mathbf{m} \cdot \mathbf{H}_{\mathrm{de}} dV \tag{2.1.3}$$

Where H_{de} is the demagnetizing field.

Zeeman energy

The potential energy of a magnetic configugration under applying an external magnetic field is the Zeeman energy (or external field energy) named after Pieter Zeeman, which also contributes to the total energy in a ferromagnet. The Zeeman energy can be written in the following equation. In the thesis, the external field is applied for altering the magnetization in the micron or submicron sized ferromagnetic devices under a modulated radiofrequency magnetic field. The Zeeman energy approaches to the minimum when the direction of the magnetization is parallel with the external field. The contribution of the Zeeman energy is described as

$$E_{\mathrm{z}} = -\int \mu_0 M_s \mathbf{m} \cdot \mathbf{H}_{\mathrm{ext}} dV \tag{2.1.4}$$

Anisotropy energy

There is another energy contribution in ferromagnetic crystals, which is the magnetic anisotropy energy resulting from the existence of preferred axes of easiest magnetization

in ferromagnetic crystals.[16, 24–27] Therefore, there is the anisotropy energy consumption while the magnetization turns away from an axis of easy magnetization to the hard magnetization by introducing a energy (eg.: electric current). The anisotropy energy originates from the interplay between spin-orbit coupling and the crystal lattice.[24–26] In a ferromagnetic cubic crystal, the anisotropy energy may be written as[26]

$$E_{\text{ani}} = -\int [K_1({\alpha_1}^2{\alpha_2}^2 + {\alpha_2}^2{\alpha_3}^2 + {\alpha_1}^2{\alpha_3}^2) + K_2({\alpha_1}^2{\alpha_2}^2{\alpha_3}^2)]d\bar{r} \tag{2.1.5}$$

where α_i are the direction cosines of magnetization. K_1 and K_2 are the anisotropy constants, respectively. The magnitude and sign of the anisotropy constants are determined by the materials. The magnetic anisotropy for permalloy is quite small which means anisotropy energy in permalloy may be ruled out.

In the thesis, the external magnetic field and the shape anisotropy in a ferromagnet arising from the demagnetization energy were considered for the research of the magnetostatic and dynamic properties in Permalloy dots. Permalloy was chose to fabricate all the ferromagnetic devices in this thesis. Therefore, the contribution of anisotropy energy was ignored because of the small magnitude.

2.1.3 Magnetic domains

Magnetization is a vector field that expresses the density of permanent or induced magnetic dipole moments in a magnetic material. An area inside a ferromagnetic material with uniform magnetization forms a magnetic domain. Under Curie temperature, the magnetization in the ferromagnetic material spontaneously divides into several small areas for the purpose of minimizing the internal energy driven by the exchange interaction between localized spins.[28] Those small areas were named magnetic domains as shown in Fig. 2.2(a). However, it requires large magnetostatic energy to maintain the parallel alignment of magnetization in a large region. Therefore, the domain would divide into several smaller domains

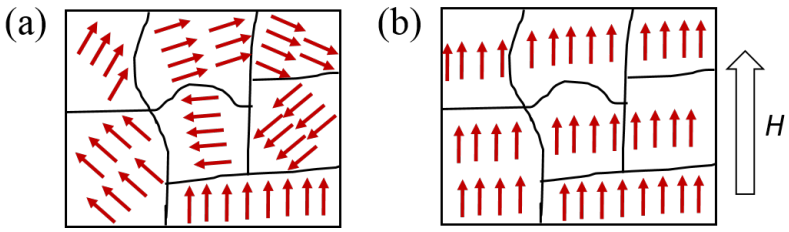

Figure 2.2: (a) The random alignment of magnetic moments in a ferromagnetic film; (b) The magnetization alignment in the same ferromagnetic film after applying a external magnetic field.

for being more stable. The size of magnetic domains is usually around a few micrometer to hundreds of micrometers.

Different magnetic domains possess different magnetization. Moreover, it exists a transition region between domains where the magnetization gradually rotates from one direction to another in the next domain. That specific region is domain wall. Magnetic domain theory was first constructed by Pierre-Ernest Weiss in 1906 then extensively developed by Landau, Lifshitz and Kennard etc.[14, 29–31] In addition, the magnetization in the magnetic domains could be rearranged by applying a external magnetic field to overcome the internal energy.

2.1.4 Patterned magnetic structure

For most of materials, the size of the magnetic domains varies from several micrometer to hundreds of micrometer. When we reduce the dimension of a ferromagnetic film to micron or sub-micron sized shapes, the boundary condition would be modified to form specific domain structures rather than uniform alignment of magnetization. The geometrical confinement in patterned structures alters their energetics and leads to new magnetic states. The rapid development in electron beam lithography technique provides good conditions for the fabrication of various patterned structures, either separated ferromagnetic arrays or 2D chained ferromagnetic devices. Those patterned magnetic structures have been paid

extensive attention due to their promising applications in patterned magnetic media, unit cell of future spintronic devices or robust topological solitons.

The magnetization distribution in patterned nano-sized structures depends on the shape and its geometrical size which can either be single domain, or non-uniform closure domain structures. Among the non-uniform domain structures, magnetic vortex is an interesting magnetization distribution with lowest energy and it is stabilized as the ground state of the patterned magnetic particles. It has become one of the hot topics in spintronic field. Therefore, the magnetic vortex would be introduced in the next section.

2.2 Magnetic vortex

From the viewpoint of microstructure, magnetic domains are considered as the elements in the ferromagnetic materials that link the fundamental physical behaviors with the macroscopic properties and applications.[1, 2] Ferromagnetic materials generally form the domain structures for the purpose of reducing the magnetostatic energy[2, 8, 17]. In the micrometer or submicrometer sized ferromagnetic dot, a constrained magnetic domain structure with the curling spin configuration appears, while the geometrical dimension satisfies the condition that the thickness of ferromagnetic dot is much smaller than the diameter or the diameter of outer circle of the dot.[32, 33] Magnetic vortex is a nonuniform magnetic structure possessing relatively lowest energy configuration even it is a bit larger than the single domain structure.[8, 17, 34]

2.2.1 Two topological parameters of magnetic vortex

A magnetic vortex usually stabilizes in a nano or micron sized ferromagnetic structures.[3, 8] There are two topological quantities introduced for characterizing the magnetic vortex, which are chirality and polarity. Those two degrees of freedom form four possible states in magnetic vortex as shown in Fig.2.3.[35] Therefore, it is suitable as a memory cell with high

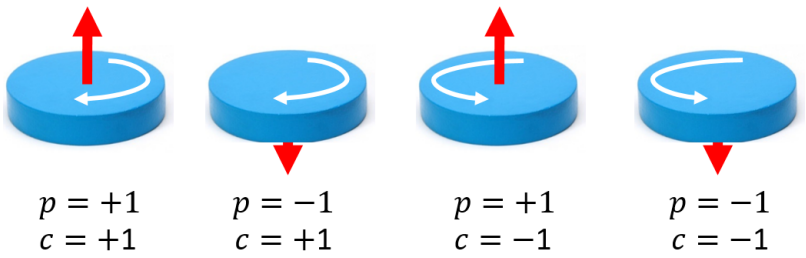

Figure 2.3: Possible states combined by different polarity (p) and chirality (c). Here those states are energetically equivalent without external field and the polarity is independent with chirality.[8]

density comparing with binary system. Chirality represents the rotational direction of magnetization in the domain structure. It could be either clockwise (CW) or counterclockwise (CCW). In the center of a ferromagnetic dot, the angle between neighboured spins becomes extremely large. Correspondingly, the magnetization in the small center area of magnetic vortex is difficult to keep in-plane. Therefore, it squeezes out and becomes perpendicular to the plane to maintain low internal energy. The magnetization in the center of vortex core is polarity, which could be either up or down, as shown in Fig.2.3.

The out-of-plane vortex core in a magnetic vortex structure has been predicted years ago but the direct experimental observation of the vortex core was realized recently by T. Shinjo et al with employing magnetic force microscope.[8, 36] They fabricated the circular type permalloy dots with the electron-beam lithography combing with electron beam evaporation. The MFM images show the different contrast at the center of Py dots implying the vortex core polarities either up or down. The polarity of vortex core is randomly distributed and it has no correlation with the chirality of the vortex structure. Moreover, the polarity of the vortex core could be adjusted to the same direction by applying a perpendicular static field even with large magnitude.[8, 37] Beside of the introduction of a perpendicular field, there are also other ways to control the vortex polarity which would be introduced in other

section. Moreover, the vortex core has also been observed in the thin film nanomagnet using spin-polarized scanning tunneling microscopy.[34] They also demonstrate the exchange stiffness and the saturation magnetization determines the size and shape of vortex core in a nanomagnet.[34]

In addition, the displacement of the vortex core could be induced by applying a in-plane magnetic field. Several studies have confirmed that the vortex core is displaced perpendicular to the direction of the external field.[38, 39] However, the chirality of magnetic vortices determines the movement direction of vortex core either this direction or opposite direction.

2.2.2 Phase diagram of geometrically stabilized vortex state

The formation of vortex structure has to satisfy specific dimensional parameters in submicron or micron size. The geometrical stability of the vortex state has been studied both theoretically and experimentally. Figure 2.4 shows the magnetic phase diagram of remanence configuration for circular permalloy disks as function of the radius R and thickness L of the disks normalized to the exchange length of permalloy. This figure was modified by taking the data from Refs.[40–42]. Figure 2.4 indicates the existence of 3 stabilized magnetic states perpendicular single domain, in-plane single domain and vortex structure. When the thickness is much larger than the radius of the disk, the energy of the magnetic charges at side surface becomes much larger and the magnetic particles form perpendicularly magnetized single domain structure. However, when the thickness becomes much smaller than the radius, the contribution of in-plane demagnetization energy exceeds the energy from exchange interaction, the magnetic configuration keeps in-plane single domain stabilized in remanence state. However, the existence of vortex structure is a balance situation between the demagnetization energy and exchange interaction located in the upper right part of Fig. 2.4 when the thickness is comparable with the radius of the circular disk.

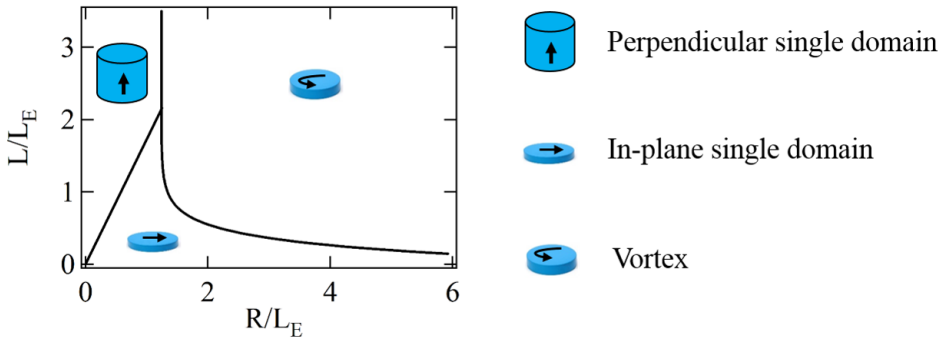

Figure 2.4: Magnetic phase diagram of circular permalloy disks with radius R and thickness L. The axis scale is expressed as the ratio with the exchange length L_E ($L_E \approx 18nm$ for permalloy). The equilibrium lines are shown as solid lines. This figure was modified according to several simulation and experimental data.[40–43]

The phase diagram representing the existence of vortex structure in ferromagnetic dot has also been experimentally revealed by R. P. Cowburn in 1999 by conducting the hysteresis loop using a sensitive magneto-optical Kerr detection.[3] After that, Lee et al. constructed the phase diagram showing the core reversal times with respect to the amplitude and frequency of magnetic field.[44] Chen and Crowell's group also studied the vortex dynamics in Py disks and established the phase diagram which enables the identification of the boundary seperating pinned and unpinned dynamics as a function of amplitude and frequency.[45] All the above results provide a valuable guidance for understanding the nonlinear properties in magnetic vortices and exploiting the application of magnetic vortices into future information storage devices.

2.2.3 Magnetostatic property of magnetic vortex structure

When we apply a external magnetic field **H** to a ferromagnet, the total magnetic moment would include two parts, one is the internal magnetization and the other part is from the external field. Therefore, the total magnetic moment could be described by

$$\mathbf{B} = \mu_0(\mathbf{M} + \mathbf{H}) \tag{2.2.1}$$

Where μ_0 and $\mathbf{M}$ are the permeability of vacuum and magnetization respectively.

When an external field is applied to a ferromagnet, the magnetization would align along the field direction. However, when the external field is removed, part of the magnetization alignment keeps remained because of the demagnetization field. Thus, the magnetization would increase and finally reach a constant value with the increasing of external field. The field corresponding to the beginning of the constant value is named saturation field. Then, if the external field is decreasing gradually, the change of magnetization would form a different curve. Moreover, when the field reduces to zero, the magnetization is not zero. This value of magnetization at zero field is remanence. According to this, the change of magnetization as a function of the external field would produce a magnetic hysteresis loop.

The hysteresis loop in a magnetic vortex structure has been investigated both theoretically and experimentally. Cowburn et al. studied the hysteresis loop of submicron circular Supermalloy ($Ni_{80}Fe_{14}Mo_5$) arrays with various diameters (500-55 nm) and thickness (6-15 nm) employing a highly sensitive magneto-optical measurement technique.[3, 46] Their results indicate that the magnetic vortex structure exists in the nanomagnet with specific diameter and thickness by presenting the typical hysteresis loop shown in Fig. 2.5 for the nanomagnet with vortex nucleation, displacement and annihilation process. The hysteresis loop also shows good agreement with other micromagnetic numerical and experimetnal results.[38, 47–52]

As indicated in Fig. 2.5, the vortex core locates in the center of the circular nanomagnet during zero field. However, the vortex shifts away from the center with the enhancement of external field. The vortex would annihilate when the field reaches the annihilation field and finally form the saturation state (uniform magnetization) with further increase of the external field. Then, a transition state "C" state appears when we reduce the external field

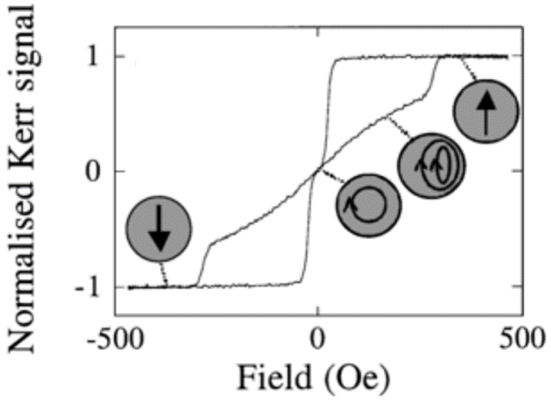

Figure 2.5: Hysteresis loop measured from the nanomagnet with diameter of 300 nm and thickness of 10 nm.[3]

from the saturation state. The vortex core would nucleate again corresponding to the rapid change of magnetization with further reduction of the field.

2.2.4 Magnetic vortex dynamics

The magnetic vortices involve rich behaviors in dynamical resonant regime. Therefore, the study of magnetic vortex dynamics is capable of providing the valuable information required for characterizing and manipulating the ferromagnets with vortex structure in the field varying from spintronics to biomagnetism. In this section, we summarized the related papers from the viewpoints including nonlinear vortex behaviors, low frequency precession mode of vortex core, detection technique, the manipulation of chirality and polarity in magnetic vortices and finally the phase diagram for the resonant frequency of magnetic vortices.

Vortex core gyration

Magnetic vortices are one kind of topological magnetic solitons where the gyration mode of vortex core is a significant characteristic.[33, 53–56] Its properties are governed by the magnetostatic potential of the vortex core. This low frequency precessional mode of vortex

core could be described by the Thiele's equation shown below with assuming the vortex core moves as a rigid body .[57]

$$-\mathbf{G}\times\frac{d\mathbf{X}}{dt}-D\frac{d\mathbf{X}}{dt}+\frac{\partial W(\mathbf{X})}{\partial\mathbf{X}}=0 \tag{2.2.2}$$

Where the gyrovector $\mathbf{G}=-G\hat{\boldsymbol{z}}$ gives rise to the gyroscopic movement of vortex core. Here, $\mathbf{G}=-G\hat{\mathbf{z}}$ is the driving force for the core motion. It could be derived by $G=2\pi qpLM_s/\gamma$, where M_s is the saturation magnetization, and L is the disk thickness. Here, p is the polarization of vortex core ($p=\pm1$ represents up or down polarity of vortex) and q determines the direction of the in-plane magnetization components($|q|$ is the vortex topological charge.) $q=+1$ and $q=-1$ correspond to the vortex structure and antivortex solution, respectively. Besides, $\mathbf{X}$ represents the displacement of the vortex core from the equilibrium position. $D=\alpha\pi M_sL(2+\ln R/R_c)/\gamma$ is the damping parameter with $R_c=0.68{L_e}^{2/3}L^{1/3}$, γ as the gyromagnetic ratio and α as the Gilbert damping parameter. Here, the exchange length L_e is calculated by $L_e=\sqrt{2A/{M_s}^2}$. In addition, $W(\mathbf{X})$ is the potential energy attributing to the harmonic equations of motion. In ideal situation, the magnetostatic potential is parabolic shape where the resonant frequency does not depend on the displacement of vortex core. However, it may deviate from the ideal situation under higher amplitude oscillation or larger displacement of vortex core. At this moment, the higher order terms has to be considered.[13, 58, 59] Thiele's equation provides important information for analyzing and understanding the dynamic properties of magnetic vortices.

Eigenfrequency of vortex oscillated in magnetic disks

The vortex core performs a gyrotropic behavior around its equilibrium position with the frequency of sub-gigahertz range driven by a restoring force from the demagnetizing field and gyrotropic force perpendicular to the velocity.[10, 12, 57, 60, 61] During oscillation, the vortex core rotates with a circular shape trajectory around its balance position in a small

range which has been demonstrated by the calculation or direct observation using x-ray photoemission electron microscopy.[6, 33, 33, 44, 54] Its eigenfrequency could be derived according to the Thiele's equation.

If we consider a sub-micron cylindrical ferromagnetic disk with radius R and thickness L. Here, we assume the thickness of the disk equates to the exchange length of the ferromagnetic material so that the dependence on coordinate along the dot thickness could be neglected. Therefore, we can only consider the magnetization distribution in two dimensional direction. The eigenfrequency of the sub-micron disk is determined by the magnetostatic energy in the disk. If we don't consider the damping of the gyroscopic motion, Thiele's equation could be written as following:

$$\mathbf{G} \times \frac{d\mathbf{X}}{dt} = \frac{\partial W(\mathbf{X})}{\partial \mathbf{X}} \tag{2.2.3}$$

As shown above, the gyroconstant G is expressed by $G = 2\pi qpLM_s/\gamma$. To simplify the analysis, q and p both are taken as 1. Thus, the relationship becomes $G = 2\pi LM_s/\gamma$.

The vortex velocity of a in-plane circular motion of vortex core could be written as

$$\mathbf{V} = \frac{d\mathbf{X}}{dt} \tag{2.2.4}$$

With considering the relationship of angular frequency vector, the vortex velocity could be written :

$$\mathbf{V} = \boldsymbol{\omega} \times \mathbf{X} \tag{2.2.5}$$

Where $\boldsymbol{\omega} = \omega\hat{\boldsymbol{z}}$. Then, we substitute Eq. 2.2.4 and eq. 2.2.5 into the left part of Eq. 2.2.3, it becomes

$$\mathbf{G} \times \frac{d\mathbf{X}}{dt} = \boldsymbol{\omega} \times \mathbf{X} = G\omega\mathbf{X} \tag{2.2.6}$$

During the vortex gyration, the vortex core has a small displacement from its equilibrium position ($\mathbf{X} = 0$), the potential energy can be written as

$$W(\mathbf{X}) = W(0) + 1/2\kappa X^2 \tag{2.2.7}$$

κ is the stiffness coefficient, which could be described by $\kappa = \frac{\pi L \xi^2 {M_s}^2}{\chi(0)}$ based on the result from Ref. [62]. ξ ($\xi \sim 1$) represents different magnetic distribution models of vortex. $\chi(0)$ is the initial susceptibility, which is determined by the geometry of vortex such as radius R and thickness L.[62]

By processing the differentiation of Eq. 2.2.7, the right side of the Eq. 2.2.3 would become

$$\frac{\partial W(\mathbf{X})}{\partial \mathbf{X}} = \kappa \mathbf{X} \tag{2.2.8}$$

After that, by substituting the expression of κ to Eq. 2.2.6 and Eq. 2.2.8, it leads to the eigenfrequency of vortex resonance.

$$\omega_0 = \kappa / G = \frac{1}{2} \gamma M_s \frac{\xi^2}{\chi(0)} \tag{2.2.9}$$

Therefore, the eigenfrequency of the vortex oscillation depends on the susceptibility and the gyroconstant G. It further indicates the eigenfrequency of sub-micron magnetic disk is established with the dependence of geometrical ratio of the thickness and diameter of the magnetic dots, which was demonstrated by K. Yu. Guslienko.[33] Furthermore, the eigenfrequency is also affected by geometrical shapes of magnetic dots because of the potential energy modulated by shape. For example, the resonant frequency exhibits a large modulation in triangular type ferromagnetic dots than that of circular dots because of modified confined potential in triangle.[63] In ellipses, resonant frequency for vortex pairs has been observed with the translational modes in sub-gigahertz frequency range.[50, 64, 65]

Nonlinear behavior of vortex core dynamics

In non-ideal behavior, the deviation from linearity is described as the nonlinear effect. So for, considerable theoretical and experimental work has been dedicated to the investigation of the nonlinear magnetization dynamic in nano- or sub-micron structures because nonlinear phenomena is indispensable not only for setting specific performance limits but also for creating novel dynamical behaviors in spintronic devices.[66–68] From the experimental side, one of the most promising findings have been discovered in the high power dynamics of nonuniform ground states, such as a magnetic vortex existing in a ferromagnetic dot.[68]

In the magnetic vortex dynamics regime, there are two typical nonlinear dynamics which have attracted enormous attention. First, when the vortex motion is excited under high amplitude, the magnetostatc potential during higher order terms should be taken account into.[13, 55] On the other hand, it has also been reported the vortex core may become deformed when the velocity of the vortex core reaches a critical value which would attribute to the reversal of vortex polarity [6, 61, 69–72] The inhomogeneities of the materials are necessary to be considered for its influence on the nonlinear behaviors of vortex dynamics.[7, 73–75]

Chapter 3

Device fabrication methods and measurements

3.1 Sample preparation process

The rapid development of the science and technology is driving the fabrication method of the nanoscale and micron-scale electronic devices more simple and effective. All the devices used in this thesis were prepared under the clean room condition. Before preparing the ferromagnetic device, a full 5-inch Si wafer is cut into 10 mm $\times$ 10 mm pieces. After that, the samples are fabricated using several steps of the electron-beam lithography and the lift-off processing of positive electron-beam resists on the silicon substrate. The whole fabrication process is briefly introduced in the following section, as illustrated in the Fig. 3.1. First, the Py layer has been fabricated by EBL and lift-off processing as shown in Fig. 3.1 (a). Then, the insulator layer has been deposited by mini-sputter then performed by EBL and dry etching processes as indicated in Fig. 3.1 (b). Finally, the nonmagnetic layer as the electrodes has been fabricated by repeating the EBL and lift-off processing as indicated in Fig. 3.1 (c). The microstructure is observed with employing the scanning electron microscopy (SEM) after finishing the fabrication process. The SEM images of part of the chained Py devices are shown in Fig. 3.1 (d). The patterned device would be used to measure the magnetostatic and dynamic properties via the microwave probe measurement

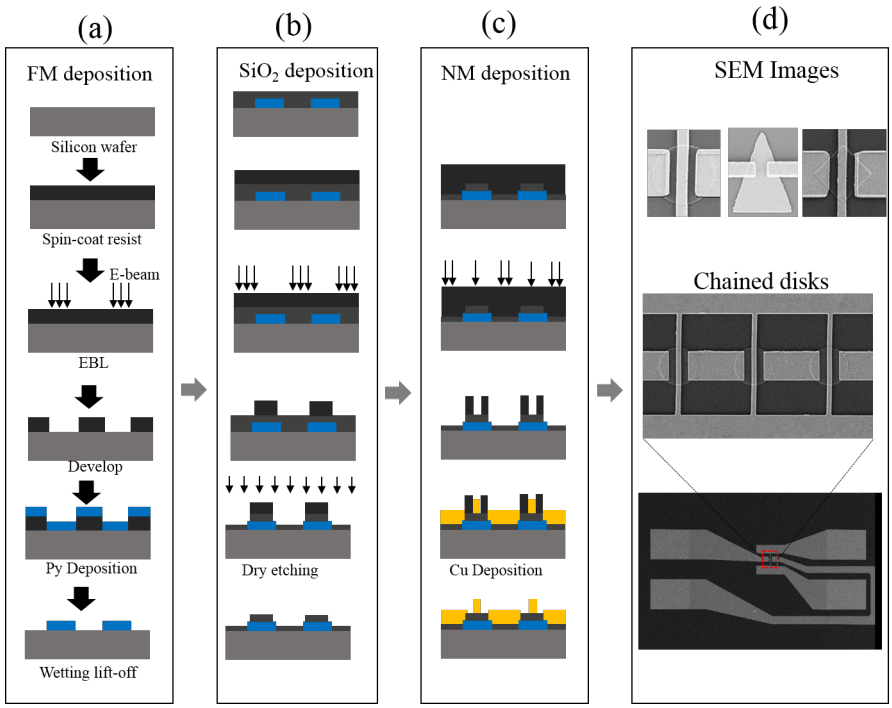

Figure 3.1: Schematic diagram of the fabrication process of the ferromagnetic device

systems. Besides, all the samples used in this thesis were fabricated on the Si substrate.

3.1.1 Substrate cleaning

After cutting into small pieces, the substrate was cleaned by high power ultrasonic. First, the substrate is cleaned by the solution Acetone and Isopropanol(IPA) with ultrasonic for 20 seconds, respectively. Then, after drying under nitrogen gas, the substrate is cleaned with the semiconductor cleaning liquid and milli-Q water for 3 minutes each. Next, the surface condition is checked by using the optical microscope. If the surface is not clean enough, several times cleaning procedure would be repeated for getting clean surface.

3.1.2 Electron beam lithography

Resist coating

The positive resist is coated on the substrate with utilizing a spinner with assistance of the hotplate for pre-baking. The thickness of the resist is adjusted by changing the rotate speed of the spinner. The pre-baking time for the resist is 2 minutes under the temperature of 180°C. Besides, ESPACER is coated on the substrate after the pre-baking in the purpose of preventing the charge-up.

Exposure under EBL

In this thesis, the exposure of all the devices are performed by using the EBL equipment ELIONIX ELS-7800 with a pressure lower than 3.0×10^{-5} Pa. The accelerate voltage used in the lithography are 80 kV. The exposure dose for our positive resist is about 200 $\mu C/cm^2$. The beam currents used in the exposure are 0.2 nA and 4 nA, respectively for the fine pattern and coarse pattern.

Development

The next process after exposure is development. First, the exposed patterned device is immersed into the solvent O-xylene for developing about 1 minute then quickly rinsed in IPA, so that the resist of exposed regions can be dissolved and removed selectively.

3.1.3 Film deposition

In this procedure, the Permalloy (Py) thin film is deposited by using the electron beam evaporator under the vacuum about 3.0×10^{-9} Torr. The deposition speed of Py is about 0.5-0.9 Å/S. Mini sputter is used for depositing the SiO_2 layer which is used for preventing the connection between the Py dots and Cu electrodes. Besides, non-ferromagnetic film Cu is deposited with employing the Joule heat evaporator under the vacuum around 5.0×10^{-6} Pa. It should be noted that the surface of the device is carefully cleaned by the low energy

Ar^+ ion milling with prior depositing Cu in the same chamber. The target material Cu is deposited with the speed of 5 Å/s.

3.1.4 Dry etching

The conduction between the Py disks and Cu electrodes is insulted by depositing SiO_2 film with thickness of 100 nm. After that, EBL exposure would be performed to get periodically space for locating Cu pad to connect the neighboured disks. Then, the exposure regions would be removed by the development. To remove the unwanted SiO_2, reactive ion etching (SAMCO RIE-10NR) would be carried out using CF_4 reactive plasma generated by a RF electromagnetic field under low pressure. After the dry etching process, the surface condition should be examined by SEM to make sure SiO_2 completely removed before starting the next step.

3.1.5 Lift-off method

After film deposition or dry etching process, the lift-off method is performed. The sample with the thin film is bathed in the ZDMAC (N, N-Dimethylacetamide) so that remaining resist together with parts of the target material would be removed. In order to remove them completely, low power sonic cleaning is required for assistance. Finally, we get the patterns in direct contact with the substrate or the underlying layer. However, if the required material is over 100 nm, long time mixer shaking usually is performed with bathing the sample in the ZDMAC solvent.

The device fabrication usually needs several steps EBL exposure together with the lift-off method. After the fabrication procedure is finished, the microstructure would be observed by using the scanning electron microscopy as shown in Fig. 3.1 (d).

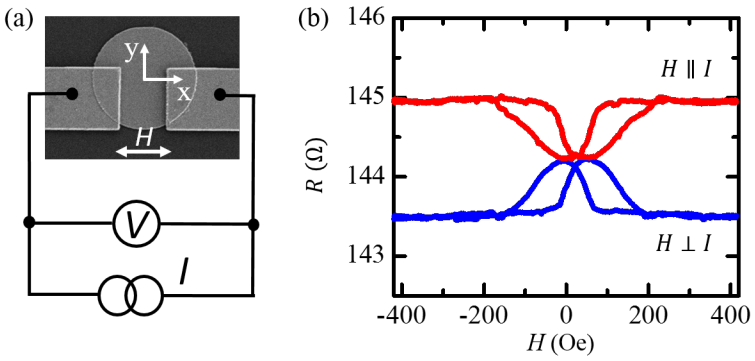

Figure 3.2: (a) Scanning electron microscope image of the fabricated device together with a probe configuration for the AMR measurement device; (b) Representative AMR curves for both $H \perp I$) or parallel ($H \parallel I$) situations.

3.2 Experimental measurement technique

So far, numerous methods have been demonstrated for characterizing the magnetostatic and dynamic properties of ferromagnetic devices with vortex structure. In this section, we would briefly introduce the measurement techniques which were used for the experiment.

3.2.1 Resistance measurement under a external field

Anisotropic magnetoresistance is one of the most important phenomena for ferromagnetic materials. In ferromagnetic metals, the resistance depends on the relative angle between the magnetization and the measuring current, which is called anisotropic magnetoresistance effect (AMR).

The typical measurement for AMR effect is monitoring the resistance change with the lock-in technique using a small AC current through the device or thin film while the external in-plane magnetic field applied perpendicular ($H \perp I$) or parallel ($H \parallel I$) to the measuring current, respectively. In our experiment, the AMR measurement was performed by two-terminal resistance measurement while sweeping the external field under a low bias ac current (55 μA).

Here the AMR measurement setup and representative AMR curves for the chain of circular disks with diameter of 2 μm is shown in Fig. 3.2. As indicated in Fig. 3.2, the device possesses higher resistance for the $H \parallel I$ than $H \perp I$.

3.2.2 RF measurement system

Lock-in measurement technique

Lock-in amplifier is one important and powerful equipment for detecting the tiny electric signal by extracting a signal with a known carrier wave from an noisy environment. The dual phase demodulation (utilization of sine and cosine demodulation at the same time) allows the signal being processed into the data including real and imaginary parts. In this thesis, a two phase lock-in amplifier together with a low noise preamplifier, and two digital multimeter constitutes the main part of the lock-in setup.

The main work principle for lock-in setup is showing here. A input signal could be multiplied with a reference signal provided by the internal oscillator from the lock-in amplifier or an external source, then be integrated over a time period. Thus, the signal which has different frequency with the reference signal would be attenuated close to zero. Only the signal with the same frequency as the reference signal is picked up as a DC signal.

For a sine reference signal and an input waveform $U_{\mathrm{in}}(t)$, the DC output signal $U_{\mathrm{out}}(t)$ could be derived as

$$U_{\mathrm{out}}(t) = \frac{1}{T}\int_{t-T}^{t} \sin[2\pi f_{\mathrm{ref}} \cdot s + \varphi] U_{\mathrm{in}}(\mathrm{s})\mathrm{ds} \tag{3.2.1}$$

Where φ is a phase which could be set on the two phase lock-in amplifier. It should be noted that the detected effective value of voltage (room-mean-square) is introduced a factor $\sqrt{2}$ with the peak amplitude of the output $U_{\mathrm{out}}(t)$ for the sinusoidal modulation.

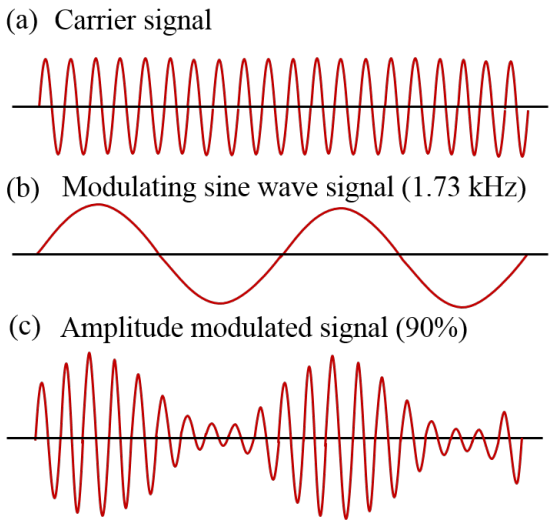

Figure 3.3: (a) and (b) are the microwave wave and low frequency modulating wave signal, respectively; The modulation frequency in the measurement is fixed on 1.73 kHz. (c) The wave signal under amplitude modulation ratio of 90%.

Amplitude modulation of RF field

In the dynamic measurement of vortex core resonance, amplitude-modulated RF signal was used to excite the core oscillation. The RF alternating field was modulated by a low frequency sinusoidal wave where the modulation frequency is 1.73 kHz. In the measurement, the ratio of amplitude modulation is 90% which is also the maximum of the signal generator. The waves for RF signal, low frequency modulation and modulated wave signal with 90% modulation are shown in Fig. 3.3. In addition, the power of the RF modulation signal was adjusted to study the influence of power on the core dynamics of magnetic vortex.

RF measurement system

Dynamic properties of magnetic vortex structures were studied by measuring the electronic response of vortex core while excited by the amplitude modulated RF magnetic field. The detection of electronic voltage as the dynamic response of vortex core is conducted by another circuit.

The equipment used for the electrical measurement of magnetic vortex devices is shown in Fig. 3.4 (a). For the measurement conducted in Chapter 5, the signal generator was employed to generate the RF magnetic field to excite the vortex core oscillation. The electronic voltage was measured using lock-in amplifier under a low frequency modulation signal by sweeping the RF frequency. For the measurement developed in Chapter 6, the signal generator together with the spectrum analyzer was used to detect the second harmonic signal. Two RF probes (ACP40-GS-150 and ACP40-SG-150 produced by Cascade Microtech) were used to connect the sample with the equipment as shown in Fig. 3.4. As shown in Fig. 3.4 (b), an optical microscope was used for precise control of the probe position on the right position of the sample. Besides, in order to minimize the noise from the mechanical change, vibration absorptive cushions are placed under four corners of the the setup stage. The details of the two RF microprobe were indicated in Fig. Fig. 3.4(c). The external static field used in the dynamic measurement is put below the sample and its magnitude is precisely controlled by a voltage source and power amplifier.

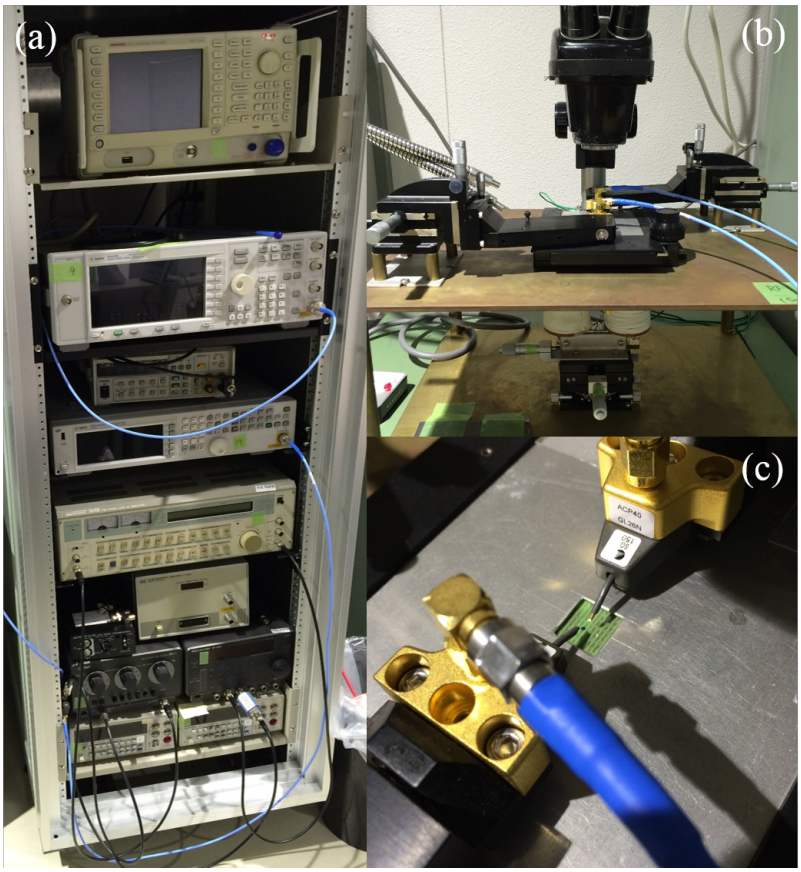

Figure 3.4: (a) Picture of the equipment setup used during the electronic measurement of magnetic vortex dynamics including the signal generator, spectrum analyzer, lock-in amplifier, etc.; (b) The stage for placing the device together with the external field (bottom) and microscope (top, used for setting the device); (c) Picture of the two RF probes used for detection.

Chapter 4

Detection of a vortex nucleation position in a circular ferromagnet using asymmetrically configured electrodes

4.1 Introduction

Study on magnetic vortex structure stabilized in a micron or submicron scaled ferromagnetic disk has been paid of great attention because of its high thermal stability, negligible magneto-static interaction and low frequency dispersion at the resonant state.[3, 5, 8, 38, 52, 76] These outstanding characteristics provide prospective application in high density storage media[77] and functional radio-frequency (RF) devices such as reconfigurable R-F filter[12, 78, 79] and spin torque oscillator [5]. Moreover, the magnetic vortex includes several intriguing fundamental properties such as Bloch point reversal[80] and the critical slowing down of the vortex formation[81]. The vortex structure can be characterized by two important quantity; polarity[8, 52] (the direction of the vortex core, either up or down) and chirality (rotational direction of the magnetization, clockwise (CW) or counterclockwise (CCW))[82]. The effective manipulation and identification of the vortex characteristics are indispensable for the realization of afore-mentioned applications and further understanding

the fundamental property of the magnetic vortex.

So far, numerous reports concerning the manipulation of the vortex polarity and chirality have been developed.[6, 70] In addition, the detection methods for the polarity and chirality have also been developed by several specific measurement techniques such as Magnetic Force Microscope (MFM)[8, 83, 84], Lorentz microscope[85, 86] or Magneto-optical Kerr effect (MOKE)[87]. However, in these techniques, complex experimental conditions such as measurement time, temperatures and sample thickness have to be satisfied. These regulations prevent the systematic and statistical considerations. The lateral spin valve also can detect the vortex chirality.[88, 89] However, the complicate fabrication process and a tiny spin-dependent signal may prevent the fair evaluation of the vortex structure at room temperature. In the method using anisotropic magnetoresistance (AMR) with four terminal electrodes, the device can be fabricated more simply.[90] However, the analysis based on the micromagnetic simulation may prevent the intuitive understanding. Therefore, to further explore the new functionalities of spin vortex and deepen the understanding on fundamental property of the vortex structure, we should seek a relatively simple and reliable method to identify the vortex chirality.

To detect the vortex chirality, in the present study, we use an anisotropic magnetoresistance (AMR) effect, in which the resistance of the ferromagnet depends on the magnetic domain structure. In the ferromagnetic disk, the magnetization reversal proceeds through the nucleation, displacement, and annihilation of the vortex.[38] The nucleation position is known to depend on the direction of the applied magnetic field and the vortex chirality. Since the nucleation of the vortex core corresponds to the phase transition of the domain structure from the uniform magnetization state[81], a significant AMR change is induced by the nucleation of the vortex, especially around the vortex core. Here, we introduce asymmetrically configured nonmagnetic Cu electrodes, which is schematically shown in Fig. 1. Because of the large difference in the resistivity between the ferromagnetic disk and

the Cu electrodes, the electric current flows favorably in the Cu electrode, leading to create an inhomogeneous current distribution. This enables to detect the local domain structure around the bottom side of the ferromagnetic disk. Therefore, when the vortex nucleates from the bottom side, we should observe the large resistance change. On the contrary, the vortex nucleation from the opposite side will be undetectable in the AMR measurement using the same electrode because the current flowing in the top side is so tiny. In this way, we can distinguish the vortex chirality by monitoring the resistance of the local area of the ferromagnetic disk.

4.2 Asymmetrically configured electrodes

We have prepared the sample consisting of a Permalloy (Py) disk, a diameter of 4 μm and a thickness of 40 nm and a pair of the nonmagnetic Cu electrodes, 200 nm thickness. Figure 4.1(a) shows a scanning electron microscope image of the fabricated sample together with the schematic configuration used for the AMR measurement. The Py disk was fabricated by using a conventional lift-off method combined with the electron beam lithography. The Cu electrodes were deposited by a Joule heat evaporator after the surface cleaning of the Py disk by a low energy Ar ion milling. Here, the vertical position of the Cu electrode is shifted by 800 nm from the center of the disk. The electrical resistivity for the Py is 29 $\mu\Omega$cm, much larger than that for the Cu electrode (2.2 $\mu\Omega$cm). The AMR measurement was performed by two-terminal resistance measurement with a low bias ac current of 55 μA. Here, the magnetic field is applied along the horizontal direction, meaning the longitudinal configuration.

The object oriented micromagnetic framework (OOMMF) was employed to calculate the domain structures. The following parameters were used in the micromagnetic simulation. The exchage constant and saturation magnetization of Py (the ferromagnetic alloy used for the device in Chapter 4) are $1.0\times10^{-11} J/m$ and 1 T respectively. Besides, the computational

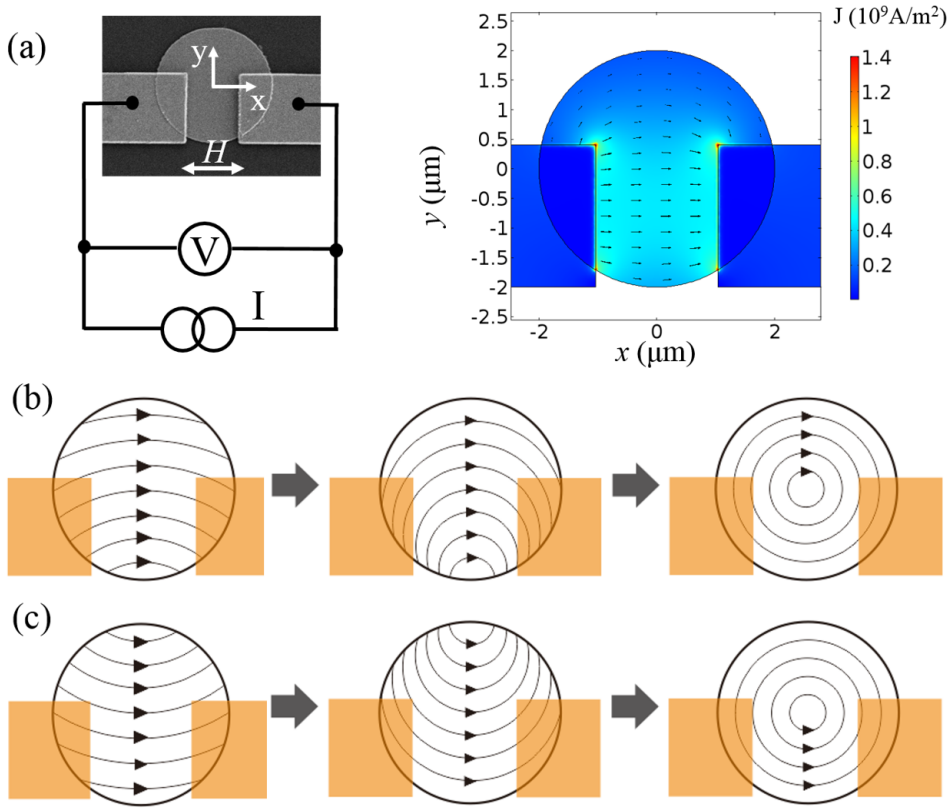

Figure 4.1: (a) Scanning electron microscope image of the fabricated device together with a probe configuration for the AMR measurement and numerically obtained 2-dimensional current-density distribution in a ferromagnetic disk with 4 μm diameter. The magnetic field is applied along the horizontal axis, parallel to the average current direction (longitudinal configuration);(b)Calculated result for the phase transition in the single ferromagnet when the vortex nucleates from the bottom side; (c)Calculated result for the phase transition in the single ferromagnet when the vortex nucleates from the top edge

cell size and damping parameter α are $4 \times 4 \times 40nm^3$ and 0.01. Besides, the size and the thickness of Py disk is in accordance with the real device fabricated in Chapter 4. which are $4\mu m$ in diameter and 40 nm as the thickness. The initial magnetic field is kept same with the AMR measurement.

COMSOL multiphysics was used for calculating the current density distribution in the Py device with asymmetrically configured Cu electrodes. As we know, the electrical resistivity of Py (29 $\mu\Omega$cm) is much larger than that for the Cu electrodes (2.2 $\mu\Omega$cm). The inhomogeneous current distribution has been confirmed in the Py disk. To confirm that the large difference in the resistivity between the Py and Cu makes an inhomogeneous current distribution in the ferromagnetic disk, we have calculated two dimensional distribution of the current density in the AMR device configured similarly to the fabricated device by using COMSOL multiphysics. As shown in Fig. 4.1(b), the current in the Py disk is found to flow mainly in the bottom part of the Py disk. This enables to detect the local domain structure of the Py disk.

4.3 AMR curves at different field range

Figure 4.2(a) shows a representative result of the AMR curve measured at room temperature. In both the forward and backward field sweeps, when the magnetic field is reduced from the saturation state, the sudden resistance change is observed at 10 Oe. These sudden changes correspond to the nucleation of the vortex core in the ferromagnetic disk. After the sudden change, the resistance gradually increases with approaching to the value for the saturation state. Figure 4.2(b) represents the domain structures calculated by OOMMF just after the vortex nucleation with CW or CCW chirality in the forward and backward sweeps. As mentioned above, since the resistance change is dominated by the domain structure in the bottom side of the ferromagnetic disk, the sudden resistance changes observed in Fig. 4.2 indicate that the vortex nucleates from the bottom edge of the disk both in the forward

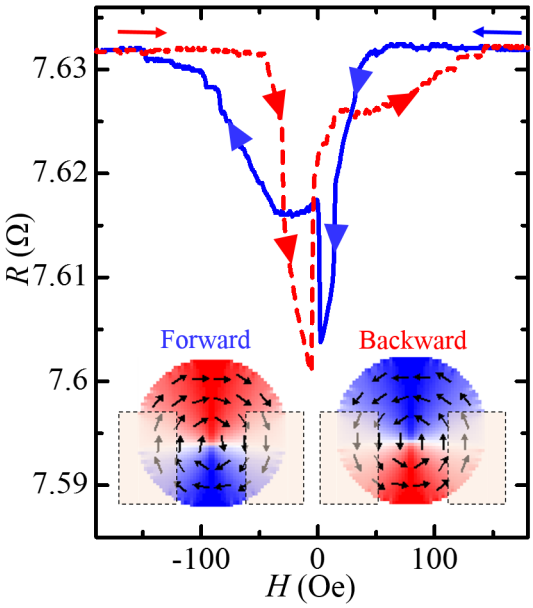

Figure 4.2: Longitudinal AMR curve of the circular disk measured at room temperature. Solid and dotted lines correspond to the forward and backward field sweeps, respectively while the inset shows the numerically calculated magnetization reversal process of the disk for the backward and forward sweeps.

and backward sweeps. Therefore, from Fig. 4.2(b), the vortex chiralities in the backward and forward sweeps are found to be CCW and CW, respectively.

From the aforementioned consideration, when the vortex nucleates from the top side, the nucleation of the vortex may become undetectable. However, as mentioned above, the observed MR curve always involves the sudden change around 10 Oe in the conventional field sweep, indicating the vortex always nucleates from the bottom side. To realize the formation of the reversed vortex, the maximum magnetic field during the field sweep was reduced. This is because the C-state just after the annihilation of the vortex is known to induce the nucleation of the vortex from the annihilated side.[91] Figure 4.3 shows the magnetoresistance curve in the field range -150 Oe $< H <$ 200 Oe. As expected above, in the backward sweep, the MR curve without the sudden resistance change has been observed

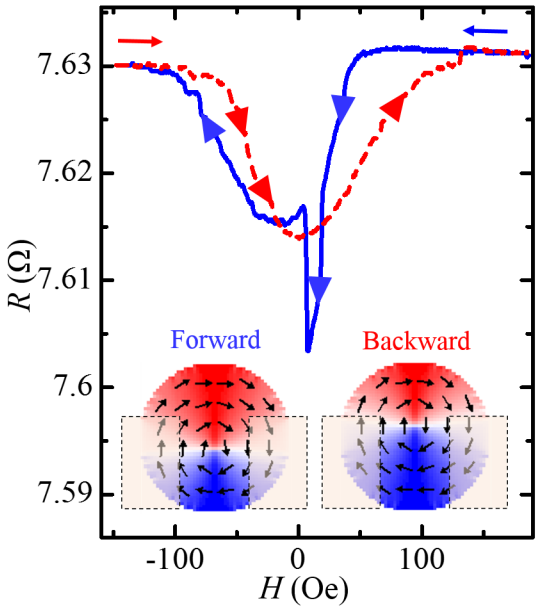

Figure 4.3: Longitudinal AMR curve in the filed range from 190 Oe to -150 Oe. The magnetic field is swept from 190 Oe to -150 Oe and then swept back to 190 Oe. Solid and dotted lines correspond to the forward and backward field sweeps, respectively with the inset of numerically calculated magnetization reversal process of the disk for the backward and forward sweeps.

which means the vortex nucleates from the top side and the chirality should be CW for both backward and forward sweeps. In addition, it should be noted that the small resistance jump has been observed at 132 Oe. This small jump can be understood by the annihilation of vortex from the bottom side. The experimental fact that the small resistance change due to the vortex annihilation has not been observed in Fig. 4.2 is also consistent with the local detection of the domain structure. Thus, we can simply distinguish the vortex chirality from the shape of the AMR curve.

4.4 Probability of appearance of CW and CCW chiralities

By using the simple evaluation method, we extend to evaluate how the vortex chirality distributes with changing the magnitude of the reversed magnetic field H_r. Figure 4.4 shows

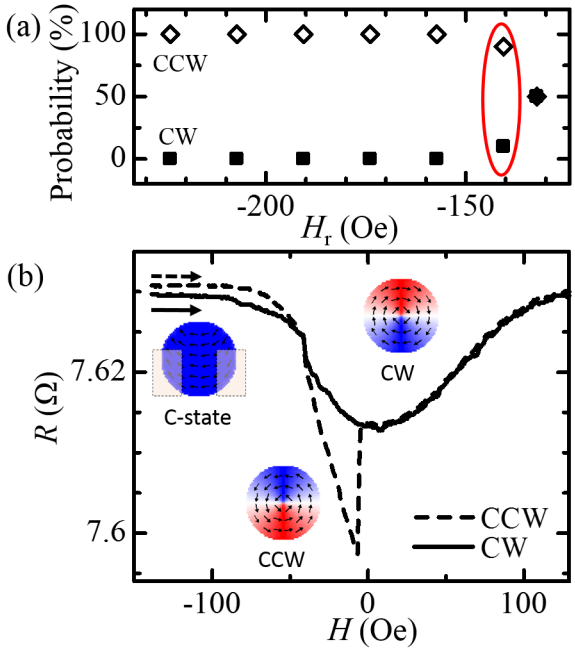

Figure 4.4: (a) Probability of the CW (solid square) and CCW (open squre) vortex formation as a function of the reversed magnetic field. (b) Representative AMR curve for chirality of CW (solid line) and CCW (dotted line) during sweep from -150 Oe to 190 Oe and the C-state domain structure after the annihilation field.

the probability of the formation of CW and CCW chiralities as a function of H_r. Here, the probability at each point was calculated by repeating the AMR measurement for 10 times. It can be clearly seen that the probability of CCW chirality formation increases with increasing H_r and reaches 100% at $|H_r| > 160$ Oe. The probability is 50% at $|H_r| \approx 135$ Oe, indicating that two possible chiralities CW and CCW were randomly formed. Since, in an ideal ferromagnetic disk, the chirality should be randomized because of its symmetric shape, this result indicates that the energy barrier for the formation of the vortex from the bottom side is reduced. To explain this, we consider the influence of slight geometrical asymmetry due to the surface cleaning. As explained above, the surface of the Py electrode underneath the Cu electrode was cleaned by Ar ion milling. This geometrical modification reduces the formation energy of the vortex from the bottom side although the etched depth is less than 2 nm, about 5% of the total thickness. The reasons for the field dependence of the probability may be due to a residual domain structure, namely C-shaped domain structure shown in the inset of Fig. 4.4(b), just after the annihilation. The domain structure of the ferromagnetic disk is known to remain the curling feature when the external magnetic field is not sufficiently large for the saturation of the magnetization. This remaining domain structure tends to form the vortex from the top side. Thus, 50% probability around the annihilation field can be understood by the competition between the non-saturated and the geometrical asymmetric effects.

4.5 AMR curves for symmetric configured electrodes

To obtain further evidence for the advantage of Py disk with asymmetrically configured electrodes, we also fabricated another AMR device consisting of a Py disk with the Cu electrodes located in the central position. Here, the dimension of the ferromagnetic disk is exactly same as that in the previous experiment. Since the Cu electrodes are located in the center of the disk, the vortex formation from both the top and bottom sides can be observed

as a sudden resistance change with the same magnitude. Therefore, the chirality cannot be distinguished from the AMR measurement. To confirm this scenario, we evaluate the AMR curve under the field sweep from -135 Oe to 190 Oe. Since the annihilation field is -130 Oe, we expect that the domain structure is not fully saturated at -135 Oe. Figure 4.5 shows a representative longitudinal AMR curve under the field sweep. The observed AMR curve for each sweep is almost symmetric with respect to the field sweep direction. Importantly, the large resistance jump at 10 Oe due to the vortex nucleation is clearly observed in both sweep. As mentioned above, the C-state domain structure tends to maintain the chirality in the reversed field sweep, the vortex nucleation side in the forward and backward sweep should be opposite each other. However, the observed AMR curve shows the same feature during 10-time repetition of the measurements. This is consistent with the above expectation that the vortex nucleation from the top and bottom sides provides the same contribution in the AMR. Thus, we cannot distinguish the vortex chirality from the AMR curve measured by the symmetrically configured electrode.

4.6 Conclusion

In short, we have studied the AMR curve for a single Py circular disk measured by non-magnetic Cu electrodes with the resistivity much lower than that for the Py disk. We showed that the asymmetrically configured electrode makes it possible to distinguish the vortex chirality in the relatively simple way. By extending this simple detection method, the vortex chirality in the AMR device is found to depend on the magnitude of the maximum magnetic field. The importance of the asymmetric configuration of the electrode is examined by evaluating the AMR device with the symmetrically configured electrodes. This simple and reliable method for the chirality detection may accelerate the development on the characterization of magnetic vortex and its future spintronic application.

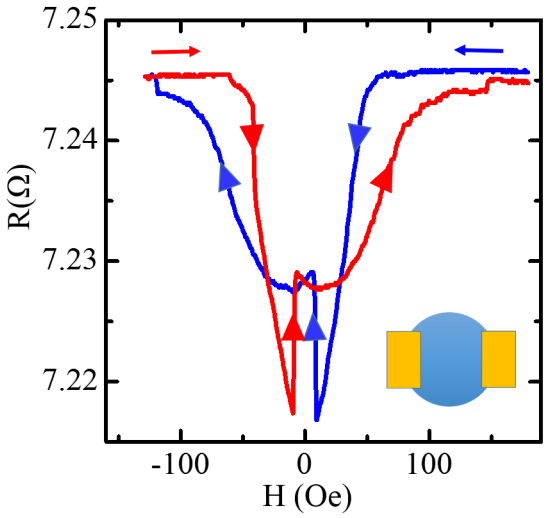

Figure 4.5: Longitudinal AMR curve of the Py circular disk measured by the symmetrically configured electrode. Since the reversed magnetic field is close to the annihilation field, the position of the vortex nucleation may be reversed in each sweep.

Chapter 5

Sensitive detection of vortex-core resonance using amplitude-modulated magnetic field

5.1 Introduction

Understanding and manipulating the dynamic properties of the magnetic vortices stabilized in patterned ferromagnetic structures are of great interest owing to the superior resonant features with the high thermal stability and their flexible tunability. So far, numerous methods for investigating the dynamic properties of the magnetic vortex have been proposed and demonstrated. However, those techniques have some regulations such as spatial resolution, experimental facility and sensitivity. Here, we develop a simple and sensitive method for investigating the vortex-core dynamics by using the electrically separated excitation and detection circuits. We demonstrate that the resonant oscillation of the magnetic vortex induced by the amplitude-modulated alternating-sign magnetic field is efficiently picked up by the lock-in detection with the modulated frequency. By extending this method, we also investigate the size dependence and the influence of the magneto-static interaction in the resonant property of the magnetic vortex.

Ferromagnetic materials with reduced dimensions show unique arrangements of magnetic spins by introducing the geometrically controlled magneto-static interactions. Such patterned domain structures are useful for application in future spintronic devices as well as for understanding of the fundamental spin-related physics.[32, 92] Especially, the magnetic vortex structure, stabilized in a ferromagnetic disk with a diameter less than a micron, has a potential as a unit cell for high density magnetic storage because of negligible magneto-static interaction.[3, 8, 52, 92] In addition, the spin dynamics of magnetic vortices stabilized in micron or submicron scaled ferromagnetic disks are of particular interest because the wide range tuning of the eigenfrequency for the vortex can be realized by its sample dimension[12, 33, 54, 78]. Moreover, its low frequency dispersion at the resonant oscillation with a high thermal stability is another great performance of the magnetic vortex.[5] Therefore, understanding the spin dynamics of the magnetic vortex is an important issue for further developments of the spin-related physics and its application.

The electronic devices based on the spin properties of magnetic elements plays a crucial role not only in scientific research but also commercial produces especially after the discovery of giant magnetoresistance and its application as magnetic read heads.[51, 93–96] A clear understanding of vortex dynamics behaviors helps pave the way for realizing the applications employing magnetic vortices. So far, there are many evaluation techniques being proposed and demonstrated which would be introduced in the following.

Magnetic optic Kerr effect (MOKE) is one of the important tools which has been used for studying the vortex dynamics from the early days.[3, 50, 82, 97–99] MOKE is a sensitive method to study the hysteresis loop, spin excitations of thin film or patterned arrays by the assisting of polarized light and external field.[97] However, the spatial resolution is limited by the wave length of the laser beam, typically sub-micron range.

Time-resolved soft X-ray microscopy is widely used to image the magnetization dynamics of ferromagnetic vortices.[11, 56, 69, 70, 100–102] Time-resolved X-ray microscopy allows

the direct observation of magnetic vortex core switching with employing a field pulse in several picosecond scale which enriches our knowledge on vortex core dynamics with the direct experimental evidence.[69] It also achieved in revealing the asymmetric formation of vortex states in Py nanodisk on account of the high resolution of magnetic transmission soft X-ray microscopy.[102] However, this kind of experiment is only carried out under the limited conditions because of the large scale facility.

Apart from the direct imaging technique, the electrical transport measurements for studying the vortex dynamics is also extensively employed. Among them, homodyne measurement can sensitively detect the resonant properties of magnetic vortices even in a single disk.[101, 103–110] The resistance of the ferromagnetic devices is monitored using the bias-Tee and lock-in technique. The resonant frequency could be distinguished as a resonant peak/dip resulting from the absorbtion when the frequency is consistent with the eigenfrequency of magnetic vortices. The origin of this detection method lies in the AMR effect where the resistance of the ferromagnetic dots is different with the relative angle between the magnetization and applied current. But its analysis is complicated because of the coexistence between the Oersted field and spin-transfer torque. In addition, the monolithic radio-frequency (RF) measurement schemes used in the homodyne electrical techniques regulate the situation of vortex excitation and prevent the detailed study of the dynamic characteristic. Sugimoto et al. developed another homodyne detection technique using two independent RF currents flowing in the excitation and detection circuits.[109] However, the RF current flowing in the detecting circuit may affect the vortex dynamics because the frequency of the detecting current is close to the resonant frequency.

Another electrical measurement is transmission impedance measurement by detecting the S_{11} signal using a vector network analyzer.[63, 111] It enables the detection of translational resonant motions of magnetic vortices. High frequency impedance measurements of a coplanar wave guide or microstrip line with nanomagnets using network analyzer enable

to detect the translational resonant motions of the magnetic vortices.[63, 104, 106] However, because of the sensitivity of the inductive coupling, approximately 1000 nanomagnets are required for detecting the vortex dynamics which enhances the difficulty of fabrication process. Based on regulations of previous evaluation methods for vortex core dynamics, a sensitive lock-in detection method for the vortex dynamics has been demonstrated by using an amplitude modulated RF magnetic field to excite the vortex resonance.

5.2 Configuration of chained device and setup

Figure 5.1 shows the schematic device structure for our measurement setup together with a scanning electron microscope image of part of the patterned circular disks. The sample consists of a chain of 40-nm-thick Permalloy (Py) dots connected by 200-nm-thick Cu pads and a periodical Cu electrode on the Py disks. Here, the number of the dot is 50, much smaller than that for network analyzer measurement.[106] The electrical connection between the Py dot and Cu electrode is insulated by a patterned SiO_2 film whose thickness is 100 nm. The Py disks with diameters varying from 2 μm to 4 μm were fabricated by using a conventional lift-off method combined with the electron beam lithography. The Cu electrodes were deposited by a Joule-heat evaporator after the surface cleaning of the Py disk by a very low energy Ar ion milling. The electrical resistivity for the Py is 30 $\mu\Omega$cm, much larger than that for the Cu electrode (2.0 $\mu\Omega$cm).[112] The anisotropic magnetoresitance (AMR) measurements under the magnetic field with the various direction were performed by two-terminal resistance measurement of 10 μA. For the vortex dynamics measurement, the static magnetic field is applied along the horizontal (x) direction where the vortex core is shifted along y direction.[86] The resonant motions of the vortices are excited by injecting the RF signal into the Cu periodical electrode. The dynamic response of the vortices under the RF magnetic field with sweeping the frequency is monitored by measuring the voltage of the chain of the disk through the AMR change, as explained below.

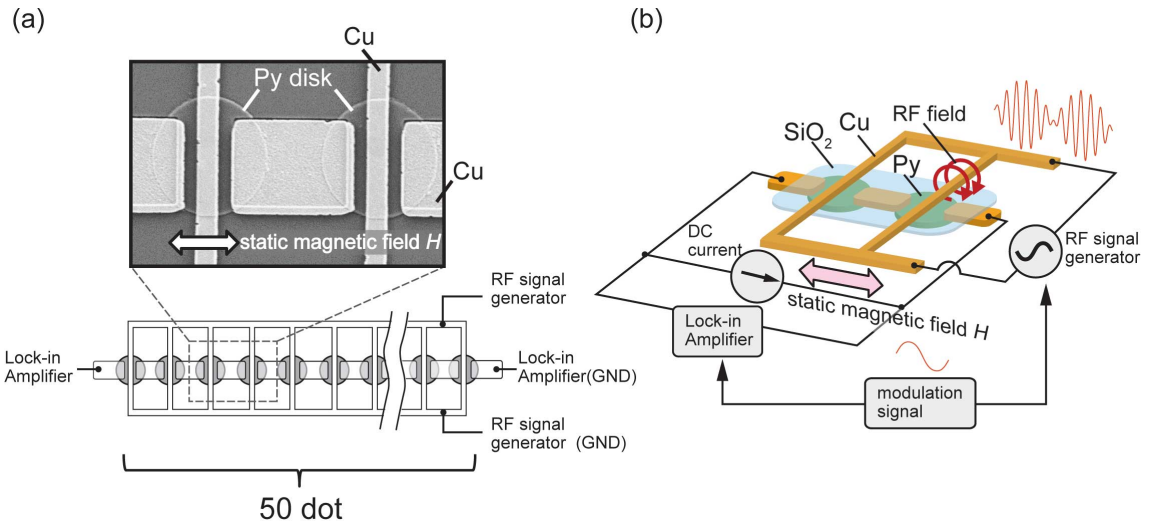

Figure 5.1: Schematic illustration of the proposed device structure for the sensitive detection of the vortex dynamics together with a SEM image of the fabricated device consisting of the chain of 50 Permalloy disks with Cu electrodes. During the measurement, an in-plane bias static magnetic field is applied parallel with the chain of Py disks. The amplitude modulated RF field is injected by flowing on the circuit of periodically patterned Cu electrode which locates on the top of the Py disk with an insulation layer of SiO_2. The voltage change is monitored by another separated circuit combining the lock-in measurement system.

5.3 AMR distribution as a function of core position in the circular disk

Figure 5.2(a) shows the longitudinal and transverse AMR curves for the sample with the diameter of 2 μm. In the measurements, the magnetic field does not exceed the annihilation field 200 Oe, meaning that the vortex core is located in the disk during the measurement. As shown in Fig.5.2(a), the field-dependence of the resistance is well fitted by the parabolic dependence. Here, the parabolic curve in the longitudinal AMR shows the horizontal shift. This is because the Cu electrode has a vertical offset from the center of the disk. By changing the direction of the magnetic field with assuming the linear field dependence of the core position under the low magnetic field, we obtain the core-position dependence of the resistance as shown in Fig.5.2(b).

To mathematically describe the position dependence of the resistance, we focus on the two-fold rotational symmetry originating from the anisotropic magnetoresistance. Moreover, the resistance change due to the vortex core displacement along the x direction should be smaller than that along the y direction because the core displacement along the x axis is partially smeared out by the Cu pads. These features are surely confirmed in the experimental results. From these considerations with parabolic dependence of the resistance change on the core position shift, we found that the resistance change (from the origin (0, 0)) $\Delta R(x, y)$ as a function of the two dimensional core position (x, y) can be given by the following equation.

$$\Delta R(x,y) = \Delta_{\mathrm{AMR}} \left(\left(1 - \alpha \left(\frac{x}{r} \right)^2 \right) \frac{(y - y_{off})^2}{r^2} - \left(\frac{x}{r} \right)^2 \right) \tag{5.3.1}$$

Here, Δ_{AMR} is the AMR change induced by the core displacement from the center to the position under magnetic field 100 Oe along the x axis. r is the displacement of the vortex core due to the application of the magnetic field 100 Oe along the x axis and α is the correction factor introduced by taking account of the influence of the Cu electrode for

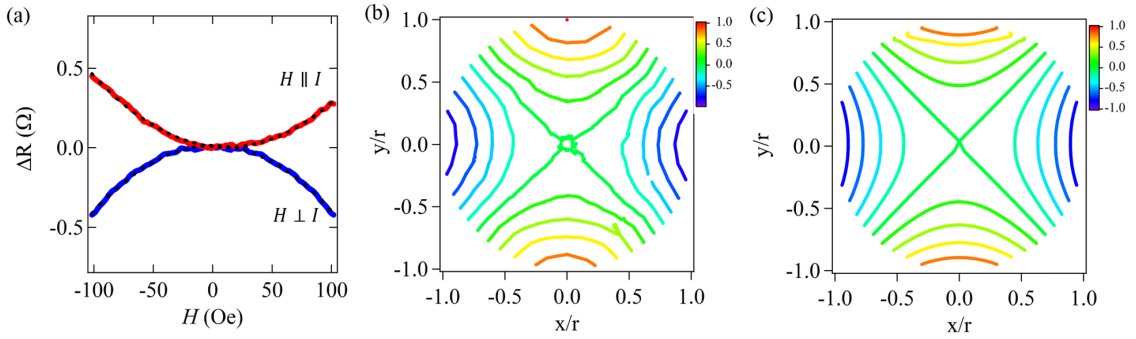

Figure 5.2: (a) Longitudinal and transverse AMR curves for the chain of the Py disks with 2 micron diameter. The AMR was measured using the traditional probe configuration for both $H \perp I$ and $H \parallel I$, respectively. (b) Experimentally obtained resistance change (normalized) as a function of the core position. The AMR curve of the device was detected with changing magnetic field directions. Since the magnitude of the magnetic field is smaller than the annihilation field, we assume a linear field dependence of the core position.(c) Calculated position dependence of the resistance change from the origin (0, 0) based on Eq. (1) with α=0.05.

flowing dc current in the Py. When the core is shifted to x direction from the center, the asymmetry with respect to the electrode increases. In such a situation, since the average y component of the magnetization becomes non zero, the resistance change due to the core displacement along y axis decrease compared to that at x=0. Thus, the position dependence of the resistance is affected by the electrode. By fitting the experimental result shown in Fig. 5.2(b) to Eq. 5.3.1, the correction factor alpha for the present device is found to be 0.05. y_{off} is the offset due to the vertical shift of the Cu electrode. As seen in Fig.5.2(c), the equation well reproduces the experimental results shown in Fig.5.2(b).

We then consider the average resistance $\langle R(x,y)\rangle$ under the amplitude-modulated RF magnetic field with the static magnetic field along the x axis. The trajectory of the vortex core induced by the RF magnetic field is known to be the circular shape not only in the absence of the magnetic field but also in the in-plane static magnetic field sufficiently smaller than the annihilation field.[33, 63, 100] Therefore, we adapt the following equations as the core trajectory under the amplitude-modulated RF magnetic field.

$$x = \delta(1 + m\cos\omega_{\mathrm{m}}t)\cos\omega_{\mathrm{RF}}t, \quad y = y_0 + \delta(1 + m\cos\omega_{\mathrm{m}}t)\sin\omega_{\mathrm{RF}}t \tag{5.3.2}$$

Here, δ is the oscillation radius of the vortex core and its frequency dependence takes the Lorentzian resonant line shape. m is the modulation ratio and y_0 is the vertical shift of the core position due to the application of the horizontal static magnetic field. ω_{m} and ω_{RF} are the modulation and RF frequencies, respectively.

The induced voltage can be calculated by substituting Eq. 5.3.2 for Eq. 5.3.1 with multiplying I_{dc}. By using lock-in detection technique with ω_{m}, we can pick up only the coefficient for $\sin\omega_{\mathrm{m}}t$ in the ac voltage. Since the experimentally detected voltage $V_{\omega_{\mathrm{m}}}$ in lock-in amplifier is the time average, we obtain the following relationship for the effective resistance R, which is defined by the average ac voltage $\langle V_{\omega_{\mathrm{m}}}\rangle$ divided by I_{dc}.

$$R \equiv \frac{\langle V_{\omega_{\mathrm{m}}}\rangle}{I_{\mathrm{dc}}} = \Delta_{\mathrm{AMR}}\frac{m\alpha}{2}\left(\frac{\delta}{r}\right)^2\left(\left(\frac{\delta}{r}\right)^2 + 2\left(\frac{y_0 - y_{\mathrm{off}}}{r}\right)^2\right) \tag{5.3.3}$$

Here, The 1st term depends on the frequency but does not depend on the vertical shift y_0. The 2nd term depends both on the frequency and the vertical shift. In the comparison between the 1st and 2nd terms, δ/r, which is the relative oscillation amplitude, depends on the input RF power, but, in general, is smaller than 0.1 even at the resonant state[33], However, $(y_0 - y_{\mathrm{off}})/r$ easily exceeds 0.1 by the application of the horizontal static magnetic field. Therefore, the 2nd term is dominant in Eq. 5.3.3. We emphasize that the detected voltage does not include any background signal, which is independent of the oscillation. This indicates that the present modulation method sensitively detects the voltage change due to the vortex oscillation.

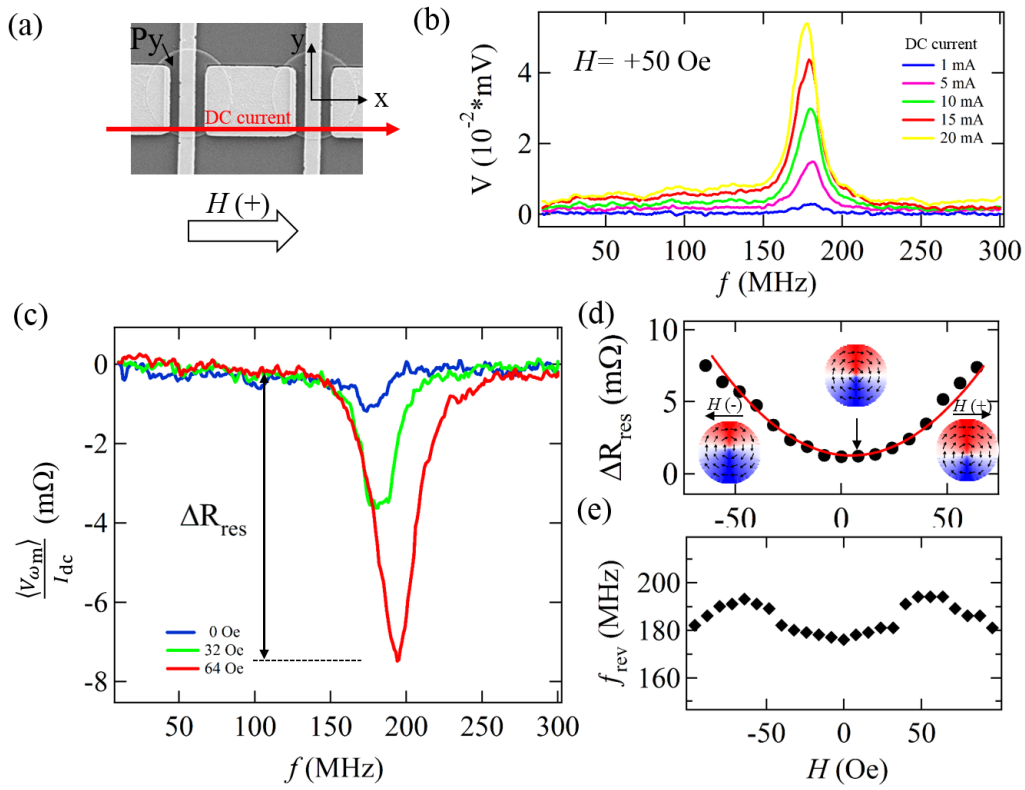

Figure 5.3: (a) Two experimental parameters; DC current $I_{\rm dc}$ for generating the voltage including the resonant signature and static magnetic field H parallel with the dc current (x axis) for moving the core position along y axis. (b) Current dependence of the voltage spectra for the chained disk with the disk diameter of 2 μ m under the static magnetic field of 50 Oe;(c) Frequency dependence of the average resistance change $\langle V_{\omega_{\rm m}}\rangle/I_{\rm dc}$ for the disk with 2 micron diameter for various static magnetic field. The voltage spectra were detected by flowing DC current of 6 mA with sweeping the RF frequency. (d) Field dependence of the resistance change ΔR_{res} due to vortex core resonance. ΔR_{res} is defined as the resistance change between base line and resonance dip. The data is well fitted by a parabolic curve (solid line) based on Eq. (3). (e) The resonant frequency of the disk with 2 micron diameter as a function of bias static field. The frequency shows a weak dependence on the static magnetic field.

5.4 Vortex core oscillation dynamical detection for ladder type circular disks

To demonstrate the proposed technique for detecting the core resonance, we measure the effective resistance $\langle V_{\omega_{\rm m}} \rangle / I_{\rm dc}$ under the RF magnetic field. First, we measured the bias current dependence of the voltage spectra under the static magnetic field of 50 Oe (Fig 5.3(b)). Here, the dc current is varied from 1 mA to 20 mA. As can be seen in Fig. 5.3(b), we do not see any significant change in this current range. The result indicates that the influence of the dc current on the vortex core resonance is negligibly small below 20 mA. This is consistent with the previous theoretical and experimental study.[79, 113] From this consideration, we decided to use 6 mA, which is sufficiently small, in the series of the measurements presented below. Figure 5.3(c) shows the effective resistance as a function of the modulation frequency at H =-40 Oe. A clear resistance dip ΔR_{res} due to the vortex-core resonance is observed. Here, the magnitude of the dip $\Delta R_{\rm res}$ in the spectra is confirmed to increase with the static field. Moreover, as shown in Fig. 5.3(d), the field dependence of $\Delta R_{\rm res}$ is well fitted by the parabolic equation. From the fitting, we find that H_{off} takes a positive value. Since the core displacement due to the application of static magnetic field is known to depend on the chirality, the chirality of the vortex is found to be CW. These experimental facts are highly consistent with the above expectation. We also point out that the resonant frequency is almost independent of the static magnetic field because the core potential is well expressed by the parabolic potential. This is clear evidence that a circular ferromagnetic disk creates a well-defined harmonic potential[63, 114]. Moreover, we also plotted the resonant frequency as a function of the static magnetic field as indicated in Fig. 5.3(e). The resonant field shows the weak field dependence although the signature expected from the ideal parabolic potential should not depend on the magnetic field. The origin of this weak dependence may be related to nonlinear behavior of the resonance frequency and/or the formation of the anharmonic magnetostatic potential in the circular devices

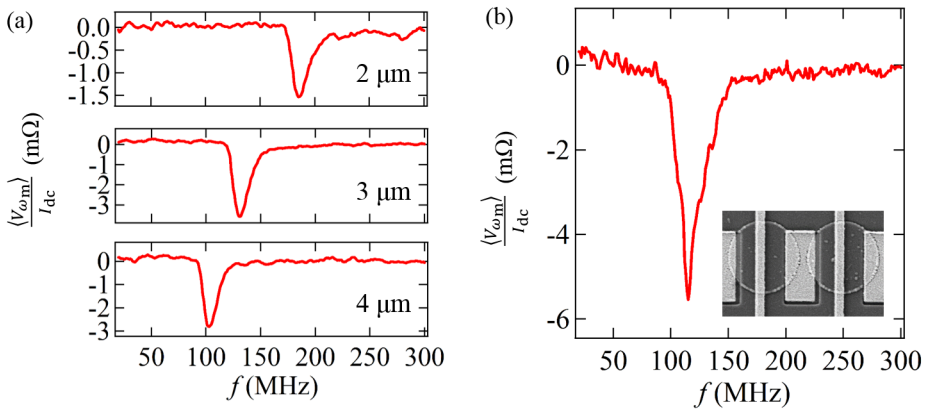

Figure 5.4: (a) $\langle V_{\omega_m}\rangle/I_{dc}$ spectra at H =-40 Oe for various disks with diameters of 2 μm, 3 μm and 4 μm. The measurements have been carried out under the DC current of 6 mA and the RF amplitude of 5 dBm; (b)$\langle V_{\omega_m}\rangle/I_{dc}$ for the magneto-statically couple vortices with the diameter of 3 μm . The inset shows a SEM image of the fabricated device where the edge-to-edge interval is 300 nm.

under a bias static field.[68]

We also perform the similar measurements for the chain of the disk with the different diameter. Figure 5.4(a) shows the spectra of the effective resistance $\langle V_{\omega_m}\rangle/I_{dc}$ at H=-40 Oe for various disk diameters, 2 μm, 3 μm and 4 μm. Here, the annihilation fields of the vortex for 2 μm-, 3 μm- and 4 μm-diameter disks are 200 Oe, 180 Oe and 160 Oe, much larger than 40 Oe. In each spectrum, a resistance dip due to the vortex resonance is clearly observed. The resonant frequencies for 2 μm-, 3 μm- and 4 μm-diameter disks are 180 MHz, 135 MHz and 105 MHz, respectively, showing the monotonic increase with reducing the diameter of the disk. The observed size dependence of the resonant frequency is well reproduced by the numerical simulation using the object-oriented micromagnetic frame network (OOMMF).[115].In addition, we study the vortex dynamics for the magneto-statically coupled vortex system. As shown in the inset of Fig.5.4(b), we have fabricated the chain of the magneto-statically coupled disks. Here, the disk diameter is 3 μm and the edge-to-edge distance between the neighboring disk is 300 nm. Figure 5.4(b) shows the

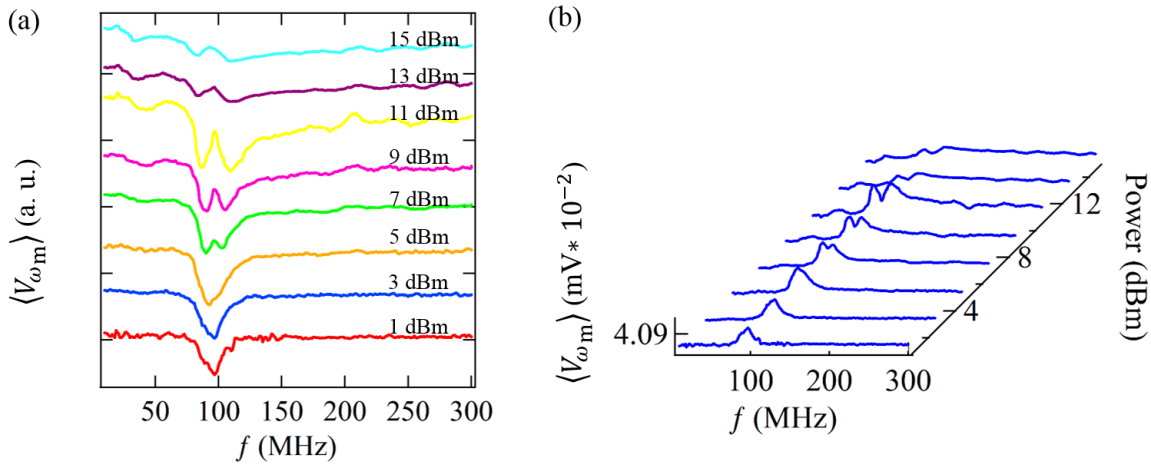

Figure 5.5: Power dependence for the meander type circular chained disks with diameter of 4 μm and edge-to-edge interval of 400 nm.

spectrum of the effective resistance $\langle V_{\omega_m} \rangle / I_{dc}$ for the chain of the coupled vortices. The resistance dip due to the vortex resonance is clearly observed at $f = 120$ MHz, which is lower than that for the isolated disk with 3 μm diameter shown in Fig.5.3(c). This reduction of the resonant frequency is well understood by the magneto-static interaction between the disks[76, 78].

5.5 Vortex core oscillation dynamical detection for meander type circular disks

In this section, the connection of Cu electrodes is changed to meander type and a chain of Py circular disks includes 51 dots.[116] Two devices were fabricated with diameter of $4\mu m$ and edge-to-edge interval of 400 nm and 16 μm, respectively. The dynamic response of vortex core in the chained Py disks is detected by the aforementioned measurement technique with core excited by the amplitude-modulated magnetic field.

The detected voltage as a function of frequency and power dependence of resonant frequency were shown in Fig. 5.5 for the device with the edge-to-edge interval of 400

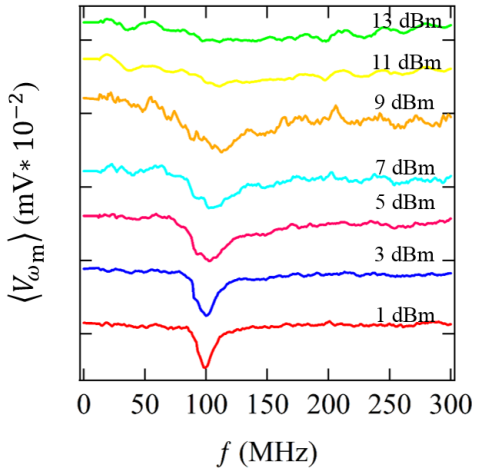

Figure 5.6: Power dependence for the meander type circular chained disks with diameter of 4 μm and edge-to-edge interval of 16 μm.

nm. As indicated in the Fig. 5.5, a clear peak due to the oscillation of vortex core was successfully observed around 100 MHz under low RF power. However, it starts to split to two peaks when the RF power is above 7 dBm. One branch of the resonant peak reduces in frequency while the other branch increases with the increase of RF power. Moreover, the peak becomes much broader from 7 dBm to 15 dBm. The resonant frequency for the device with the edge-to-edge interval of 16 *mum* as a function of the RF power was also provided in Fig. 5.6 The resonant peak broadens with the increase of RF power but it doesn't spilt into two peaks at the high excitation power as shown in Fig. 5.6. Therefore, the results suggest the stronger magneto-static coupling for the device with the edge-to-edge interval of 400 nm is one possible contribution of the splitting of resonant frequency by comparing the data in Fig. 5.5 and Fig. 5.6. Furthermore, the higher order terms of the magnetostatic potential should be taken into consideration for this translational mode when the vortex motion is excited under high amplitude.[13, 55] The above dynamic behaviors enrich our understanding towards the nonlinear dynamic phenomena of magnetic vortices and are anticipated to offer some guidance for the spintronic application of magnetic vortices.

5.6 Conclusion

A sensitive technique for detecting the magnetic vortex core oscillation was developed. A desperately prepared excitation and detection circuits allow us to pick up the vortex oscillation without any background signal. Thus, the sensitive detection of the vortex resonance was achieved. The obtained size and interval dependences of the resonant property show good agreement with the previously reported numerical and experimental results[33, 101]. By extending the present technique to the application of the spatially modulated magnetic field, it is possible to excite the unique high-energy resonant mode[78, 79]. In addition, the detection technique makes the evaluation of vortex core dynamics at strong RF amplitude possible. By employing the meander type configured electrodes, a translational mode with two splitting resonant peaks has been observed when the RF amplitude is higher than 7 dBm. It may result from the magnetostatic interaction or the higher orders terms of the magnetostatic potential during the high amplitude excitation of vortex core motion.

Chapter 6

2nd harmonic detection of nonlinear vortex oscillation in ferromagnets

6.1 Introduction

A magnetic vortex stabilized in the micron or sub-micron sized ferromagnetic disks have been intensively studied because they opened up the possibilities of advanced spintronic applications such as the high density spintronic memory devices, vortex based spin torque oscillators as well as logic operation devices.[3, 5, 8, 51] The attention on magnetic vortices also arises from the numerous advantages including negligible magnetostatic interaction, high thermal stability and remarkably low frequency dispersion at resonant oscillation state.[3, 52, 92] Moreover, the static and dynamic characteristics of the magnetic vortex can be controlled by the geometrical confinement such as the shape of the dot and the ratio between the thickness and the diaster.[33, 76, 78] However, further developments in the experimental characterization of the vortex characteristics, especially for the vortex dynamics are indispensable for the further manipulation of magnetic vortices and promotion of the practical application. So far, numerous methods for evaluating the dynamic properties of the magnetic vortex have been demonstrated.[69, 103, 104, 117]. Especially, electrical

measurement techniques such as homodyne detection and high frequency impedance measurement sensitively detect the vortex motion in small ferromagnetic disks. These electrical techniques are based on monolithic RF measurement scheme. However, this simplification strongly regulates the situation of vortex excitation and prevents the detailed study of the dynamic characteristic.

Recently, we have developed a novel detection method for the vortex dynamics, in which the excitation and detection circuits are electrically separated.[112] This technique provides the sensitive detection and the flexible experimental situations, leading to the detailed study of the dynamic response of the magnetic vortex. However, owing to its detection scheme, it is difficult to measure the core dynamics at remanent state because of the spatially symmetric domain structure. However, the dynamic behaviors at remanent field may provide useful information as guidance for exploring applications based on magnetic vortex. Therefore, in the present study, a novel method has been proposed to study the core dynamics at remanent state by detecting the second harmonic voltage based on the two fold symmetry of magnetoresistance distribution in circular Py disks.

6.2 Development of vortex core resonance measurement technique using 2nd harmonic voltage detection

50 permalloy (Py) ferromagnetic circular disks were prepared on non-doped Si substrate by using the electron beam lithography in the combination with conventional lift-off technique. The circular Py disks with the thickness of 40 nm and diameter of 2 μm were deposited by using electron-beam evaporation equipment under high vacuum. The center-to-center interval between the disks is 4 μm. The Py dots are connected by the Cu pads in order to make a series circuit of the chained disk. In addition, periodic Cu strip lines, which generates microwave magnetic field with high frequency, are formed on each Py disk. Here, the electrical connection between Py disks and Cu electrodes was insulated by the patterned

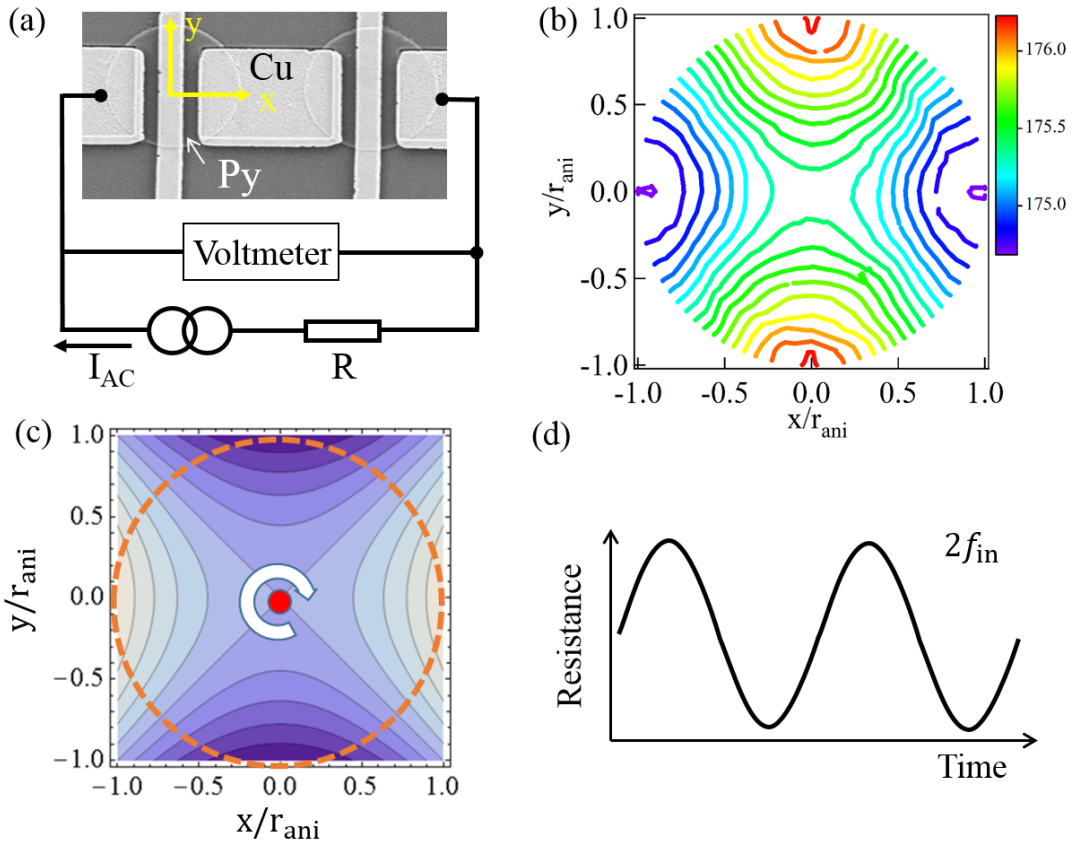

Figure 6.1: (a) Scanning electron microscope image of a part of the fabricated device together with the probe configuration for anisotropic magnetoresistance measurement;(b) The resistance of the circular disks as a function of the vortex core position; (c) and (d) show the schematic illustrations for the mechanism of the 2nd harmonic signal generation due to the circular core oscillation.

SiO_2 film with the thickness of 100 nm.

Here, we explain the detection mechanism of the vortex oscillation at the remanent state. Figure 6.1(a) shows the schematic configuration of the anisotropic magnetoresistance (AMR) measurement together with the scanning electron microscopy image of part of the device. The resistance of the chain of the Py disks as a function of the core position is shown in Fig. 6.1(b). We obtained this plot by changing the magnitude and the direction of the magnetic field. Here, we assume that the vortex core linearly displaces perpendicularly to

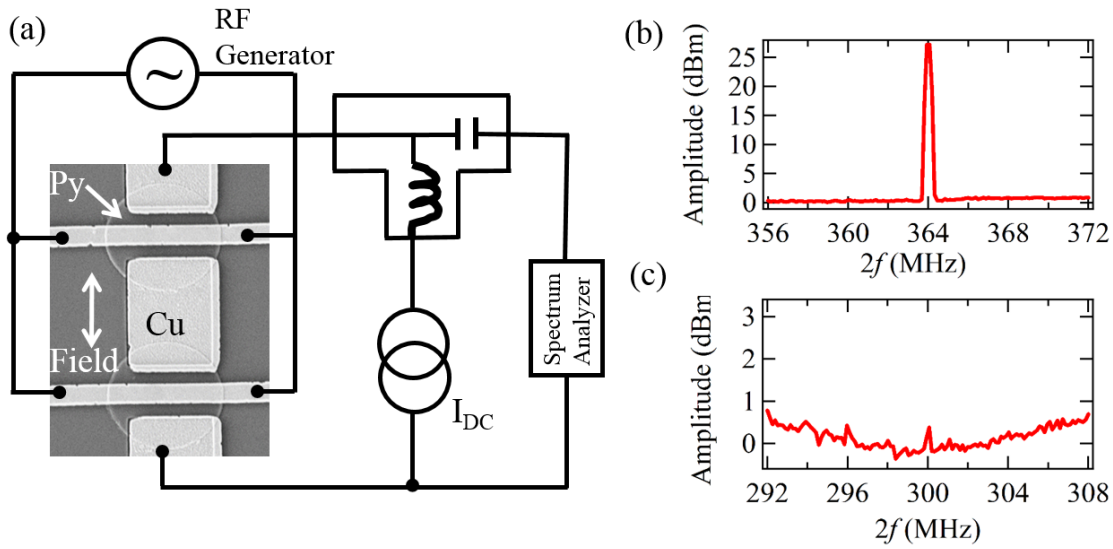

Figure 6.2: (a) Circuit diagram used for the 2nd harmonic signal measurement together with part of the scan electron microscope image of fabricated device. (b) A representative voltage spectrum under the microwave magnetic field with the frequency of 182 MHz. (on-resonant state) and (c) that for the frequency of 150 MHz. (off-resonant state)

the direction of the external field when the applied magnetic field is sufficiently smaller than the annihilation field of the magnetic vortex. [38, 118] It is clearly seen that the resistance change shows the two-fold symmetry. This indicates that when the vortex core has a circular trajectory with the frequency f, the 2nd harmonic resistance change is expected. Therefore, when the dc current flows in the disk, the 2nd harmonic voltage will be induced as indicated in Figs. 6.1(c) and (d). By using spectrum analyzer, we can detect the signal related to the vortex oscillation.

Figure 6.2(a) shows the diagram for the measurement circuit. We flow the microwave current with the specific frequency f_{in} in the periodical Cu electrodes. This induces the voltage change with the frequency $2f_{in}$ under the dc current flow. Especially, when the vortex core is resonantly excited, the induced voltage with the frequency $2f_{in}$ becomes large. However, when f_{in} is far from the resonant frequency of the vortex core, the core oscillation becomes very small. Therefore, by changing the input microwave frequency f_{in}

with monitoring the spectrum of the voltage, we can characterize the resonant motion of the magnetic vortex core.

6.2.1 Frequency dependence of 2nd harmonic spectra

First, to confirm the validity of the aforementioned detection scheme, we measured the spectrum of the voltage induced by the dc current under the microwave magnetic field. Figures 6.2(b) and (c) show the 2nd harmonic voltage spectra for f_{in}=182 MHz and f_{in}=150 MHz, respectively. The Y axis in Fig. 6.2(b) and (c)

We confirmed that a clear voltage peak at f=364 MHz corresponding to $2f_{in}$ in the spectra for f_{in}=182 MHz. However, for f_{in}=150 MHz, only a small peak same as the noise level is observed. This indicated that the resonant frequency of the vortex core is close to 182 MHz.

To evaluate the resonant property more clearly, we measure the spectra for various input RF frequency around 180 MHz. Here, the spectra under the input RF frequency in the range from 150 MHz to 208 MHz was measured every 4 MHz. As can be seen in Figure 6.3(a), the spectra for various input frequency show the resonant feature. From the results, the resonant frequency can be recognized as 182 MHz, where the signal becomes the maximum value. To verify the reliability of the present results, we confirmed the resonant properties of the magnetic vortex by using our previously developed technique.[112] Here, to introduce the spatial asymmetry, we introduce the small in-plane magnetic field with the magnitude of 30 Oe, much smaller than the annihilation field of the magnetic vortex. Since the resonant frequency of the magnetic vortex confined in the circular disk is almost independent of the core position, the resonant property similar to the remanent state is expected. As can be seen in Fig.6.3(c), we confirmed that the resonant frequency of the vortex is approximately 180 MHz, which is consistent with the results in Figs. 6.3(a) and (b).

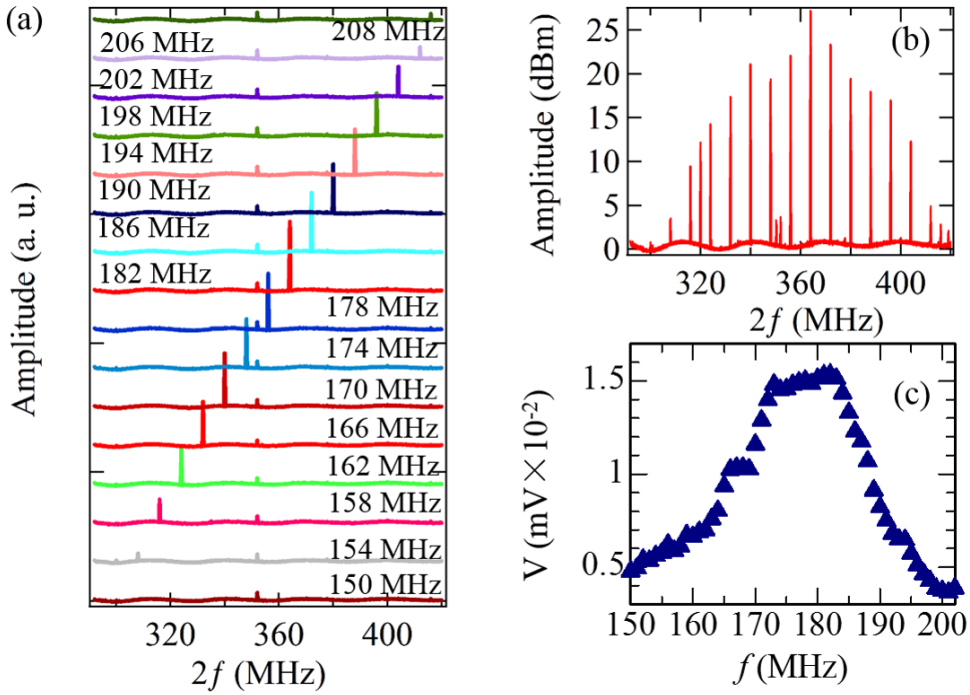

Figure 6.3: (a) Voltage spectra for various input RF frequencies in the range from 150 MHz to 208 MHz. Here, the spectrum was measured every 4 MHz and each spectrum is vertically shifted to clarify. (b) Voltage spectra for various input RF frequencies signals without offset; (c) Frequency dependence of the dc voltage measured by previously developed lock-in technique under a small in-plane magnetic field.

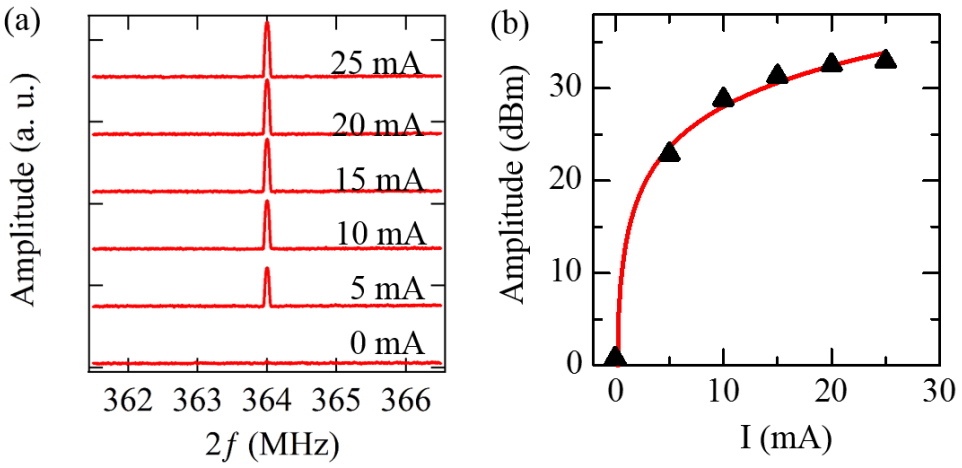

Figure 6.4: (a) Voltage spectra under the microwave magnetic field with the frequency of 182 MHz for various dc current in the absence of the magnetic field. (b) The current dependence of the amplitude of the resonant peak of the 2nd harmonic signal. A solid line is a logarithmic curve fitted to the experimental data.

6.2.2 Current dependence and field dependence at resonant frequency

The dc current dependence of the induced voltage at resonant frequency 182 MHz has also been studied. Since the voltage is linearly proportional to the current, we expect a logarithmic dependence on the dc current in the signal. Figure 6.4(a) shows the spectrum induced by the RF magnetic field with the frequency of 182 MHz for various dc current. The peak magnitude monotonically increases with increasing the dc current. Moreover, as can be seen in Fig. 6.4(b), its dependence clearly shows the logarithmic dependence.

After that, the 2nd harmonic voltage spectra at resonant frequency 182 MHz has been measured under different magnetic field. As can be seen in Fig.6.5, the signal does not show the significant change below 62 Oe both for the positive and negative magnetic field. However, above 90 Oe, the peak amplitude starts to decrease and finally disappears. This is because the core potential deviated from the ideal parabolic shape when the magnetic field is close to the annihilation.[33, 114] When the magnetic field exceeds 120 Oe, the vortex core

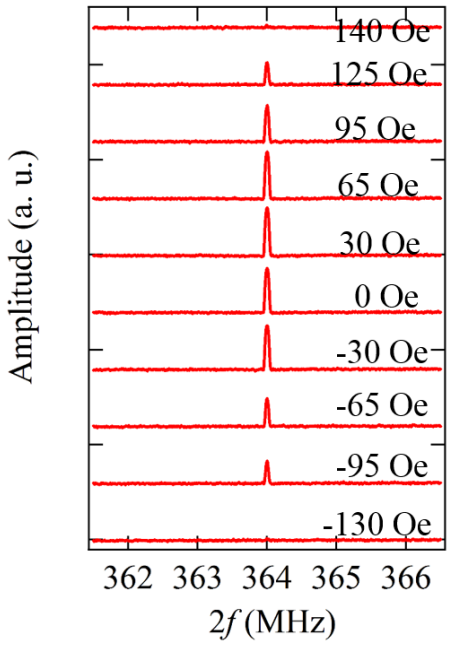

Figure 6.5: Voltage spectra under the microwave magnetic field with the frequency of 182 MHz for various static in-plane magnetic field.

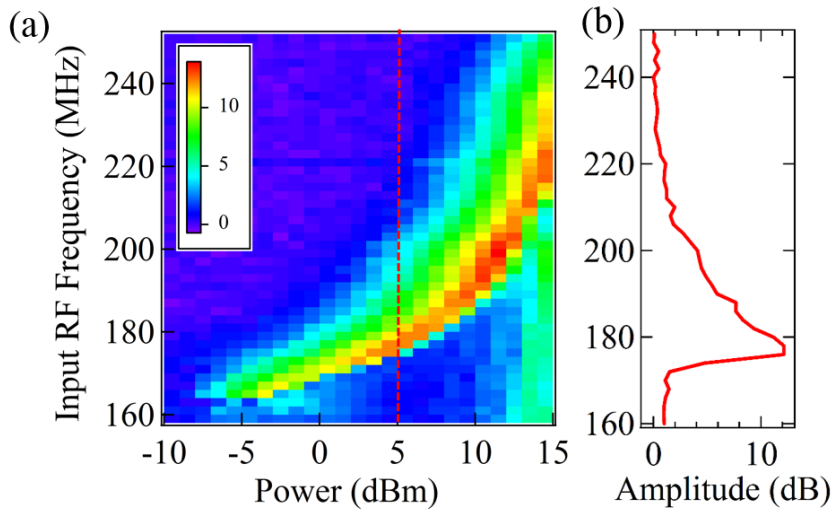

Figure 6.6: Power dependence of the resonance properties of the ferromagnetic circular device at remanent state.

annihilates, resulting in the perfect elimination of the two-fold symmetry in the resistance.

6.2.3 Power dependence of resonant frequency at remanent field

To further check the sensitivity of the 2nd harmonic detection technique, we decreased the numbers of the circular disks from 50 to 10. Then, the 2nd harmonic response of the vortex core at remanent state was evaluated using the spectrum analyzer at various RF frequency and different RF power. As expected, the resonant peak was successfully detected. The obtained spectra were processed into a image plot showing the 2nd harmonic signal as a function of input frequency and RF power in Fig. 6.6. The spectrum representing the frequency dependence of 2nd harmonic signal at 5 dBm is also provided in Fig. 6.6b. As indicated in Fig. 6.6, the resonant frequency increases with the enhancement of the RF power which is deviated from the ideal linear situation. It may attributes to the higher order terms of the magnetostatic potential at high excitation amplitude[13, 55] or the nonlinear behavior contribution when the vortex core has a large displacement from the equilibrium place under high power[6, 61, 69–72].

6.3 Conclusion

To investigate the magnetic vortex core dynamics at the remanent state, we have developed a novel method based on the electrically separated excitation and detection circuits with the spectrum analyzer. The signature of the vortex core resonance is well detected as the 2nd harmonic signal induced by the two-fold symmetric resistance change. The current and field dependence of the 2nd harmonic signal show the features consistent with the previously reported results. The enhancement of resonant frequency of magnetic vortex during remanent state has been indicated at high RF amplitude. This technique may be extended to the higher order frequency generator voltage, faster than the intrinsic precession frequency.

Chapter 7

Magnetostatic and dynamic properties in isosceles triangular and square ferromagnet

7.1 Introduction

Magnetic vortices represent one of the novel structures that form the cornerstone of a series of promising applications including magnetoelectric random access memory[119], microwave signal-processing devices[6, 12, 72, 78, 79], vortex based oscillators[5, 120] or even medical use such as biofunctionalized microdiscs[7]. In addition to the technological interest, there are also interests from the fundamental standpoint towards understanding the fascinating magnetostatic and dynamic behaviors of sub-micron sized ferromagnetic patterns because of their unique properties such as such as the superior thermal stability and negligible anisotropy [3, 8]. Especially, with considering the geometrical effect, magnetic devices with various domain structures and resonant properties could be effectively constructed by choosing specific geometrical shape and tailoring the particle aspect ratio[33, 76, 103]. So far, most of studies on the magnetic vortex have been carried out by employing simple circular ferromagnetic disk [103, 111, 118, 121], several unique features have been reported in the magnetic vortex confined in other shapes. For example, in a ferromagnetic dot with a regular triangle shape, the chirality of the vortex core can be well controlled and its resonant

frequency is strongly modified by adjusting the core position.[63] In a elliptical ferromagnetic disk, an anisotropic field dependence of the core resonant frequency has been reported.[64, 65] Thus, the resonant properties of the magnetic vortex can be flexibly modified by tuning the geometrical shape as well as their dimension.[33, 45] These facts imply that excellent novel properties are anticipated by exploring the magnetic vortex confined in a specific-shaped ferromagnetic dot with tailoring geometrical ratio.

To realize the promising applications based on magnetic vortices, the independent manipulation of polarity and chirality is indispensable. In the last couple of years, it has drawn considerable of attention on developing effective ways to control both chirality and polarity.

In the first place, one of the effective approaches to control the magnetic chirality is the introduction of a slight asymmetry in the magnetic geometry. For example, both Schneider and Kimura's groups have successfully realized the control of chirality by introducing a flat edge to a magnetic disk because the vortex easily nucleates from the flat edge due to the larger demagnetizing field under a static field parallel to the flat edge[85, 91] In addition, Yakata et al also proposed a method to control the chirality in the regular polygons with odd-symmetry structures such as in triangle, pentagons.[83, 84] They succeeded in manipulating the vortex chirality with the MFM image by changing the initialized magnetic field direction. Cambel et al. also achieved the manipulation of chirality in a ferromagnetic nanodot with gap.[122] Another issue to manipulate the chirality is addressed by applying time dependent spatially distributed magnetic field such as field pulse and short bursts, aiming at modulating the remanent state of the ferromagnet.[44, 61, 69, 121] Furthermore, other methods have also been presented based on spin-transfer toque, nano-local spin valve signal, or utilization of C state vortex after expelling the vortex core.[89, 123, 124]

The polarity could be switched by applying a perpendicular static field but the magnitude of the field is quite large.[37] At the same time, defects and thermal agitation may

help to lower the switching field by the means of assisting the Bloch-point inject according to Thiaville's calculation.[80] However, there are also other approaches to effectively reverse the polarity of vortex core by exciting the gyrotropic precession mode of vortex core.[10–12, 33] Guslienko et al. investigated the dynamic origin of vortex core switching in magnetic nanodots by analytical and micromagnetic calculation and their result reveals that vortex core switching is driven by a gyrotropic field which is proportional to the velocity of the moving vortex.[61] What's more, when the vortex core comes to a critical velocity, the polarity of vortex core would reverse to the opposite.[6, 44, 61] Until now, it has been confirmed that vortex core polarity could be efficiently reversed by introducing a spin-polarized current, short bursts of a alternating field, coherent excitation of resonant microwave pulse.[5, 69, 71, 72, 125, 126] In addition, excitation of spin waves could assist the reversal of vortex core polarity attributing to the instability of vortex core.[127–129] During the reversal process of vortex polarity, some anti-vortex structure may appear to contribute the formation of a vortex structure with opposite polarity but it only exists in a very short time.[130, 131]

In the linear response regime, the dynamic property of the magnetic vortex core can be described by Thiele's equation, where the trajectory of the vortex core exhibits a rotational motion around its equilibrium position about sub-gigahertz range.[9–11, 57, 61] The gyration motion of vortex core offers abundant fundamental behaviors because the motion equation of the core is mathematically equivalent situation for the mass point confined in the parabolic potential. Moreover, the characterization of core motion including the non-linear regime may deepen the understanding towards the basic property of vortex core and pave the way for improving the performance of the spin-based nanoelectronic devices using a magnetic vortex.[10–13] Two or more vortices are known to be stabilized by modifying the shape of the ferromagnet, where further intriguing properties and new possibilities for the application are anticipated[50, 64, 65, 132]. Up to now, experiments on magnetic structure with two vortex

has been limited to ferromagnetic ellipses and the resonance frequencies of the vortex pairs are quite close possibly due to the complete symmetry structure or weak coupling between the vortex pairs[50, 64]. However, evidence for control of two vortices in isosceles triangle and its dynamic results is still lacking.

In this chapter, for seeking new functionalities of magnetic vortex, the chirality of vortex core numbers in an isosceles triangle ferromagnet at remanent state under various directions of initialized in-plane magnetic field has been demonstrated. Moreover, the core dynamics of the magnetic vortex confined in both isosceles triangle and square-shaped ferromagnetic dot have been studied.

7.2 Static and dynamic investigation in isosceles triangle

The exploitation of high density magnetic memory and other spin-based devices requires effective control and well understanding on both the magnetostatic and dynamical properties of the magnetic vortices. In this section, magnetic force microscopy imaging has been employed to study the magnetic structure of isosceles triangular dot and two vortices have been successfully created by applying a specific initialing in-plane magnetic field. Furthermore, the resonance dynamic properties of the stabilized vortices in the isosceles triangular dots have been investigated with employing the transmission impedance technique. These results have revealed an effective manipulation of the numbers of the vortices in addition to the chirality, demonstrated large variation of resonant frequency in the two vortices states with dependence of the magnetic field resulting from the strong magnetic coupling. Besides, the experimental results are reproduced by conducting micromagnetic simulations. What's more, the numerical results further confirmed the two oscillation peaks corresponding to the low frequency mode and high frequency mode of the bottom vortex. Both the experimental and simulation results suggest a possible approach to develop the reconfigurable

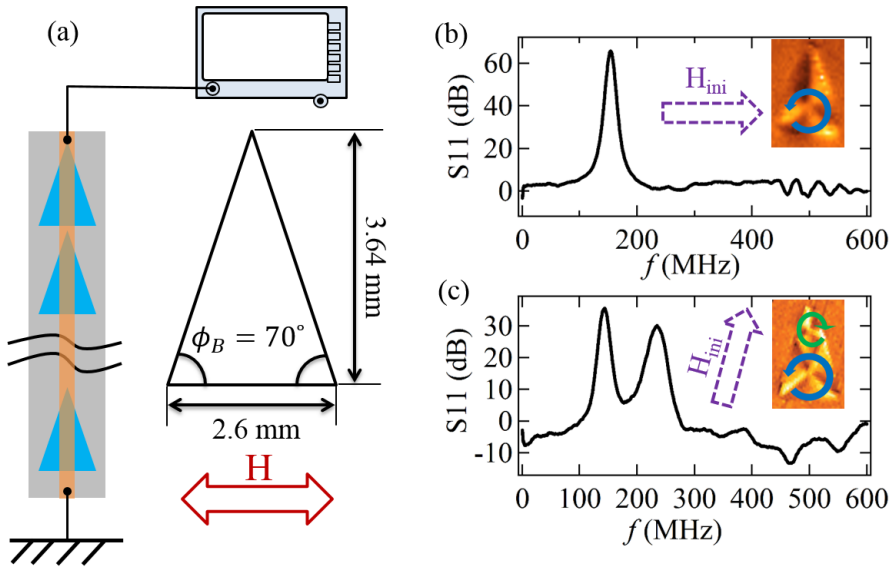

Figure 7.1: (a) Sample size for the isosceles triangle used in the measurement and the schematic setup for the impedance measurement employing the network network analyzer. (b) and (c) show the representative spectra of S_{11} signal of frequency dependence observed at zero field $H = 0$ as a function of horizontal magnetic field H for isosceles ferromagnetic triangle with (b) Single vortex (c) double vortices, respectively. Before the measurement, the initial magnetic field with specific directions was applied in order to obtain the single vortex and double vortices domain structure. The S_{11} signal spectra were obtained by the impedance measurement indicated in (a) employing the Vector Network Analyzer.

logic and microwave assisted filter devices. Besides, the conducted micomagnetic simulation supports the dynamic behaviors of the device and offers extensive information about the low frequency mode and high frequency mode as the dominant role in the dynamics.

7.2.1 Configuration of the fabricated device

The patterned isosceles triangular Py dots were prepared using the electron beam lithography combining with traditional lift-off method. The Py film with the thickness of 40 nm was deposited using the E-gun evaporation. The sample consists of a one dimensional chain with 1000 isosceles triangular dots which are connected by Cu line. The base length of the sampled used in the experiment is 2.6 μm and the base angle ϕ_B is 70 deg, as shown in

Fig. 7.1. A single Cu strip line, 500 nm in width and 200 nm in thickness, has been fabricated also by the electron-beam lithography and was placed on the center of the Permalloy dots for detecting the dynamic response of the magnetic vortices. The dynamic properties of the magnetic vortex in the triangular dots have been evaluated by performing the 1-port transmission impedance measurements (S_{11}) using the Vector Network Analyzer as schematically shown in Fig. 7.1. The position of the vortex core was controlled by adjusting the external magnetic field. The vortex chirality in the triangle dots was set to CCW by using an initialized in-plane magnetic field.

7.2.2 Phase diagram of the vortex domain structure under various initialized field directions

In order to characterize the remanent domain structure in the isosceles triangular Permalloy (Py) dot, magnetic force microscopy (MFM) was used for the magnetic imaging evaluation. An initialized in-plane magnetic field with different directions was applied before starting the measurement. After removing the magnetic field, the magnetic structure of the sample were measured using MFM. Fig. 7.2 shows the phase diagram of the remanent domain structures as a function of the direction of the initialized in-plane field. Hereafter, the angle between the direction of the magnetic field and the baseline of the isosceles triangle is referred as ϕ_{H}. As shown in Fig. 7.2, it could be found that when the angle ϕ_{H} is between -20° and 20°, which means the external field is parallel with the positive x axis direction or possessing a small angle with the x axis, the Py isosceles triangle exhibits the single vortex structure, which is similar to the domain structure of the regular triangle[133]. In addition, the chirality of the vortex shows clockwise (CW) as indicated in Fig. 7.2. However, when the field direction becomes steeper, the domain structure of the isosceles triangle transforms to double-vortex structure. The double vortices show opposite chiralities with each other. The chirality of the up vortex is CW while the bottom one shows counter-clockwise (CCW) domain structure in the range of ϕ_{H} 20° to 90°. However, the experimental result also

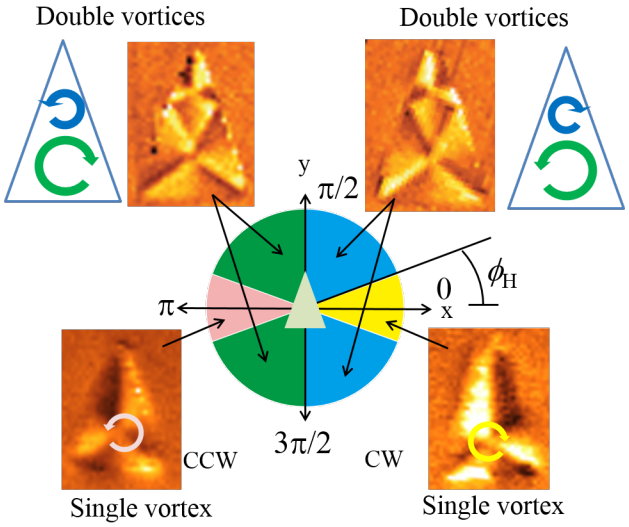

Figure 7.2: The phase diagram of nucleation vortices and MFM images in the isosceles triangular dot with various in-plane initialized field angle ϕ_H. ϕ_H represents the angle between the initial magnetic field direction and positive horizontal direction. The MFM images show the domain structure after initialization. The chirality of the vortex state is labeled in the MFM images. X axis and Y axis are the horizontal and vertical direction respectively.

indicates that chiralities for the double vortices transforms into the opposite direction when ϕ_H exceeds 90°. Besides, the isosceles triangle has single and double-vortex domain structure under ϕ_H range of (160°, 200°) and (200°, 340°), respectively. The chirality reverses when the external field changes to the opposite direction. Therefore, it obviously indicates that the domain structure of the isosceles triangular Py device shows strong dependence of the initialized external magnetic field. These results also suggest that both the vortex chirality and the number of the vortex cores in the isosceles triangular dot could be effectively and simply controlled only by adjusting the direction of initialized in-plane magnetic field.

The domain structure after applying the magnetic field is governed by the competition of the formation energy among various domain structures. When the angle ϕ_H locates in the range 20° to 160°, the nucleation of the up vortex in the magnetic structure may result from the lower formation energy of the double vortices comparing with single vortex in

combination of the strong demagnetization field induced around the vertex angle. In other words, the double vortex magnetic structure in the isosceles triangular Py dot is more stable when the angle ϕ_H is around 90° or 270°, respectively.

7.2.3 AMR measurement of the ferromagnetic Isosceles triangle

As shown above, the magnetic domain structure with two vortices in the isosceles triangular dot was confirmed via the MFM images. However, it is not enough by the realization of domain structures. AMR measurement is another approach to characterize the properties of ferromagnetic devices by electrical measurements which attributes to the significant AMR change during the vortex core nucleation or annihilation induced by the phase transition of the domain structure.[81, 91] Therefore, in order to gain further insight into magnetostatic properties of the isosceles triangular dot, the AMR detection of the isosceles triangle has also been performed under different directions of external magnetic field.

The AMR was measured by using traditional two probes configuration. The representative spectra for the single isosceles triangle under external field direction of ϕ_H of 0° and 70° as plotted in Fig. 7.3. For both situations, the ac current was flowing along the direction of ϕ_H= 0°. As seen in Fig.7.3,the resiestance was monitored first by sweeping the field from negative to positive direction (blue curve) then sweeping back (red curve). It can be seen in Fig. 7.3 (a), the resistance jumps around 50 Oe and -50 Oe have been obtained for the situation H||I which probably result from the vortex nucleation from the uniform domain structure with the increase of positive magnetic field. The only resistance jump during the field sweep is supposed to correspond to the single vortex structure shown in the MFM image of the isosceles triangle. On the other hand, when the external filed is along the direction of ϕ_H=70°, two significant resistance jumps appear round 45 Oe and 55 Oe for both sweep from negative to positive direction and from positive to negative direction. As we know, a significant AMR change is induced by the nucleation of the vortex. The AMR

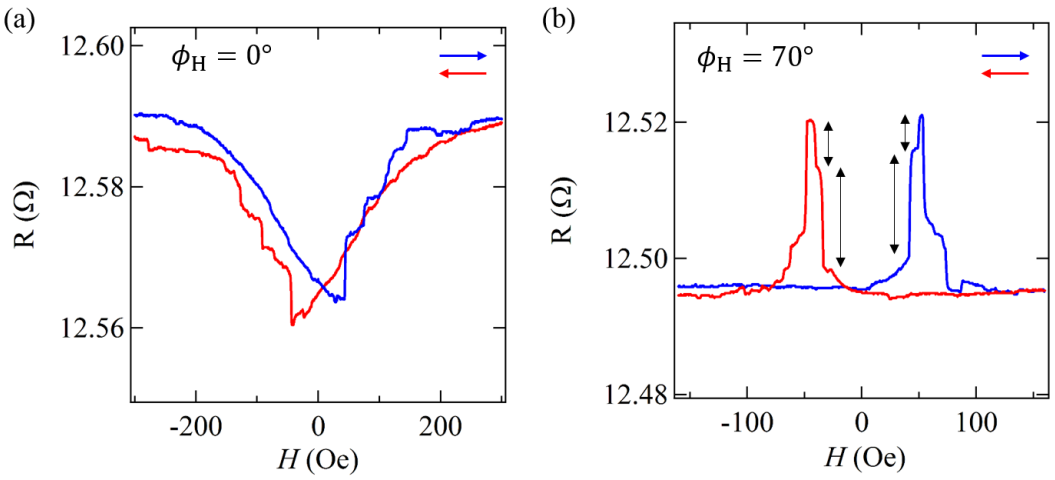

Figure 7.3: AMR curves for the single isosceles triangle under the external field direction ϕ_H of 0° and 70°, respectively.

curves in Fig. 7.3(b) suggest the nucleation of two vortices during the field sweep which extensively confirmed the two vortices structure obtained in Fig. 7.2 when ϕ_H locates in 20° to 160°. Therefore, the AMR curves obtained under difference magnetic field directions exhibit good agreement with the domain structure from the MFM detection.

7.2.4 Dynamic measurement of the Isosceles triangle based on impedance measurement

To further explore the new functionalities of spin vortex, it is not enough with the realization of magnetostatic structure. The dynamic properties of the magnetic vortices in the isosceles triangles oscillated by radiofrequency (RF) field are highly expected. Therefore, as the first step, we studied the dynamic properties of the single vortex domain structure in the isosceles triangular Py dot using impedance measurement method. In order to observe strong signal from the impedance measurement, a sample containing a chain of 1000 isolated isosceles triangle dots was prepared by using the electron beam lithography and traditional lift-off method. The whole measurement was carried out in the room temperature. The vector network analyzer was used to estimate the oscillation properties of the sample.

To start with, the single vortex and double vortex structure were created, respectively, by applying the initialized magnetic field with appropriate directions according to the phase diagram presented in Fig. 7.2. After that, the dynamic response of the vortex cores was monitored with the existence of a horizontal external magnetic field (parallel to the base line of the isosceles triangle). Fig. 7.1 illustrates the S_{11} spectra for the single vortex and double vortex states under remanent fields and the resonance frequency of the vortex cores as a function of external magnetic field for both single vortex and double vortex situations, respectively. As shown in Fig. 7.1(b), a clear single peak in the spectrum corresponding to the resonant frequency of the single vortex core in the isosceles triangle was observed in the measurement. Besides, the resonant frequency of the vortex core varies in a relatively small range with the change of the magnetic field which exhibits great difference comparing with the tendency of resonant frequency in regular triangular ferromagnetic dots. The results indicate that the resonant frequency performs a gradual upward trend with the enhancement of magnetic field along the negative direction as the vortex core approaches the device boundary. However, the resonant frequency decreases slightly as the field increases from zero, then it starts to increase again while the magnetic field exceeds 40 Oe which may originates from the variation of the confined potential[33, 57, 114] of the vortex core along with the movement of vortex core towards to the vertex.

As expected, two well-defined peaks were obviously observed in the spectrum in association with the double vortex magnetic structure obtained above. The high resonant frequency is for the upper vortex owing to the relatively higher potential in this asymmetric triangle structure while the low resonant frequency is for the downside vortex. By studying the field dependence of the resonant frequency in the range from -20 Oe to 100 Oe, we identify that the upper vortex and downside vortex show different behaviors. Apparently, the resonant frequency of the downside vortex performs weak field dependence with slightly reduction. On the contrary, figure 7.1(c) illustrates the resonant frequency of the upper

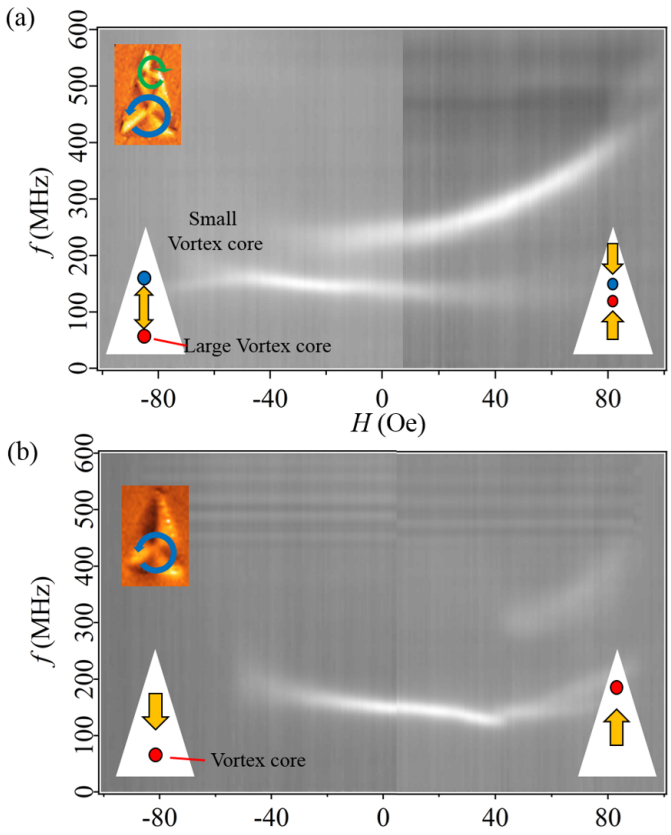

Figure 7.4: The resonant response of vortex core as a function of the external field for isosceles triangular device with single vortex and double vortices, respectively with the schematic figure showing the displacement of vortex cores with the external field.

vortex core showing great modification as the in-plane field varies from negative to positive and reaching to the maximal resonant frequency over 400 MHz. In the meanwhile, the downside vortex reaches to the minimum. As the magnetic field increases positively from zero, the two vortices are getting closer to each other implying that the magnetic interaction between two vortices becomes stronger correspondingly, which may attribute to the splitting between the resonant frequencies of the two vortices. However, there is no big difference between the resonant frequencies of the two vortices during negative magnetic field range which could be understood as a consequence of relatively small magnetic interaction rooted in the deviation of two vortex cores. These results indicate the resonant frequency could be modified by choosing the specific domain structure and specific field and may give us a suggestion that the magnetic coupling plays an important role in determining the oscillation properties of the upper vortex and the downside vortex.

7.2.5 Micromagnetic simulations

To gain further insight into the resonant dynamic properties of vortices in isosceles triangle, micromagnetic simulations were conducted on the triangular Py dot with same size and same experimental conditions. The results are shown in figure 3 and mainly are in good agreement with the experimental results. As we expected in the experiment result for the triangle with single vortex, the displacement direction of the vortex core is confirmed in the numerical result shown in Fig. 7.5(a), which moves vertically upward while sweeping field from negative to positive direction. The resonance frequency of the vortex core ranges between 100 MHz and 200 MHz for both experimental and the simulation results. The resonant frequency exhibits a downward trend with respect to the H from -80 Oe to 80 Oe and the minimum of the resonant frequency appears at field of 80 Oe in the numerical plot. However, the resonant frequency reduces from -80 Oe to 40 Oe then starts to increase from 40 Oe to 80 Oe according to the experimental result shown in Fig. 7.4(a). This difference

between the experimental and numerical results may originate from the small excitation field (H_ac=0.5 Oe). Besides, the result in Fig. 7.5(c) indicates that the oscillation radius on x axis and y axis is different with each other but both less than 25 nm, demonstrating the ellipse shape rotation under resonant state. The radius reaches the minimum as the vortex core is closest to the vertex angle of the triangle at field of 80 Oe, probably due to the enhanced potential near the vertex comparing with the initial position of vortex core.

On the other hand, the triangle with two vortices and their dynamic properties were also successfully reproduced by the numerical calculation even there are some differences between the experimental and simulation results. The plot of vortex core positions as a function of the external dc field shown in Fig. 7.5(d) demonstrates that the vortices shift away from each other as horizontal field on negative direction is applied while the two vortices approach each other with the increasing horizontal field on positive direction based on the competition of two vortices. However, according to the relationship between resonant frequency and external field indicated in Fig. 7.5(e), the oscillation of the large vortex core downwards dominated at low field ($< 30Oe$) with a resonant frequency around 180 MHz, probably because the interaction between two vortex cores is negligibly small when there is a large distance between the two vortex cores at negative field then the large vortex core plays a dominant role. The splitting of the resonant frequency of the two vortices was observed only when the external field exceeds 30 Oe. In this case, two resonant frequency curves appear as a result of the strong interaction between two vortices while the two vortex cores get close to each other. Besides, the maximum of the resonance frequency for the small vortex core was achieved at the field of 80 Oe. At the same time, the large vortex core also reaches its minimum resonant frequency. But the magnitude of the observed resonant frequency for the experimental and numerical result are different. The maximum of the resonant frequency from the experimental data is over 400 MHz while the maximum of the numerical one is about 300 MHz. The field dependence of resonant frequency may be in

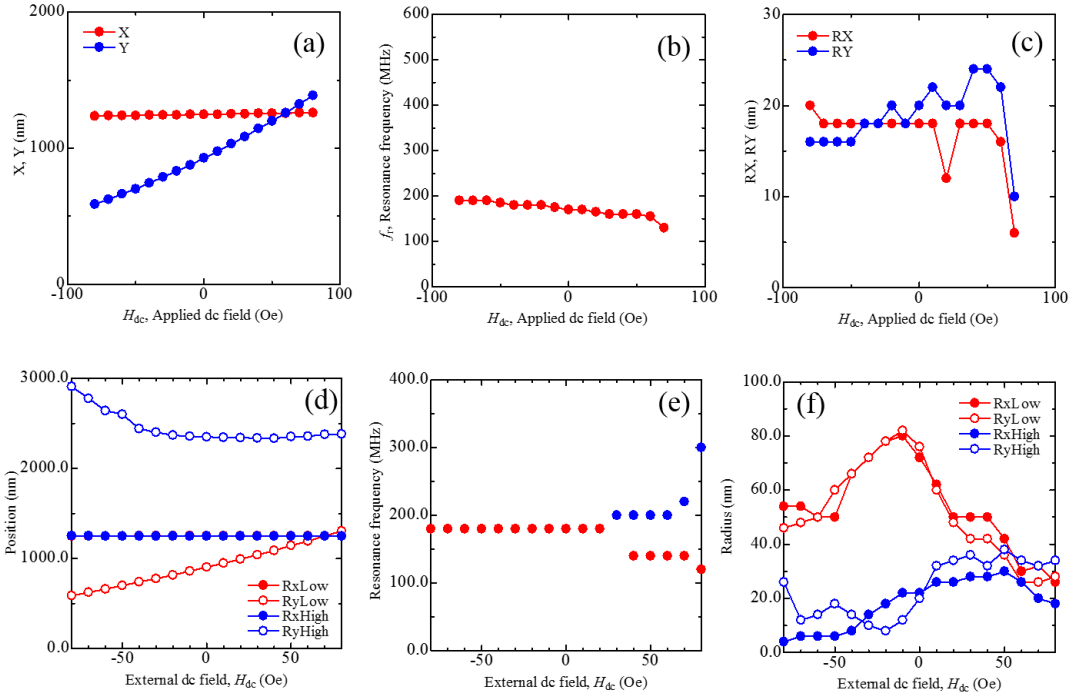

Figure 7.5: Numerically calculated results for the sample with single vortex and double vortices. The simulation results were conducted for the triangle with same size and same experiment conditions. (a) vortex position as a function of applied dc field for the triangle with single vortex; (b) resonant frequency as a function of the applied dc field for the triangle with single vortex; (c) The field dependence of the rotation radius on both R_x and R_y for the field range from -80 Oe to 80 Oe for the triangle with single vortex; (d) vortex positions as a function of applied dc field for the triangle with double vortices; (e) resonant frequencies as a function of the applied dc field for the triangle with double vortices; (f) The field dependences of the rotation radius on both Rx and Ry for the field range from -80 Oe to 80 Oe for the triangle with double vortices.

close association with the dc field dependence of radium of the core rotation. As shown in Fig. 7.5(f), the downside vortex core possesses the larger oscillation radius comparing to the upper vortex core at low field range (<30 Oe), however, the radius of the upper vortex core becomes larger than the downside vortex core under the interaction between the two vortices. In short, the mismatch between the experimental and simulation result may originate from the inaccuracy in the thickness and saturation magnetization as well as the structural imperfections in the samples.

7.3 Directional dependence of vortex core resonance in a square-shaped ferromagnetic dot

In this section, the resonant property of the magnetic vortex confined in a square-shaped ferromagnetic dot has been investigated. The field dependence of the resonant frequency performs a unique directional dependence originating from a four fold rotational symmetry of the square. The resonant frequency is found to be strongly modulated by the magnetic field along the diagonal direction although the magnetic field applied along the side of the square hardly modified the resonant frequency. The modulation ratio of the resonant frequency was found to be tuned by the lateral dimension of the ferromagnetic dot. These tunable properties of the field dependence may provide an additional function in the application of magnetic vortex systems.

A chain of the square ferromagnetic dots on a non-doped Si substrate was fabricated by the conventional lift-off technique. Here, the 40-nm-thick ferromagnetic Permalloy (Py) film was evaporated by a electro-beam evaporation under the pressure of 2×10^{-7} Pa. About the lateral dimensions of the square dots, we prepared three kinds of samples with different lateral dimension. Here, the diagonal distance of the square l varied from 1 μm to 3 μm. We note that the diagonal distance corresponds to the diameter of the circumscribed circle for the square dot. We confirm that the domain structures at the remanent state for the square

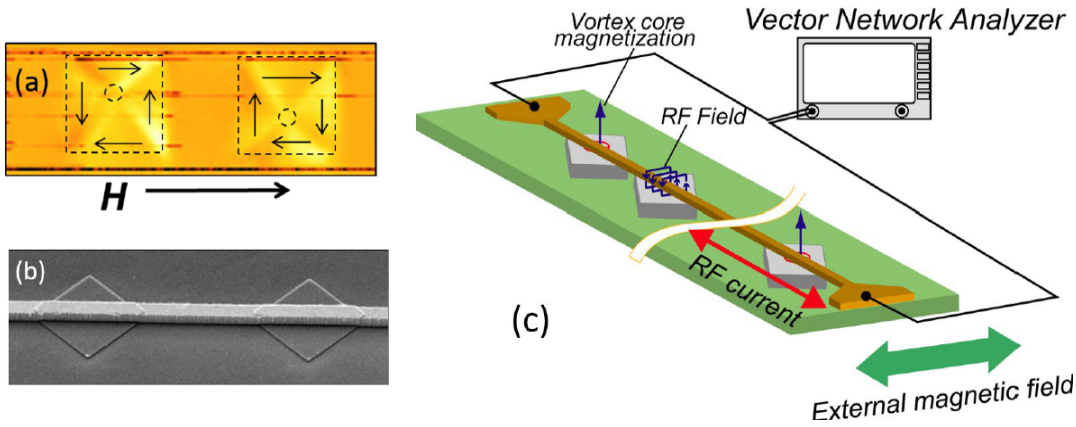

Figure 7.6: (a) Spatial distribution of the spin structure in the squared Permalloy dot observed by magnetic-force microscope; (b) SEM image of part of the fabricated device; (c)Schematic illustration of the sample structure with the measurement setup.

dots perfectly form magnetic vortex structure even for the square dot with $l = 3$ μm by using magnetic force microscopy (MFM) (model NanoNavi/E-sweep, SII NanoTechnology) with low moment magnetic probes. The chirality distribution was random because the nucleation energy for both chiralities is degenerate.[83] The dynamic properties of the vortex core confined in the square dot have been evaluated by the reflection impedance (S_{11}) measurements using a standard vector network analyzer.[12, 63] As shown in Fig. 7.6(b), a single Cu strip line with 500 nm in width and 200 nm in thickness was deposited on the top of the ferromagnetic dots. We note that the narrow strip line enables to detect the resonant oscillation of the magnetization sensitively.[63] The in-plane static magnetic field at an angle ϕ with respect to the strip line was applied to adjust the equilibrium position of the vortex core. Here, we study the field dependence of the resonant property at $\phi = 0, \pi/4$ and $\pi/2$.

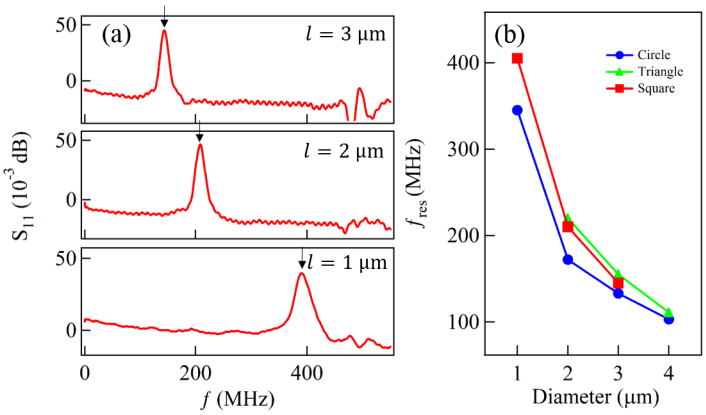

Figure 7.7: (a) Reflection spectra as a function of the input RF frequency for the square-shaped ferromagnetic dot with the diagonal distance $l = 1$ μm, 2 μm and 3 μm, respectively at the remanent state. (b) Comparison of the resonant frequency of the magnetic vortex confined in circular, square and triangular ferromagnetic dot as a function the diameter of the circumscribed circle.

7.3.1 Diagonal distance and field dependence of resonant frequency

Fig. 7.7(a) shows S_{11} signals as a function of the input RF frequency at the remanent state for the three different samples. In all of the samples, the resonant signature was clearly observed as a peak of the signal. The resonant frequencies for the samples with l= 1μ m, 2 μm and 3 μm are 405 MHz, 210 MHz and 145 MHz, respectively. These monotonic changes with the lateral dimension come from the change of the magneto-static energy and are consistent with the conventional understandings.[33] In Fig. 7.7(b), we compare the resonant frequency at the remanent state for the various shapes of the ferromagnetic dots.[63, 104] Here, the horizontal axis corresponds to the diameter of the circumscribed circle. The square dot was found to have intermediate values between the circle and the triangle. This indicates that the confined potential for the vortex core is related to the area size of the ferromagentic dot. So, the magnetic vortex confined in the triangular dot feels the largest restoring force because the average distance from the edges is shortest.

We then study the field dependence of the resonant property of the magnetic vortex in the square dot as well as its anisotropy. First we apply the magnetic field perpendicular to the Cu strip ($\phi = \pi/2$), which is a diagonal direction for the square. In this case, the equilibrium core position shifts along the Cu strip. As can be seen in Fig. 7.8(a), the resonant frequency increases with increasing the magnitude of the magnetic field for both polarities. We note that a similar modulation feature has been observed in a magnetic vortex confined in the regular triangle. In the triangular ferromagnetic dot, when the vortex core approaches to the vertex of the triangle, the resonant frequency increases because of the enhancement of the confined potential.[63] Since the similar situation is also expected in the square-shaped ferromagnetic dot by moving the core around the corner of the square, the modulation of the resonant frequency observed in Fig. 7.8(a) is caused by the enhancement of the confined potential. On the other hand, as shown in Fig. 7.8(b), when the magnetic field is applied along the side of the square ($\phi = \pi/4$), the change of the resonant property is negligibly small. We also want to emphasize that the similar in-sensitive behavior was obtained in the triangular dot when the core moves toward the side of the triangle.[63] This is exactly the same situation in the case for Fig. 7.8(b). Therefore, the effective confined potential for the vortex core is not modified when the core moves towards the side of the ferromagnetic dot. Thus, in the square-shaped ferromagnetic dot, the field dependence of the resonant frequency strongly depends on the direction of the magnetic field.

7.3.2 Modulation ratio and field direction dependence of resonant frequency

As pointed above, in the square dot, the resonant frequency is significantly modulated by the application of the magnetic field along the diagonal direction. Here, we discuss about the size dependence of the modulation ratio of the resonant frequency. Figure 7.9(a) shows the image plot of the spectra as a function of the magnetic field along the diagonal direction ($\phi = \pi/2$) for the samples with $l = 1$ μm, 2 μ m and 3 μm. In all of the samples, the resonant

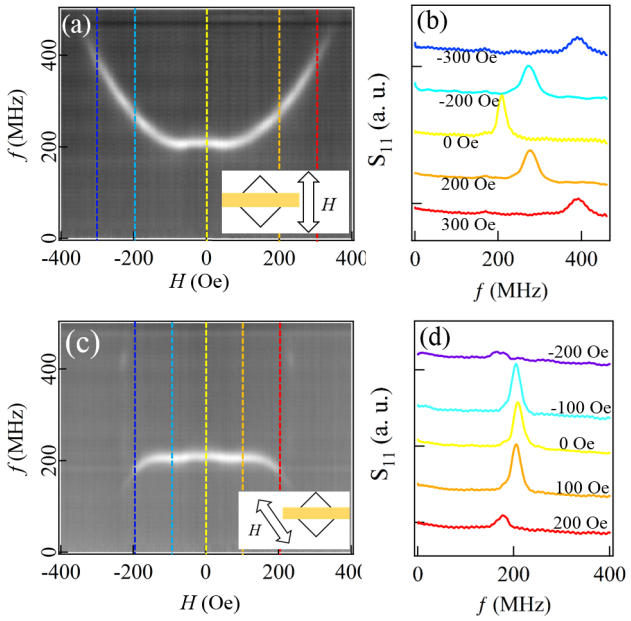

Figure 7.8: (a) Image plot of the reflection signal spectra as a function of external magnetic field perpendicular to the strip line ($\phi = \pi/2$) and (b) the representative spectra observed at $H = \pm 300$ Oe, ± 200 Oe and zero field . (c) Image plot of the reflection signal spectra as a function of external magnetic field along the side of the square ($\phi = \pi/4$) and (d) the representative spectra observed at $H = \pm 200$ Oe, ± 100 Oe and zero field.

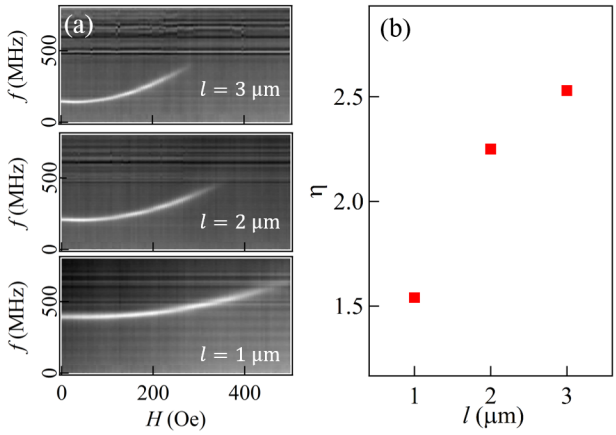

Figure 7.9: (a) Image plot of the reflection spectra for the square dot with $l = 3$ μm as a function of the external magnetic field along the diagonal direction ($\phi = \pi/2$); (b) The modulation ratio η as a function of the diameter distance, where the modulation ratio is defined as the ratio of maximum resonant frequency to the resonant frequency at remanent state.

frequency increases with increasing the magnitude of the magnetic field. We now focus on the modulation ratio η defined by the maximum resonant frequency divided by the resonant frequency at $H = 0$. Figure 7.9(b) shows the modulation ratio η as a function of the diagonal distance l. It can be clearly seen that η monotonically increases with increasing the size of the square. We want to emphasize that the difference in the maximum resonant frequency is smaller than the difference in the minimum resonant frequency, which corresponds to the resonance at the remanent state. This means that the confined potential for the magnetic vortex does not depend on the lateral dimension so much when the core is located in the vicinity of the corner. This can be understood by the fact that one square is perfectly fit at the corner of the other square.

Finally, the importance of the relationship between the device configuration and the direction of the core displacement has been indicated. Figures 7.10(a) and (b) show the image plots for the field dependence of the reflection spectra for the square with the diameter of

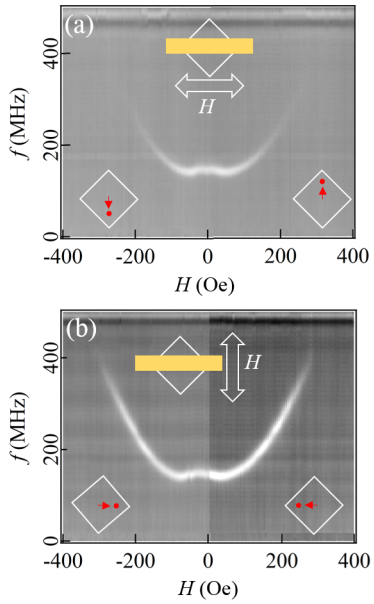

Figure 7.10: Image plots of reflection spectra for the square dot with l =3 μm as a function of external magnetic field at (a) $\phi = \pi/2$ and (b)$\phi = 0$

3 μm, where the magnetic field is applied along two different diagonal direction. We clearly confirm that the resonant signature in Fig. 7.10(b) disappears at much lower magnetic field than that in Fig. 7.10(a). Since the vortex core moves perpendicular to the magnetic field[39], the core should shift out of the strip line by the application of the magnetic field along the strip line ($\phi = 0$). Therefore, the results indicate that the narrow strip line can detect the core oscillation only in the vicinity the Cu strip line.

7.4 Conclusion

To summarize, in the first place, we have achieved the identification of magnetic structure with two vortices in the isosceles triangular device using magnetic force microscopy imaging, indicated that the transition between the single and double vortex structure could be simply manipulated by controlling the direction of the initialized in-plane magnetic field and suggested that the existence of the double vortex state is stable due to the lower formation energy. The realization of the double vortex may enrich new fundamental studies of magnetostatic structure and related dynamic properties. Furthermore, we provide the detailed experimental and numerical information about the dynamic changes of the resonant frequency with the dependence of horizontal magnetic field for both single and double vortices and clarify that the large splitting of oscillation frequency between the upper vortex and downside vortex. Comparing with the resonant frequency of the two vortex states in patterned ellipses[64, 65], the double vortex in the isosceles triangular Py dots maintains larger deviation of two resonant frequencies especially when the magnetic field exceeds +30 Oe. That should be contributed from the stronger dynamic interaction of the two vortices in the asymmetric domain structure of the patterned isosceles triangles while the ellipses possess exactly symmetric structure. The simple realization of the transition between single and double vortex and the effective modification of the resonant frequency based on the magnetic coupling between two vortices imply that a possibility for the development of the

reconfigurable logic and microwave assisted spin based devices.

On the other hand, the resonant property of the magnetic vortex stabilized in a square-shaped ferromagnetic dot has been investigated. The resonant frequency takes an intermediate value between the circular and triangular disks with the same diameter of the circumscribed circle. This is because the magnitude of the confined potential decreases with increasing the area size of the dot. The field dependence of the resonant frequency shows a unique directional dependence reflecting the four-fold rotational symmetry. The significant modulation of the resonant frequency can be realized in the square with the diagonal distance of 3 μm under the in-plane magnetic field perpendicular to the strip line. These results indicate that the dynamic properties of vortex core can be modified by adjusting the direction of in-plane magnetic field and these characteristics provide a possibility for technological applications such as the reconfigurable logic and filtering devices.

Chapter 8

Conclusion

This thesis concentrates on the experimental characterization and manipulation of vortex chirality, as well as the development of detection techniques for vortex dynamics and further exploitation of interesting dynamic behaviors. There are several results which have been concluded shown as follows:

The measurement of AMR curves demonstrates the introduction of asymmetrically configured electrodes for a single Py circular disk offers a simple solution to distinguish the nucleation position of vortex structure. That should attribute to the inhomogeneous distribution of current density from the large difference of resistivity of Py and Cu electrodes. The chirality is further determined because the nucleation depends on direction of applied field and chirality. The observation of AMR curves at different field range suggest the vortex chirality relying on the magnitude of the maximum magnetic field. This approach for chirality detection may accelerate the development on characterization of magnetic vortex and its future spintronic application.

The dynamic property of magnetic vortex during oscillation was also studied by a new developed measurement technique in this thesis which allows to pick up the vortex oscillation without any background signal by the separately prepared excitation and detection circuits. The obtained size and interval dependences of the resonant property show good agreement with the previously reported numerical and experimental results. By extending the present

technique to the application of the spatially modulated magnetic field, it is possible to excite the unique high-energy resonant mode. Moreover, the power dependence of a chain of meander type circular was detected by this method. The result indicates a splitting of the resonant frequency during high RF amplitude which may originates from some translational mode under nonlinear regime. This method is limited to the investigation of magnetic vortex dynamics at remanent state. To exploit the magnetic vortex core dynamics at the remanent state, we have developed a novel method based on the electrically separated excitation and detection circuits with the spectrum analyzer. The signature of the vortex core resonance is well detected as the 2nd harmonic signal induced by the two-fold symmetric resistance change. The current and field dependence of the 2nd harmonic signal show the features consistent with the previously reported results. This technique may be extended to the higher order frequency generator voltage, faster than the intrinsic precession frequency. In addition, the resonant frequency as a function of RF power measured by the 2nd harmonic method at remanent state deviates from the linear behavior which may results from the high order contributions under high power.

Apart from the devotion to magnetic vortex in circular disks, magnetic vortex confined in the isosceles triangle or square was also paid attention to. In the first place, the experimental evidence of two stabilized vortices in an isosceles triangular ferromagnet has been provided by imaging the domain structure employing MFM under remanent state. Moreover, the numbers and chirality of the magnetic vortices can be controlled by adjusting the initialized field direction. By performing the transmission impedance measurement to analyze the oscillation dynamic behaviors for isosceles triangular devices with single vortex and double vortices structure, two resonance frequency peaks were observed where the high frequency peak increases further larger while the low frequency peak reduces gradually with the increase of positive field, indicating stronger magnetic vortices coupling under large positive field. Besides, the conducted micromagnetic simulation afterwards reproduces

the experimental results in a good way and offers a more extensive understanding about the low resonant frequency mode and high frequency mode in the core oscillation dynamic. Furthermore, the dynamic response of vortex core stabilized in chained square Py dots was also investigated. The experimental results indicate a unique directional field dependence of resonant frequency reflecting the four-fold rotational symmetry. In addition, significant modulation of the resonant frequency was realized in the square device with diagonal distance of 3 μm under the in-plane field perpendicular to the strip line. The results suggest the dynamic properties of vortex core could be modified by adjusting the direction of external field.

The above results indicate much simple but sensitive detection techniques for investigating of static and dynamic properties of vortex core, and provide a possibility for technological application based on magnetic vortex such as magnetic vortex based memories or microwave assisted filters.

Bibliography

[1] A. Bogdanov and A. Hubert. Thermodynamically stable magnetic vortex states in magnetic crystals. *Journal of Magnetism and Magnetic Materials*, 138(3):255–269, 1994.

[2] Hubert Alex and Rudolf Schäfer. *Magnetic Domains*. Springer, 1998.

[3] R. P. Cowburn, D. K. Koltsov, A. O. Adeyeye, M. E. Welland, and D. M. Tricker. Single-Domain Circular Nanomagnets. *Physical Review Letters*, 83(5):1042–1045, August 1999.

[4] K. Guslienko, S. Demokritov, B. Hillebrands, and a. Slavin. Effective dipolar boundary conditions for dynamic magnetization in thin magnetic stripes. *Physical Review B*, 66(13):8–11, 2002.

[5] V. S. Pribiag, I. N. Krivorotov, G. D. Fuchs, P. M. Braganca, O. Ozatay, J. C. Sankey, D. C. Ralph, and R. a. Buhrman. Magnetic vortex oscillator driven by d.c. spin-polarized current. *Nature Physics*, 3(7):498–503, May 2007.

[6] Keisuke Yamada, Shinya Kasai, Yoshinobu Nakatani, Kensuke Kobayashi, Hiroshi Kohno, André Thiaville, and Teruo Ono. Electrical switching of the vortex core in a magnetic disk. *Nature materials*, 6(4):269–3, April 2007.

[7] Dong-Hyun Kim, Elena a Rozhkova, Ilya V Ulasov, Samuel D Bader, Tijana Rajh, Maciej S Lesniak, and Valentyn Novosad. Biofunctionalized magnetic-vortex microdiscs for targeted cancer-cell destruction. *Nature materials*, 9(2):165–71, February 2010.

[8] T Shinjo, T Okuno, R Hassdorf, K Shigeto, and T Ono. Magnetic Vortex Core Observation in Circular Dots of Permalloy. *Science*, 289(5481):930–932, August 2000.

[9] B. E. Argyle, E. Terrenzio, and J. C. Slonczewski. Magnetic Vortex Dynamics Using the Optical Cotton-Mouton Effect. *Physical Review Letters*, 53(2):190–193, July 1984.

[10] J. P. Park, P. Eames, D. M. Engebretson, J. Berezovsky, and P. A. Crowell. Imaging of spin dynamics in closure domain and vortex structures. *Physical Review B*, 67(2):020403, January 2003.

[11] S B Choe, Y Acremann, a Scholl, a Bauer, a Doran, J Stöhr, and H a Padmore. Vortex core-driven magnetization dynamics. *Science (New York, N.Y.)*, 304(5669):420–422, 2004.

[12] V. Novosad, F. Fradin, P. Roy, K. Buchanan, K. Guslienko, and S. Bader. Magnetic vortex resonance in patterned ferromagnetic dots. *Physical Review B*, 72(2):024455, July 2005.

[13] Konstantin Y. Guslienko, Rafael Hernández Heredero, and Oksana Chubykalo-Fesenko. Nonlinear gyrotropic vortex dynamics in ferromagnetic dots. *Physical Review B*, 82(1):014402, July 2010.

[14] L Landau and E Lifshits. on the Theory of the Dispersion of Magnetic Permeability in Ferromagnetic Bodies. *Phys. Zeitsch. der Sow.*, 169(14):14–22, 1935.

[15] William Fuller Brown. Theory of the approach to magnetic saturation. *Physical Review*, 58(8):736–743, 1940.

[16] Charles Kittel. Theory of the structure of ferromagnetic domains in films and small particles. *Physical Review*, 70(11-12):965–971, 1946.

[17] Brown W. F. Jr Frei. E. H. The fundamental theorem of fine-ferromagnetic-particle theory. *Journal of Applied Physics*, 39(2):993–994, 1968.

[18] W. Heisenberg. Mehrkörperproblem und Resonanz in der Quantenmechanik. *Zeitschrift für Physik*, 38(6-7):411–426, 1926.

[19] P. A. M. Dirac. On the Theory of Quantum Mechanics, 1926.

[20] J. C. Slater. The ferromagnetism of nickel colloids. *Physical Review*, 49(7):537–545, 1936.

[21] E C Stoner. Collective electron ferromagnetism. *Proceedings of the Royal Society of London, Series A (Mathematical and Physical Sciences)*, 165(A922):372–414, 1938.

[22] R. M. Bozorth and D. M. Chapin. Demagnetizing factors of rods. *Journal of Applied Physics*, 13(5):320–326, 1942.

[23] J. A. Osborn. Demagnetizing factors of the general ellipsoid. *Physical Review*, 67(11-12):351–357, 1945.

[24] F. Bloch and G. Gentile. Zur Anisotropie der Magnetisierung ferromagnetischer Einkristalle. *Zeitschrift für Physik*, 70(5-6):395–408, 1931.

[25] J. H. Van Vleck. On the anisotropy of cubic ferromagnetic crystals. *Physical Review*, 52(11):1178–1198, 1937.

[26] Harvey Brooks. Ferromagnetic anisotropy and the itinerant electron model. *Physical Review*, 58(10):909–918, 1940.

[27] T. McGuire and R. Potter. Anisotropic magnetoresistance in ferromagnetic 3d alloys. *IEEE Transactions on Magnetics*, 11(4):1018–1038, 1975.

[28] Richard P Feynman, Robert B Leighton, and Matthew Sands. *The Feynman Lectures on Physics, Desktop Edition Volume I*, volume 1. Basic Books, 2013.

[29] Pierre Weiss. La variation du ferromagnétisme avec la température. *Comptes Rendus*, 143:1136, 1906.

[30] E. H. Kennard. Shape of the domains in ferromagnetics. *Physical Review*, 55(3):312–314, 1939.

[31] C Kittel. physical theory of ferromagnetic domians. *Reviews of Modern Physics*, 21(4):745, 1949.

[32] Michel Hehn, Kamel Ounadjela, J.-P. Bucher, Franqoise Rousseaux, Dominique Decanini, Bernard Bartenlian, and C. Chappert. Nanoscale Magnetic Domains in Mesoscopic Magnets, June 1996.

[33] K. Yu. Guslienko, B. A. Ivanov, V. Novosad, Y. Otani, H. Shima, and K. Fukamichi. Eigenfrequencies of vortex state excitations in magnetic submicron-size disks. *Journal of Applied Physics*, 91(10):8037, 2002.

[34] A Wachowiak, J Wiebe, M Bode, O Pietzsch, M Morgenstern, and R Wiesendanger. Direct observation of internal spin structure of magnetic vortex cores. *Science (New York, N.Y.)*, 298(5593):577–80, October 2002.

[35] R. Pulwey, M. Rahm, J. Biberger, and D. Weiss. Switching behavior of vortex structures in nanodisks. *IEEE Transactions on Magnetics*, 37(4):2076–2078, July 2001.

[36] T. Okuno, K. Shigeto, T. Ono, K. Mibu, and T. Shinjo. MFM study of magnetic vortex

cores in circular permalloy dots: behavior in external field. *Journal of Magnetism and Magnetic Materials*, 240(1-3):1–6, February 2002.

[37] N. Kikuchi, S. Okamoto, O. Kitakami, Y. Shimada, S. G. Kim, Y. Otani, and K. Fukamichi. Vertical bistable switching of spin vortex in a circular magnetic dot. *Journal of Applied Physics*, 90(12):6548–6549, 2001.

[38] K. Guslienko, V. Novosad, Y. Otani, H. Shima, and K. Fukamichi. Magnetization reversal due to vortex nucleation, displacement, and annihilation in submicron ferromagnetic dot arrays. *Physical Review B*, 65(2):024414, December 2001.

[39] Thomas Uhlig, M. Rahm, Christian Dietrich, Rainer Höllinger, Martin Heumann, Dieter Weiss, and Josef Zweck. Shifting and pinning of a magnetic vortex core in a permalloy dot by a magnetic field. *Physical Review Letters*, 95(23):1–4, 2005.

[40] C. Ross, M. Hwang, M. Shima, J. Cheng, M. Farhoud, T. Savas, Henry Smith, W. Schwarzacher, F. Ross, M. Redjdal, and F. Humphrey. Micromagnetic behavior of electrodeposited cylinder arrays. *Physical Review B*, 65(14):1–8, 2002.

[41] Konstantin L. Metlov and Konstantin Yu Guslienko. Stability of magnetic vortex in soft magnetic nano-sized circular cylinder. *Journal of Magnetism and Magnetic Materials*, 242-245(PART II):1015–1017, 2002.

[42] W. Scholz, K. Yu Guslienko, V. Novosad, D. Suess, T. Schrefl, R. W. Chantrell, and J. Fidler. Transition from single-domain to vortex state in soft magnetic cylindrical nanodots. *Journal of Magnetism and Magnetic Materials*, 266(1-2):155–163, 2003.

[43] Konstantin Yu. Guslienko. Magnetic vortex state stability, reversal and dynamics in restricted geometries. *Journal of Nanoscience and Nanotechnology*, 8(7):2745–2760, July 2008.

[44] Ki-suk Lee, Sang-koog Kim, Young-sang Yu, Youn-seok Choi, Konstantin Yu. Guslienko, Hyunsung Jung, and Peter Fischer. Universal Criterion and Phase Diagram for Switching a Magnetic Vortex Core in Soft Magnetic Nanodots. *Physical Review Letters*, 101(26):267206, December 2008.

[45] T. Y. Chen, A. T. Galkiewicz, and P. A. Crowell. Phase diagram of magnetic vortex dynamics. *Physical Review B*, 85(18):180406, May 2012.

[46] R. Cowburn, A. Adeyeye, and M. Welland. Configurational Anisotropy in Nanomagnets, December 1998.

[47] A. Fernandez and C. J. Cerjan. Nucleation and annihilation of magnetic vortices in submicron-scale Co dots. *Journal of Applied Physics*, 87(3):1395–1401, 2000.

[48] M. Schneider, H. Hoffmann, S. Otto, Th. Haug, and J. Zweck. Stability of magnetic vortices in flat submicron permalloy cylinders. *Journal of Applied Physics*, 92(3):1466, 2002.

[49] M. Rahm, M. Schneider, J. Biberger, R. Pulwey, J. Zweck, D. Weiss, and V. Umansky. Vortex nucleation in submicrometer ferromagnetic disks. *Applied Physics Letters*, 82(23):4110, 2003.

[50] P. Vavassori, N. Zaluzec, V. Metlushko, V. Novosad, B. Ilic, and M. Grimsditch. Magnetization reversal via single and double vortex states in submicron Permalloy ellipses. *Physical Review B*, 69(21):214404, June 2004.

[51] S. D. Bader. Colloquium: Opportunities in nanomagnetism. *Reviews of Modern Physics*, 78(January), 2006.

[52] Roman Antos, YoshiChika Otani, and Junya Shibata. Magnetic Vortex Dynamics. *Journal of the Physical Society of Japan*, 77(3):031004, March 2008.

[53] A.M. Kosevich, B.A. Ivanov, and A.S. Kovalev. Magnetic Solitons. *Physics Reports*, 194(3-4):117–238, 1990.

[54] K. Guslienko, X. Han, D. Keavney, R. Divan, and S. Bader. Magnetic Vortex Core Dynamics in Cylindrical Ferromagnetic Dots. *Physical Review Letters*, 96(6):067205, February 2006.

[55] K. S. Buchanan, M. Grimsditch, F. Y. Fradin, S. D. Bader, and V. Novosad. Driven dynamic mode splitting of the magnetic vortex translational resonance. *Physical Review Letters*, 99(26):267201, December 2007.

[56] V Uhlíř, M Urbánek, L Hladík, J Spousta, M-Y Im, P Fischer, N Eibagi, J J Kan, E E Fullerton, and T Šikola. Dynamic switching of the spin circulation in tapered magnetic nanodisks. *Nature nanotechnology*, 8(5):341–6, May 2013.

[57] A. A. Thiele. Steady-state motion of magnetic domains. *Physical Review Letters*, 30(6):230–233, 1973.

[58] B. A. Ivanov, H. J. Schnitzer, F. G. Mertens, and G. M. Wysin. Magnon modes and magnon-vortex scattering in two-dimensional easy-plane ferromagnets. 1998.

[59] K. S. Buchanan, P. E. Roy, M. Grimsditch, F. Y. Fradin, K. Yu Guslienko, S. D. Bader, and V. Novosad. Magnetic-field tunability of the vortex translational mode in micron-sized permalloy ellipses: Experiment and micromagnetic modeling. *Physical Review B - Condensed Matter and Materials Physics*, 74(6):1–5, 2006.

[60] B. A. Ivanov and C. E. Zaspel. High frequency modes in vortex-state nanomagnets. *Physical Review Letters*, 94(2):23–26, 2005.

[61] Konstantin Guslienko, Ki-Suk Lee, and Sang-Koog Kim. Dynamic Origin of Vortex

Core Switching in Soft Magnetic Nanodots. *Physical Review Letters*, 100(2):027203, January 2008.

[62] K. Yu Guslienko, V. Novosad, Y. Otani, H. Shima, and K. Fukamichi. Field evolution of magnetic vortex state in ferromagnetic disks. *Applied Physics Letters*, 78(24):3848–3850, 2001.

[63] Satoshi Yakata, Terumitsu Tanaka, Kohei Kiseki, Kimihide Matsuyama, and Takashi Kimura. Wide range tuning of resonant frequency for a vortex core in a regular triangle magnet. *Scientific reports*, 3:3567, January 2013.

[64] Kristen S. Buchanan, Pierre E. Roy, Marcos Grimsditch, Frank Y. Fradin, Konstantin Yu. Guslienko, Sam D. Bader, and Valentyn Novosad. Soliton-pair dynamics in patterned ferromagnetic ellipses. *Nature Physics*, 1(3):172–176, December 2005.

[65] Kristen S. Buchanan, Pierre E. Roy, Frank Y. Fradin, Konstantin Yu Guslienko, Marcos Grimsditch, Sam D. Bader, and Val Novosad. Vortex dynamics in patterned ferromagnetic ellipses. *Journal of Applied Physics*, 99(2006):97–100, 2006.

[66] P. A. Franken and J. F. Ward. Optical harmonics and nonlinear phenomena. *Reviews of Modern Physics*, 35(1):23–39, 1963.

[67] Andrei Slavin and Vasil Tiberkevich. Nonlinear auto-oscillator theory of microwave generation by spin-polarized current. *IEEE Transactions on Magnetics*, 45(4):1875–1918, 2009.

[68] O. V. Sukhostavets, B. Pigeau, S. Sangiao, G. De Loubens, V. V. Naletov, O. Klein, K. Mitsuzuka, S. Andrieu, F. Montaigne, and K. Y. Guslienko. Probing the anharmonicity of the potential well for a magnetic vortex core in a nanodot. *Physical Review Letters*, 111(24):1–5, 2013.

[69] B Van Waeyenberge, a Puzic, H Stoll, K W Chou, T Tyliszczak, R Hertel, M Fähnle, H Brückl, K Rott, G Reiss, I Neudecker, D Weiss, C H Back, and G Schütz. Magnetic vortex core reversal by excitation with short bursts of an alternating field. *Nature*, 444(7118):461–4, November 2006.

[70] A. Vansteenkiste, K. W. Chou, M. Weigand, M. Curcic, V. Sackmann, H. Stoll, T. Tyliszczak, G. Woltersdorf, C. H. Back, G. Schütz, and B. Van Waeyenberge. X-ray imaging of the dynamic magnetic vortex core deformation. *Nature Physics*, 5(5):332–334, March 2009.

[71] Markus Weigand, Bartel Van Waeyenberge, Arne Vansteenkiste, Michael Curcic, Vitalij Sackmann, Hermann Stoll, Tolek Tyliszczak, Konstantine Kaznatcheev, Drew Bertwistle, Georg Woltersdorf, Christian Back, and Gisela Schütz. Vortex Core Switching by Coherent Excitation with Single In-Plane Magnetic Field Pulses. *Physical Review Letters*, 102(7):077201, February 2009.

[72] Benjamin Pigeau, Grégoire de Loubens, Olivier Klein, Andreas Riegler, Florian Lochner, Georg Schmidt, and Laurens W. Molenkamp. Optimal control of vortex-core polarity by resonant microwave pulses. *Nature Physics*, 7(1):26–31, October 2010.

[73] R. Compton and P. Crowell. Dynamics of a Pinned Magnetic Vortex. *Physical Review Letters*, 97(13):137202, September 2006.

[74] A Dussaux, B Georges, J Grollier, V Cros, a V Khvalkovskiy, A Fukushima, M Konoto, H Kubota, K Yakushiji, S Yuasa, K a Zvezdin, K Ando, and A Fert. Large microwave generation from current-driven magnetic vortex oscillators in magnetic tunnel junctions. *Nature communications*, 1(1):8, 2010.

[75] A. Dussaux, A. V. Khvalkovskiy, P. Bortolotti, J. Grollier, V. Cros, and A. Fert.

Field dependence of spin-transfer-induced vortex dynamics in the nonlinear regime. *Physical Review B*, 86(1):014402, July 2012.

[76] V. Novosad, M. Grimsditch, J. Darrouzet, J. Pearson, S. D. Bader, V. Metlushko, K. Guslienko, Y. Otani, H. Shima, and K. Fukamichi. Shape effect on magnetization reversal in chains of interacting ferromagnetic elements. *Applied Physics Letters*, 82(21):3716, 2003.

[77] Naoki Nishimura, Tadahiko Hirai, Akio Koganei, Takashi Ikeda, Kazuhisa Okano, Yoshinobu Sekiguchi, and Yoshiyuki Osada. Magnetic tunnel junction device with perpendicular magnetization films for high-density magnetic random access memory. *Journal of Applied Physics*, 91(8):5246, 2002.

[78] Junya Shibata, Kunji Shigeto, and Yoshichika Otani. Dynamics of magnetostatically coupled vortices in magnetic nanodisks. *Physical Review B*, 67(22):224404, June 2003.

[79] Junya Shibata and Yoshichika Otani. Magnetic vortex dynamics in a two-dimensional square lattice of ferromagnetic nanodisks. *Physical Review B*, 70(1):012404, July 2004.

[80] André Thiaville, José García, Rok Dittrich, Jacques Miltat, and Thomas Schrefl. Micromagnetic study of Bloch-point-mediated vortex core reversal. *Physical Review B*, 67(9):094410, March 2003.

[81] Sergey Savelfev and Franco Nori. Magnetic and mechanical buckling: Modified Landau theory approach to study phase transitions in micromagnetic disks and compressed rods. *Physical Review B*, 70(21):214415, December 2004.

[82] M. Grimsditch, P. Vavassori, V. Novosad, V. Metlushko, H. Shima, Y. Otani, and K. Fukamichi. Vortex chirality in an array of ferromagnetic dots. *Physical Review B*, 65(17):172419, May 2002.

[83] S. Yakata, M. Miyata, S. Nonoguchi, H. Wada, and T. Kimura. Control of vortex chirality in regular polygonal nanomagnets using in-plane magnetic field. *Applied Physics Letters*, 97(22):222503, 2010.

[84] M. Jaafar, R. Yanes, D. Perez de Lara, O. Chubykalo-Fesenko, A. Asenjo, E. M. Gonzalez, J. V. Anguita, M. Vazquez, and J. L. Vicent. Control of the chirality and polarity of magnetic vortices in triangular nanodots. *Physical Review B*, 81(5):054439, February 2010.

[85] M. Schneider, H. Hoffmann, and J. Zweck. Magnetic switching of single vortex permalloy elements. *Applied Physics Letters*, 79(19):3113, 2001.

[86] M. Schneider, H. Hoffmann, and J. Zweck. Lorentz microscopy of circular ferromagnetic permalloy nanodisks. *Applied Physics Letters*, 77(18):2909, 2000.

[87] M. Natali, A. Popa, U. Ebels, Y. Chen, S. Li, and M. E. Welland. Correlated vortex chiralities in interacting permalloy dot patterns. *Journal of Applied Physics*, 96(8):4334, 2004.

[88] T. Kimura, Y. Otani, and J. Hamrle. Determination of magnetic vortex chirality using lateral spin-valve geometry. *Applied Physics Letters*, 87(17):172506, 2005.

[89] S. Yakata, M. Miyata, S. Honda, H. Itoh, H. Wada, and T. Kimura. Chirality control of magnetic vortex in a square Py dot using current-induced Oersted field. *Applied Physics Letters*, 99(24):242507, 2011.

[90] P. Vavassori, M. Grimsditch, V. Metlushko, N. Zaluzec, and B. Ilic. Magnetoresistance of single magnetic vortices. *Applied Physics Letters*, 86(7):072507, 2005.

[91] T. Kimura, Y. Otani, H. Masaki, T. Ishida, R. Antos, and J. Shibata. Vortex motion

in chilarity-controlled pair of magnetic disks. *Applied Physics Letters*, 90(13):132501, 2007.

[92] C Stamm. Two-Dimensional Magnetic Particles. *Science*, 282(5388):449–451, October 1998.

[93] M.N. Baibich and J.M. Broto. Giant Magnetosresistance of (001)Fe/(001)Cr Magnetic Superlattices. *Physical Review Letters*, 61(001):2472–2475, 1988.

[94] G. Binasch, P. Grünberg, F. Saurenbach, and W. Zinn. Enhanced magnetoresistance in layered magnetic structures with antiferromagnetic interlayer exchange. *Physical Review B*, 39(7):4828–4830, 1989.

[95] Gary A Prinz. Magnetoelectronics applications. *Journal of Magnetism and Magnetic Materials*, 200(1):57–68, 1999.

[96] S. A. Wolf, D. D. Awschalom, R. A. Buhrman, J. M. Daughton, S. von Molnár, M. L. Roukes, A. Y. Chtchelkanova, and D. M. Treger. Spintronics: a spin-based electronics vision for the future. *Science (New York, N.Y.)*, 294(5546):1488–1495, November 2001.

[97] V. Novosad, M. Grimsditch, K. Guslienko, P. Vavassori, Y. Otani, and S. Bader. Spin excitations of magnetic vortices in ferromagnetic nanodots, August 2002.

[98] J. Sort, A. Hoffmann, S. H. Chung, K. S. Buchanan, M. Grimsditch, M. D. Baró, B. Dieny, and J. Nogués. Magnetization reversal in submicron disks: Exchange biased vortices. *Physical Review Letters*, 95(6):1–4, 2005.

[99] Thomas Gerrits, Pavol Krivosik, Michael L. Schneider, Carl E. Patton, and T. J. Silva. Direct detection of nonlinear ferromagnetic resonance in thin films by the magneto-optical kerr effect. *Physical Review Letters*, 98(20):1–4, 2007.

[100] Markus Bolte, Guido Meier, Benjamin Krüger, André Drews, René Eiselt, Lars Bocklage, Stellan Bohlens, Tolek Tyliszczak, Arne Vansteenkiste, Bartel Van Waeyenberge, Kang Wei Chou, Aleksandar Puzic, and Hermann Stoll. Time-resolved X-ray microscopy of spin-torque-induced magnetic vortex gyration. *Physical Review Letters*, 100(17):1–4, 2008.

[101] Shinya Kasai, Peter Fischer, Mi-Young Im, Keisuke Yamada, Yoshinobu Nakatani, Kensuke Kobayashi, Hiroshi Kohno, and Teruo Ono. Probing the Spin Polarization of Current by Soft X-Ray Imaging of Current-Induced Magnetic Vortex Dynamics. *Physical Review Letters*, 101(23):237203, December 2008.

[102] Mi-Young Im, Peter Fischer, Keisuke Yamada, Tomonori Sato, Shinya Kasai, Yoshinobu Nakatani, and Teruo Ono. Symmetry breaking in the formation of magnetic vortex states in a permalloy nanodisk. *Nature communications*, 3:983, January 2012.

[103] Shinya Kasai, Yoshinobu Nakatani, Kensuke Kobayashi, Hiroshi Kohno, and Teruo Ono. Current-Driven Resonant Excitation of Magnetic Vortices. *Physical Review Letters*, 97(10):107204, September 2006.

[104] M. Miyata, S. Nonoguchi, S. Yakata, H. Wada, and T. Kimura. Static and Dynamical Properties of a Magnetic Vortex in a Regular Polygonal Nanomagnet. *IEEE Transactions on Magnetics*, 47(10):2505–2507, October 2011.

[105] Satoshi Sugimoto, Yasuhiro Fukuma, Shinya Kasai, Takashi Kimura, Anjan Barman, and YoshiChika Otani. Dynamics of Coupled Vortices in a Pair of Ferromagnetic Disks. *Physical Review Letters*, 106(19):197203, May 2011.

[106] Andreas Vogel, Anna Corinna Niemann, Charlotte Stenner, Andrú Drews, Mi-Young Im, Peter Fischer, and Guido Meier. Vortex dynamics in triangular-shaped confining potentials. *Journal of Applied Physics*, 112(6):063916, 2012.

[107] Takayuki Nozaki, Yoichi Shiota, Shinji Miwa, Shinichi Murakami, Frédéric Bonell, Shota Ishibashi, Hitoshi Kubota, Kay Yakushiji, Takeshi Saruya, Akio Fukushima, Shinji Yuasa, Teruya Shinjo, and Yoshishige Suzuki. Electric-field-induced ferromagnetic resonance excitation in an ultrathin ferromagnetic metal layer. *Nature Physics*, 8(6):492–497, April 2012.

[108] J.-S. Kim, M. Kläui, M. V. Fistul, J. Yoon, C.-Y. You, R. Mattheis, C. Ulysse, and G. Faini. Double resonance response in nonlinear magnetic vortex dynamics. *Physical Review B*, 88(6):064402, August 2013.

[109] Satoshi Sugimoto, Norinobu Hasegawa, Yasuhiro Niimi, Yasuhiro Fukuma, Shinya Kasai, and YoshiChika Otani. Detection of a symmetric circular gyration of the vortex core via the second-order harmonic magnetoresistance oscillation. *Applied Physics Express*, 7(2):023006, February 2014.

[110] Ajay Gangwar, Hans G. Bauer, Jean-Yves Chauleau, Matthias Noske, Markus Weigand, Hermann Stoll, Gisela Schütz, and Christian H. Back. Electrical determination of vortex state in submicron magnetic elements. *Physical Review B*, 91(9):2–6, 2015.

[111] Andreas Vogel, André Drews, Thomas Kamionka, Markus Bolte, and Guido Meier. Influence of dipolar interaction on vortex dynamics in arrays of ferromagnetic disks. *Physical Review Letters*, 105(3):037201, July 2010.

[112] Xiaomin Cui, Shaojie Hu, and Takashi Kimura. Detection of a vortex nucleation position in a circular ferromagnet using asymmetrically configured electrodes. *Applied Physics Letters*, 105(8):082403, August 2014.

[113] T. Ishida, T. Kimura, and Y. Otani. Current-induced vortex displacement and annihilation in a single permalloy disk. *Physical Review B*, 74(1):014424, July 2006.

[114] Benjamin Krüger, André Drews, Markus Bolte, Ulrich Merkt, Daniela Pfannkuche, and Guido Meier. Harmonic oscillator model for current- and field-driven magnetic vortices. *Physical Review B*, 76(22):224426, December 2007.

[115] Numerically obtained resonant frequencies for 2 μm, 3 μm and 4 μm disks are 177 MHz, 132 MHz and 86 MHz, respectively.

[116] K. Kiseki, S. Yakata, and T. Kimura. Efficient excitation and detection of standing spin wave in Permalloy film: Demonstration of spin wave resonator. *Applied Physics Letters*, 101(21):212404, 2012.

[117] Y. Acremann, J. Strachan, V. Chembrolu, S. Andrews, T. Tyliszczak, J. Katine, M. Carey, B. Clemens, H. Siegmann, and J. Stöhr. Time-Resolved Imaging of Spin Transfer Switching: Beyond the Macrospin Concept. *Physical Review Letters*, 96(21):217202, May 2006.

[118] Junya Shibata, Yoshinobu Nakatani, Gen Tatara, Hiroshi Kohno, and Yoshichika Otani. Current-induced magnetic vortex motion by spin-transfer torque. *Physical Review B*, 73(2):020403, January 2006.

[119] K. Bussmann, G. A. Prinz, S.-F. Cheng, and D. Wang. Switching of vertical giant magnetoresistance devices by current through the device. *Applied Physics Letters*, 75(16):2476, 1999.

[120] A Ruotolo, V Cros, B Georges, A Dussaux, J Grollier, C Deranlot, R Guillemet, K Bouzehouane, S Fusil, and A Fert. Phase-locking of magnetic vortices mediated by antivortices. *Nature nanotechnology*, 4(8):528–32, August 2009.

[121] Yuri Gaididei, Denis D. Sheka, and Franz G. Mertens. Controllable switching of vortex chirality in magnetic nanodisks by a field pulse. *Applied Physics Letters*, 92(1):012503, 2008.

[122] V. Cambel and G. Karapetrov. Control of vortex chirality and polarity in magnetic nanodots with broken rotational symmetry. *Physical Review B*, 84(1):014424, July 2011.

[123] B. C. Choi, J. Rudge, E. Girgis, J. Kolthammer, Y. K. Hong, and a. Lyle. Spin-current pulse induced switching of vortex chirality in permalloyCuCo nanopillars. *Applied Physics Letters*, 91(2):2005–2008, 2007.

[124] Roman Antos and Yoshichika Otani. Simulations of the dynamic switching of vortex chirality in magnetic nanodisks by a uniform field pulse. *Physical Review B*, 80(14):140404, October 2009.

[125] Keiki Fukumoto, Kuniaki Arai, Takashi Kimura, Yoshichika Otani, and Toyohiko Kinoshita. Nonlinear motion of magnetic vortex cores during fast magnetic pulses. *Physical Review B*, 85(13):134414, April 2012.

[126] Young-Sang Yu, Dong-Soo Han, Myoung-Woo Yoo, Ki-Suk Lee, Youn-Seok Choi, Hyunsung Jung, Jehyun Lee, Mi-Young Im, Peter Fischer, and Sang-Koog Kim. Resonant amplification of vortex-core oscillations by coherent magnetic-field pulses. *Scientific reports*, 3:1301, January 2013.

[127] J. Park and P. Crowell. Interactions of Spin Waves with a Magnetic Vortex. *Physical Review Letters*, 95(16):167201, October 2005.

[128] Sangkook Choi, Ki Suk Lee, Konstantin Yu Guslienko, and Sang Koog Kim. Strong radiation of spin waves by core reversal of a magnetic vortex and their wave behaviors in magnetic nanowire waveguides. *Physical Review Letters*, 98(8):98–101, 2007.

[129] Matthias Kammerer, Markus Weigand, Michael Curcic, Matthias Noske, Markus

Sproll, Arne Vansteenkiste, Bartel Van Waeyenberge, Hermann Stoll, Georg Woltersdorf, Christian H Back, and Gisela Schuetz. Magnetic vortex core reversal by excitation of spin waves. *Nature communications*, 2:279, January 2011.

[130] Georgios Roumpos, Michael D. Fraser, Andreas Löffler, Sven Höfling, Alfred Forchel, and Yoshihisa Yamamoto. Single vortex-antivortex pair in an exciton-polariton condensate. *Nature Physics*, 7(2):129–133, November 2010.

[131] K. Nakano, K. Tanabe, R. Hiramatsu, D. Chiba, N. Ohshima, S. Kasai, T. Sato, Y. Nakatani, K. Sekiguchi, K. Kobayashi, and T. Ono. Real-time observation of electrical vortex core switching. *Applied Physics Letters*, 102(7):072405, 2013.

[132] Nickolai A. Usov, Ching Ray Chang, and Zung Hang Wei. Nonuniform magnetization structures in thin soft type ferromagnetic elements of elliptical shape. *Journal of Applied Physics*, 89(11 II):7591–7593, 2001.

[133] M. Miyata, K. Kiseki, S. Yakata, H. Wada, and T. Kimura. Formations of magnetic vortices in a chain array of triangle Py dots and an isosceles triangle Py dot. *Journal of Applied Physics*, 111(7):07B902, 2012.

Research Activities

Journal Publications

1. Xiaomin Cui, Satoshi Yakata and Takashi Kimura. *Directional dependence of vortex core resonance in a square-shaped ferromagnetic dot.* Appl. Phys. Lett., submitted.

2. Kazuto Yamanoi, Yuki Yokotani, Xiaomin Cui, and Takashi Kimura. *Stability of standing spin wave in NiFe thin film studied by using anisotropic magnetoresistance effect.* Phys. Rev. B, submitted.

3. Xiaomin Cui, Shaojie Hu, Makoto Hidegara, and Takashi Kimura. *Sensitive detection of vortex-core resonance using amplitude-modulated magnetic field.* Sci. Rep. submitted.

4. Xiaomin Cui, Satoshi Yakata,and Takashi Kimura. *Detection of vortex core oscillation using 2nd harmonic voltage detection technique.* IEEE Trans. on Magn. **15**, 0018-9464 (2015).

5. Xiaomin Cui, Shaojie Hu, and Takashi Kimura, *Detection of a vortex nucleation position in a circular ferromagnet using asymmetrically configured electroes.* Appl. Phys. Lett. **105**, 082403 (2014).

Conference Presentations

1. Xiaomin Cui, Satoshi Yakata, and Takashi Kimura. *Detection of vortex core oscillation using 2nd harmonic voltage detection technique*(Poster), IEEE International Magnetics Conference (Intermag 2015). May 11-15, 2015, Beijing, China.

2. Satoshi yakata, Xiaomin Cui, and Takashi Kimura. *Reconfigurable dynamic properties using a polygonal Py dot*(Poster). IEEE International Magnetics Conference (Intermag 2015), May 11-15, Beijing, China.

3. Makoto Hidegara, Xiaomin Cui, and Takashi Kimura. *Angular dependence of the vortex nucleation process in a regular triangle nanomagnet* (Poster). IEEE International Magnetics Conference (Intermag 2015), May 11-15, 2015, Beijing, China.

4. Xiaomin Cui, Satoshi Yakata, Terumitsu Tanaka, and Takashi Kimura. *Reconfigurable vortex oscillations using isosceles triangular ferromagnetic dots* (Oral). 5th Zing Bionanomaterials Conference, Apr. 25-28, Carvoeiro, Portugal.

5. Makoto Hidegara, Xiaomin Cui, Kohei Ohnishi and Takashi Kimura. *Spin dynamics and instability of the magnetic vortex formation process of polygonal nanomagnets* (Poster). Annual meeting of the Physical Society of Japan in 2014, Sept. 7-10, Nagoya, Japan.

6. Xiaomin Cui, Satoshi Yakata, and Takashi Kimura. *2nd harmonic detection of nonlinear vortex oscillation under strong RF magnetic field based on the anisotropic magnetoresistance effect* (Poster). The 15th International Union of Materials Research Societies, International Conference in Asia (IUMRS ICA 2014), Aug. 24-30, 2014, Fukuoka, Japan.

7. Xiaomin Cui, Satoshi Yakata and Takashi Kimura. *Detection of nonlinear vortex oscillation under strong RF magnetic field using anisotropic magnetoresistance effect*

(Oral). The 58th Annual Conference on Magnetism and Magnetic Materials (MMM 2013), Nov. 4-8, 2013, Denver, USA.

8. Satoshi Yakata, Xiaomin Cui, and Takashi Kimura. *Sensitive detection of magnetic vortex dynamics using anisotropic magnetoresistance effect* (Oral). The 37th Annual Conference on Magnetics in Japan, Sep. 3-6, 2013, Sapporo, Japan.

9. Xiaomin Cui, Kohei Kiseki, Satoshi Yakata, and Takashi Kimura. *Resonant vortex core oscillation detected by anisotropic magnetoresistance effect* (Poster). The 8th International Symposium on Metallic Multilayers (MML 2013), May 19- 24, 2013, Kyoto, Japan.

10. Xiaomin Cui, Kohei Kiseki, Satoshi Yakata and Takashi Kimura. *Resonant vortex core oscillation detected by anisotropic magnetoresistance effect* (Poster), Spring meeting of the Physical Society of Japan, Mar. 26- 29, 2013, Hiroshima, Japan.